Fiber Optical Parametric Oscillator and Its Application to All-Optical Clock Recovery

Jia Li

A Thesis Submitted to the Faculty of Graduate Studies and Research

in Partial Fulfillment of the Requirements for

the Degree of Doctor of Philosophy at the

McGill University

Montreal, Quebec, Canada

May, 2014

VITA

Jia Li received his Bachelor of Science degree in optical information science and technology at Huazhong University of Science and Technology, Wuhan, China, in 2007, and Master of Philosophy degree in electrical engineering at The University of Hong Kong, Hong Kong SAR, in 2009. From September 2009, he has being working towards his Ph. D. degree under the supervision of Prof. Lawrence Chen in electrical engineering at McGill University, Montreal, Quebec, Canada. From November 2011 to March 2012, he was a visiting student in the Optical and Quantum Communication Group in the Universidad Politecnica de Valencia, Valencia, Spain. From May 2013, he has being working as an optical system designer at Ciena Corporation, Ottawa.

His research at McGill focuses on nonlinear phenomena in optical fiber, in particular fiber optical parametric amplifiers and oscillators, and their applications in all-optical clock recovery. He is also interested in photonic integrated circuits including integrated multi-wavelength SOA lasers and silicon based nonlinear signal processors. He has published 14 journal papers and 14 conference proceedings during his graduate studies, and these papers have been cited more than 130 times. He is the reviewer for many top-ranked photonic journals such as Optics Letters, Optics Express, Photonics Technology Letters, Optical Fiber Technology, Applied Optics, and Optics Communications.

He is a student member of IEEE, IEEE Photonics Society, and Optical Society of America.

ABSTRACT

The ever increasing demand for broader bandwidth in recent decades arises from various aspects simultaneously such as the increase in the number of users, the advent of new access methodologies, and the demand for higher access rate as well as high-quality multimedia services. Fiber optical communication technology has being developed at an unprecedented speed to meet the increasing demand. High-speed optoelectronic devices and sophisticated transmission schemes have been invented in order to fully utilize the huge transmission bandwidth provided by optical fiber. Despite the fact that different technologies exhibit their own merits and drawbacks, they share some common but critical optical components such as lasers, amplifiers, signal processing and networking devices. Innovation on these optical devices improves the optical system performance while lowering down the overall cost. Lasers that produce high repetition-rate and short duration optical pulses are essential for high-speed OTDM/WDM communication systems. The cost of a WDM transmitter could be significantly reduced if highly stable multi-wavelength laser sources could be implemented to replace the traditional DFB laser diode arrays. All-optical signal processing functions such as all-optical clock recovery are vital for the future ultra-high-speed optical transport networks as the electronic signal processing speed might be limited to a few hundred Gb/s.

In this dissertation, a novel type of fiber laser – fiber optical parametric oscillator (FOPO) is analyzed and demonstrated as a simple and cost-effective solution to the above mentioned applications. It will be demonstrated that FOPOs can be configured as multi-wavelength laser sources if a narrowband transmission grating filter is included in the cavity. Inherent four-wave mixing in the parametric process helps to stabilize the power distribution of the lasing wavelengths by reducing the gain competition among multiple longitudinal modes. As a result, simultaneous lasing of 129 wavelengths with 25 GHz frequency spacing is demonstrated with spectral tuning and reconfigurable features. Following the study of continuous-wave operation, actively mode-locked FOPO is studied in detail by analyzing the impact of pump requirements and cavity designs on the characteristics of the mode-locked pulses. The results provide useful guidelines for such design that high-quality optical pulses can be generated from a simple configuration.

Based on a similar configuration, rational harmonic mode-locking is investigated following the harmonic mode-locking counterpart. Optical pulses generation with various repetition-rates is demonstrated through this mechanism by simply tuning the cavity length without changing the cavity configuration. Mode-locked pulses with repetition rates from 10 GHz up to 240 GHz have been generated in the experiments. Finally, the application of actively mode-locked FOPOs in all-optical clock recovery is demonstrated. A detailed investigation is performed on the 10 Gb/s operation case. The results show that this method is promising as an all-optical clock recovery solution in terms of its robustness to the input signal quality degradations over a large range, namely duty cycle from 33% to 60%, average input power from -23 dBm to 6 dBm, extinction ratio above 8.7 dB, OSNR above 27 dB, residual dispersion between -600 ps/nm to 550 ps/nm, and DGD below 48 ps. All-optical clock recovery operating at 40 Gb/s is also demonstrated following the analysis.

RÉSUMÉ

Plusieurs facteurs tels que le nombre accru des utilisateurs, la découverte de nouvelles méthodes d'accès, l'attrait pour la haute-vitesse de même que les services de haute-qualité pour les multimédia justifient concomitamment l'utilisation toujours plus croissante de bande passante au cours des dernières décennies. La technologie de communication par fibre optique a connu un développement sans précédent de manière à satisfaire la demande. Les composants ultra-optiques à haute vitesse ainsi que les programmes sophistiqués de transmission ont été développés afin d'utiliser au maximum le débit fourni par fibre optique. Nonobstant les succès et les inconvénients respectifs de ces technologies, ces dernières ont en commun des composants électroniques essentiels tels que les lasers, les amplificateurs et les éléments pour le traitement du signal et pour la gestion de réseau. L'innovation de ces composants optiques améliore leur performance tout en baissant leurs coûts. Les lasers ayant un taux de reproduction élevé et des vibrations de courte durée, sont essentiels pour les systèmes de communication OTDM/WDM à haute vitesse. Le coût d'un émetteur WDM serait réduit en utilisant des sources à multiples longueurs d'onde très stables plutôt que des matrices de lasers DFB traditionnellement utilisées à cet effet. Comme le traitement électronique du signal pourrait être limité à quelques centaines de Go par seconde, les fonctions du traitement du signal entièrement optique comme celles de la réparation de l`horloge électronique sont vitales pour l'avenir des réseaux de transport à vitesse ultra-rapide.

Ce travail de recherche scientifique analyse et présente le nouveau type de laser à base de fibre optique - un oscillateur paramétrique à base de fibre optique (FOPO) - comme une solution simple et rentable pour les applications susmentionnées. Il vise à démontrer que les FOPO peuvent être conçus comme des sources à multiples longueurs d'ondes si un filtre à base de réseau de Bragg (grating) est inclus dans la cavité. Le phénomène des quatre-vagues de mixage présent dans le processus paramétrique aide à stabiliser la distribution de puissance des longueurs d'onde du laser en réduisant l'excès obtenu dans des multiples modes longitudinales. À l'issu du processus, on a obtenu simultanément un laser comprenant 129 longueurs d'ondes à fréquences séparées par 25 GHz ayant les possibilités d'ajustement et de reconfiguration. Se basant sur l'étude de

l`opération à onde continue, le FOPO étant en mode Verrouiller est scruté à travers l'analyse de l'impact des spécificités de la pompe et les types de cavité sur la nature des pulsations en mode Verrouiller. Les résultats fournissent des instructions utiles pour ce genre de conception qui atteste de la haute qualité des pulsations optiques suite à une configuration simple. S'inspirant d'une configuration similaire, ce phénomène rationnel et harmonique en mode Verrouiller est examiné en fonction de celui du système opposé. La génération des pulsations à différents niveaux de répétition est démontrée en ajustant la longueur de la cavité sans changer sa configuration. Des pulsations en mode Verrouiller ayant des taux de répétition de 10 GHz à 240 GHz ont été expérimentalement produites. Au final, l'application du FOPO en mode Verrouiller dans la réparation d'une horloge est démontrée. Une recherche détaillée est effectuée dans le cas de l'opération à 10 Go/s. Les résultats montrent que cette méthode est une solution prometteuse pour la réactivation d'une horloge causée par des dégradations de la qualité du signal entrant sur un champ d'action considérable, c'est-à-dire, un cycle d'utilisation de 33% à 60%, et une puissance d'énergie moyenne en amont de -23 dBm à 6 dBm, un ratio d'extinction supérieur à 8.7 dB, OSNR au-dessus de 27 dB, perte résiduelle entre -600 ps/nm et 550 ps/nm et un DGD inférieur à 48 ps. Le processus de réparation de l''horloge à un niveau de 40 Go/s est démontrée à partir de cette analyse.

ACKNOWLEDGEMENTS

First of all, I would like to thank my supervisor Prof. Lawrence Chen for his guidance over the past four years. I am always impressed by his profound knowledge in photonics and deep understanding in the area of fiber optics and optical communications. He is always able to provide his valuable insights to any theoretical or experimental problems I encountered. I am grateful for his kindness to support my study in Spain as an exchange student, and later my research project in silicon photonics from the UBC-CMC workshop. My thesis would not be finished without his unconditional support and continuous encouragement.

I would also like to thank other professors in the photonic systems group: Prof. David Plant, Prof. Andrew Kirk, Prof. Martin Rochette, and Prof. Odile Liboiron-Ladouceur. It is not possible to conduct research at our world-class lab without their generous contribution and management. A few more people I would like to thank are the lab managers Dr. Philip Roche, Dr. Pegah Seddighian, and the booking system manager Dr. Zhaobing Tian, who made their great effort to keep the lab running smoothly and efficiently.

I would like to thank the people who helped me during my PhD study: Dr. Victor Torres-Company, Dr. Pegah Seddighian, Dr. Payman Samadi, Mr. Junjia Wang, Mr. Lu Zhang, Ms. Maria-Iulia Comanici, Mr. Alireza Nezam-alhosseini, Mr. Mohammad Rezagholipour Dizaji, Mr. Rhys Adams, and Miss Mina Spasojevic. I would like to express special thanks to Dr. Tianye Huang. The hard working days in the lab and the fruitful discussions on papers and experiments will remain as the most precious memory of my PhD life.

Last but not least, I would like to express my sincere gratitude to my parents Mr. Chunfang Li and Mrs. Cuilian Zhong for their love and support.

TABLE OF CONTENTS

VITA i

ABSTRACT ii

RÉSUMÉ iv

ACKNOWLEDGEMENTS vi

TABLE OF CONTENTS vii

LIST OF FIGURES xi

LIST OF TABLES xv

LIST OF ABBREVIATIONS xvi

Chapter 1 Introduction 1

1.1 Fiber optical communication systems 3

1.2 Motivation 8

1.3 Contributions 9

1.3.1 Significance of the work 9

1.3.2 List of published journal and conference papers 11

1.4 Outline of the dissertation 14

Chapter 2 Nonlinear Effects in Optical Fiber 17

2.1 Stimulated inelastic scattering 19

2.1.1 Stimulated Brillouin scattering (SBS) 19

2.1.2 Stimulated Raman scattering (SRS) 21

2.2 Optical Kerr effect 22

2.2.1 Self-phase modulation (SPM) and cross-phase modulation (XPM) 22

2.2.2 Four-wave mixing 24

2.3 Fiber optical parametric amplifiers and oscillators 25

2.3.1 FOPA gain 25

2.3.2 One-pump and dual-pump FOPAs....28
2.3.3 Performance of FOPAs....30
2.3.4 FOPOs....31
2.3.5 Performance of FOPOs....33
2.4 Summary....36
Chapter 3 Multi-wavelength CW-FOPO....39
3.1 Introduction....39
3.1.1 EDFA based multi-wavelength fiber lasers....39
3.1.2 SOA based multi-wavelength fiber lasers....41
3.1.3 FOPA based multi-wavelength fiber lasers....42
3.2 Experimental setup and principle of operation....43
3.3 Experimental results and discussions....44
3.4 Conclusions....53
Chapter 4 Actively Harmonically Mode-Locked FOPO....55
4.1 Introduction....56
4.1.1 Fiber ring laser basics....56
4.1.2 EDFRLs and SFRLs....59
4.1.3 Mode-locked FOPOs....62
4.2 Operating principle and experimental setup....64
4.3 Experimental results and analysis....67
4.3.1 Pump pulse duty cycle....67
4.3.2 Pump power....69
4.3.3 Pulse chirp compensation....70
4.3.4 Filter bandwidth (FBW)....71
4.3.5 Wavelength tuning characteristics....72

4.3.6 Pump phase modulation 75
4.4 Discussion and conclusion 77
Chapter 5 Rational Harmonically Mode-locked FOPO 79
5.1 Pulse repetition rate multiplication methods 80
5.1.1 Amplitude-only spectral filtering 80
5.1.2 Phase-only spectral filtering 81
5.1.3 Temporal fractional Talbot effect 82
5.1.4 Rational harmonic mode-locking 83
5.2 Nonlinear frequency doubling using MZMs in a FOPO 84
5.3 RHML from 10 GHz to 30 GHz 87
5.3.1 Operating principle and experimental setup 87
5.3.2 Results and discussions 90
5.4 RHML from 40 GHz to 240 GHz 94
5.5 Conclusions 99
Chapter 6 All-optical Clock Recovery Based on a FOPO 101
6.1 Review of clock recovery approaches 102
6.1.1 PLLs 102
6.1.2 Self-pulsating laser 103
6.1.3 Spectral filtering 104
6.1.4 Actively mode-locked fiber ring laser 105
6.2 Experimental setup of a FOPO based all-optical clock recovery 106
6.3 Detailed analysis of 10 Gb/s all-optical clock recovery 108
6.3.1 Duty cycle 110
6.3.2 Average power 111
6.3.3 Extinction ratio 112

6.3.4 OSNR 113
6.3.5 Residual dispersion 113
6.3.6 DGD 114
6.3.7 Tunability 116
6.3.8 Electrical spectrum 118
6.4 Demonstration of 40 Gb/s all-optical clock recovery 118
6.5 Conclusions 122
Chapter 7 Conclusions and Future work 125
7.1 Summary of contributions 125
7.2 Future work 127
7.2.1 > 40 Gb/s all-optical clock recovery 127
7.2.2 Multi-wavelength mode-locking and all-optical clock recovery 128
7.2.3 Silicon based optical parametric amplifier and oscillator 130
REFERENCES 131

LIST OF FIGURES

Figure 1.1 New capacity deployment on major submarine cable routes vs. year over year growth. Data according to TeleGeography [1]. 2
Figure 1.2 Global IP traffic in Extra-Bytes (EB = 10^{18} Bytes) per month vs. year over year growth. Data according to Cisco Visual Network Index [2]. 1 EB/s corresponds to a deployed capacity of 10 Tb/s assuming a peak to average factor of 3.3 in the variation of demand. 2
Figure 1.3 A typical OTDM system [8]. Copyright © 2006, IEEE. Reproduced with permission from IEEE. 4
Figure 1.4 WDM based optical transport networks [22]. Copyright © 1999, Lucent Technologies Inc. Reproduced with permission from John Wiley & Sons.....6
Figure 1.5 Subsystems in a digital coherent receiver [26]. Copyright © 2010, IEEE. Reproduced with permission from IEEE.....7
Figure 1.6 Example of various research work in FOPOs. Contributed research directions are highlighted with referenced journal and conference publications. 10
Figure 2.1 Brillouin gain spectrum of a 700-m single-mode fiber [31]. Copyright © 1997, IEEE. Reproduced with permission from IEEE.....20
Figure 2.2 Parallel- and cross-polarized Raman gain spectra [32]. Copyright ©1995, OSA. Reproduced with permission from OSA. 22
Figure 2.3 Measured and calculated net "black-box" gain for three different pump powers [33]. Copyright © 2002, IEEE. Reproduced with permission from IEEE. 28
Figure 2.4 Measured and calculated gain spectra for a dual-pump FOPA [34]. Copyright © 2003, IET. Reproduced with permission from IET. 29
Figure 2.5 A typical configuration of an actively mode-locked FOPO. 32
Figure 3.1 Experimental setup of a multiwavelength FOPO. 43
Figure 3.2 Gain spectrum of the FOPA in the anti-Stokes band. 45
Figure 3.3 The dependence of the FOPA gain on the pump peak power.....45
Figure 3.5 Evolution of FOPO lasing spectrum at different pump powers. OSA RBW: 0.06 nm.....47
Figure 3.6 Output wavelength number and power nonuniformity vs. input pump power.48

Figure 3.7 FOPO spectrum at 1 W pump power (a) without flattening, and (b) with flattening. OSA RBW: 0.06 nm. 48
Figure 3.8 Repeated scans of the FOPO output spectrum in 20 min period. OSA RBW: 0.06 nm. 51
Figure 3.9 Multiwavelength FOPO with arbitrary lasing spectrum. OSA RBW: 0.06 nm. 51
Figure 3.10 Multiwavelength FOPO with tunable wavelength range over the entire lasing spectrum. OSA RBW: 0.06 nm. 52
Figure 4.1 A typical configuration of an actively mode-locked fiber ring laser....56
Figure 4.2 (a) Frequency distribution of M waves of equal intensity and phase. (b) Temporal distribution of M waves in mode-locking condition [102]. 58
Figure 4.3 Experimental setup for an actively mode-locked FOPO working at 10 GHz. .64
Figure 4.4 Impact of pump pulse duty cycle on the mode-locked pulse. 68
Figure 4.5 Impact of pump power on the mode-locked pulse. (Filter BW=0.8 nm). 68
Figure 4.6 Impact of intra-cavity dispersion management on the mode-locked pulse. (Filter BW=0.8 nm)....70
Figure 4.7 Impact of intra-cavity FBW on the mode-locked pulse. 71
Figure 4.8 Characteristics of a 10 GHz harmonically mode-locked FOPO. (a) Waveform of the input pump pulses with 33% duty cycle. 20 ps/div. (b) Waveform of the output mode-locked pulses. 20 ps/div (c) Pulsewidth and TBW product characteristics vs. tunable wavelength. (d) RSM timing jitter performance vs. tuning wavelength. (e) Tunable lasing spectra of the FOPO. RBW = 0.06 nm. (f) Electrical spectrum of the mode-locked pulses (waveform shown in figure (b)) from the FOPO. RBW= 10 kHz. ...73
Figure 4.9 Dependence of SNSR on average pump power for different values of filter bandwidth. 75
Figure 4.10 Characteristics of the mode-locked pulses when no PPM is applied. (a) Waveforms of the input pump pulses and the output mode-locked pulses. 20ps/div. (b) Electrical spectrum of the mode-locked pulses. RWB: 10 kHz. (c, d) RMS timing jittr, pulsewidth, and TBW product vs. tuning wavelength. 76
Figure 5.1 (a) Waveform of the input pump pulses with 20 GH repetition rate and 50% duty cycle. (b) Waveform of the output mode-locked pulses. (c) Lasing spectra of the 20

GHz harmonically mode-locked FOPO. RBW = 0.06 nm. (d, e) Pulsewidth, TBW product and RMS timing jitter vs. tuning wavelength. (f) Electrical spectrum of the mode-locked pulses. 85
Figure 5.2 Experimental setup of a rational harmonic mode-locked FOPO working at 10 - 30 GHz. 87
Figure 5.3 (a) Waveform of 20 GHz mode-locked pulses at 1551.7 nm. Time scale: 20 ps/div. (b) Optical spectrum of the mode-locked pulses at 20 GHz. (c) Pulsewidth and TBW product vs. wavelength. (d) RMS timing jitter vs. wavelength. 91
Figure 5.4 (a) Waveform of 30 GHz mode-locked pulses at 1551.8 nm. Time scale: 20 ps/div. (b) Optical spectrum of the mode-locked pulses at 30 GHz. (c) Pulsewidth and TBW product vs. wavelength. (d) RMS timing jitter vs. wavelength. 92
Figure 5.5 Experimental setup for a rational harmonic mode-locked FOPO working at 40 – 240 GHz. 94
Figure 5.6 Impact of FBW on the characteristics of the output pulses at 40 GHz. 96
Figure 5.7 Wavelength tuning characteristics of a RHML FOPO working at 40 GHz (a, b) and 80 GHz (c, d). (a, c) show the autocorrelation traces of the 40 GHz and 80 GHz pulses. 96
Figure 5.8 Waveforms of the pulses with various repetition rates generated from a RHML FOPO. 98
Figure 5.9 Characteristics of the pulses with various repetition rates generated from a RHML FOPO. 98
Figure 6.1 Experimental setup of a FOPO based clock recovery circuit. 107
Figure 6.2 Dependence of clock recovery performance on the signal duty cycle. (a) RMS timing jitter vs. duty cycle. (b) Pulsewidth, TBW product vs. duty cycle. 110
Figure 6.3 Dependence of clock recovery performance on the signal average input power. (a) RMS timing jitter vs. average input power. (b) Pulsewidth, TBW product vs. average input power. 111
Figure 6.4 Dependence of clock recovery performance on the signal extinction ratio. (a) RMS timing jitter vs. extinction ratio. (b) Pulsewidth, TBW product vs. extinction ratio. 111
Figure 6.5 Dependence of clock recovery performance on the signal OSNR. 112

Figure 6.6 Dependence of clock recovery performance on the signal residual dispersion. (a) Waveforms of the input signal with 500 ps/nm residual dispersion and its corresponding recovered clock. (b) Waveforms of the input signal with -600 ps/nm residual dispersion and its corresponding recovered clock. (c) RMS timing jitter vs. residual dispersion. (b) Pulsewidth, TBW product vs. residual dispersion. 114
Figure 6.7 Dependence of clock recovery performance on the signal DGD. (a) Waveforms of the input signal with 36 ps DGD and its corresponding output recovered clock. 20 ps/div. (b) Waveforms of the input signal with 48 ps DGD and its corresponding output clock. 20 ps/div. (c) RMS timing jitter vs. DGD. (b) Pulsewidth, TBW product vs. DGD. 115
Figure 6.8 Dependence of clock recovery performance on the clock wavelength. (a) RMS timing jitter vs. clock wavelength. (b) Pulsewidth, TBW product vs. clock wavelength. 116
Figure 6.9 Electrical spectrum of the recovered clock from input signal without impairments. ESA RBW: 1 kHz. 116
Figure 6.10 Experimental setup of FOPO based all-optical clock recovery operating at 40 Gb/s. 117
Figure 6.11 Characteristics of the recovered clock as a function as SOA current. 120
Figure 6.12 Waveforms of the recovered clock signal as a function of SOA current. (a) Waveform of the clock signal without SOA amplification. (b, c, d) Waveforms of the clock signals when the SOA operates at 70 mA, 150 mA, and 250 mA, correspondingly. 120
Figure 6.13 Characteristics of the recovered clock signal as a function of clock wavelength. 121
Figure 6.14 Waveforms of the recovered clock signal as a function of clock wavelength. (a) Waveform of the input signal. 10 ps/div. (b, c, d) Waveforms of the output clock at 1546.7 nm, 1549.8 nm, and 1551.5 nm, correspondingly. 10ps/div. 121

LIST OF TABLES

Table 3.1 Comparison of various types of multi-wavelength lasers discussed in this chapter.....53
Table 4.1 Waveform results of the mode-locked lasers.....58
Table 4.2 Specifications of the HNLF 67
Table 4.3 Default operation condition of the mode-locked FOPO.....67
Table 5.1 Comparison of pulse characteristics using different schemes and with different repetition rates.....99
Table 6.1 Characteristics of the the input signal without impairments..... 109

LIST OF ABBREVIATIONS

AM	amplitude modulator
AOFS	acousto-optic frequency shifter
ASIC	application-specific integrated circuit
ASE	amplified spontaneous emission
BPF	band-pass filter
CD	chromatic dispersion
CW	continuous wave
DCA	digital communication analyzer
DFB	distributed feedback laser
DGD	differential group delay
DSF	dispersion-shifted fiber
DSP	digital signal processing
EAM	electro-absorption modulator
EDFA	erbium-doped fiber amplifier
EDFRL	erbium-doped fiber ring laser
EOM	electro-optic modulator
ER	extinction ratio
ESA	electrical spectrum analyzer
FBG	fiber Bragg grating
FBW	filter bandwidth
FOPO	fiber optical parametric oscillator
FOPA	fiber optical parametric amplifier
FP	Fabry-Perot
FSR	free spectral range
FWM	four-wave mixing
FWHM	full width half maximum
GVD	group velocity dispersion
LCM	liquid crystal modulator
LOA	linear optical amplifier

MZI	Mach-Zehnder interferometer
NALM	nonlinear amplifying loop mirror
NFSI	nonlinear fiber Sagnac interferometer
NLSE	nonlinear Schrodinger equations
NOLM	nonlinear optical loop mirror
NPR	nonlinear polarization rotation
OADM	optical add/drop multiplexer
OC	optical coupler
ODL	optical delay line
OEM	opto-electronic modulator
OEO	opto-electronic oscillator
OEOL	oscillating electro-optical loop
OSA	optical spectrum analyzer
OSNR	optical signal-to-noise ratio
OTDM	optical time-division multiplexing
OXC	optical cross connect
PC	polarization controller
PD	photodetector
PDM	polarization-division multiplexing
PHB	polarization hole burning
PM	phase modulator
PMD	polarization-mode dispersion
PLL	phase-locked loop
PPLN	periodically poled lithium niobate
PZT	piezoelectric transducer
QAM	quadrature-amplitude modulation
RBW	resolution bandwidth
RMS	root-mean square
SBS	stimulated Brillouin scattering
SC-FDM	single-carrier frequency-division multiplexing
SCG	supercontinuum generation

SFRL	semiconductor fiber ring laser
SHB	spectral hole burning
SMF	single-mode fiber
SNSR	supermode noise suppression ratio
SOA	semiconductor optical amplifier
SOP	state of polarization
SPM	self-phase modulation
SRS	stimulated Raman scattering
SSA	semiconductor saturable absorber
TBW	time-bandwidth
TGF	transmission grating filter
THG	third harmonic generation
TLS	tunable laser source
VCO	voltage controlled oscillator
WDM	wavelength-division multiplexing
WDMC	wavelength-division multiplexing coupler
XGM	cross-gain modulation
XAM	cross-absorption modulation
XPM	cross-phase modulation
XPolM	cross-polarization modulation

Chapter 1 Introduction

The demand for broader bandwidth grows at an unprecedented speed in the recent few years. It has been reported from the service providers as well as the telecom analysts that the demand on international bandwidth grew 39% in 2012, and at a compounded annual rate of 53% between 2007 and 2012. A study of the new capacity deployment on some major submarine cable routes reveals the growing appetite of bandwidth in the past 15 years (see Figure 1.1) [1]. The bandwidth demand on the trans-Atlantic submarine cable route increased 36% annually between 2007 and 2012; the demand for bandwidth between U.S. to Latin America grew 70% annually over the same period; and the demand for capacity on the Europe-Asia route via Egypt grew at 87% per year. With such growth rate, the total internet traffic will anticipate a jump from around 100 Tb/s in 2008 up to 1000 Tb/s in 2016 (see Figure 1.2) [2]. The average monthly data consumption will climb up to 100 EB by 2016. Much of the bandwidth need comes from the ever-increasing audio/video streaming, peer-to-peer file sharing, social networking, and the booming new services such as data centers and cloud computing. In April 2013, the IEEE announced the launch of IEEE 802.3 Standard for Ethernet study to explore the development of 400 Gb/s Ethernet standard to support ever-increasing, exponential network bandwidth growth [3].

The growing demand on broader bandwidth arises from different aspects simultaneously such as the increase in the number of users, access methodologies, access rates, and multimedia services. One of the key technologies that we rely on to meet the ever-increasing demand on bandwidth is fiber optical communication. With the continuous progress in the research and development of electro-optical devices such as lasers, modulators, and photodetectors (PDs), and the progress in the fiber-optic devices such as low-loss optical fibers, fiber amplifiers, and optical filters, the bit rate of the fiber optical communication system has been increased by a factor of 100,000 over a period of less than 30 years [4]. The transmission distances have also increased from 10 to 10,000 km over the same time period. In particular, the loss of the optical fiber has dropped

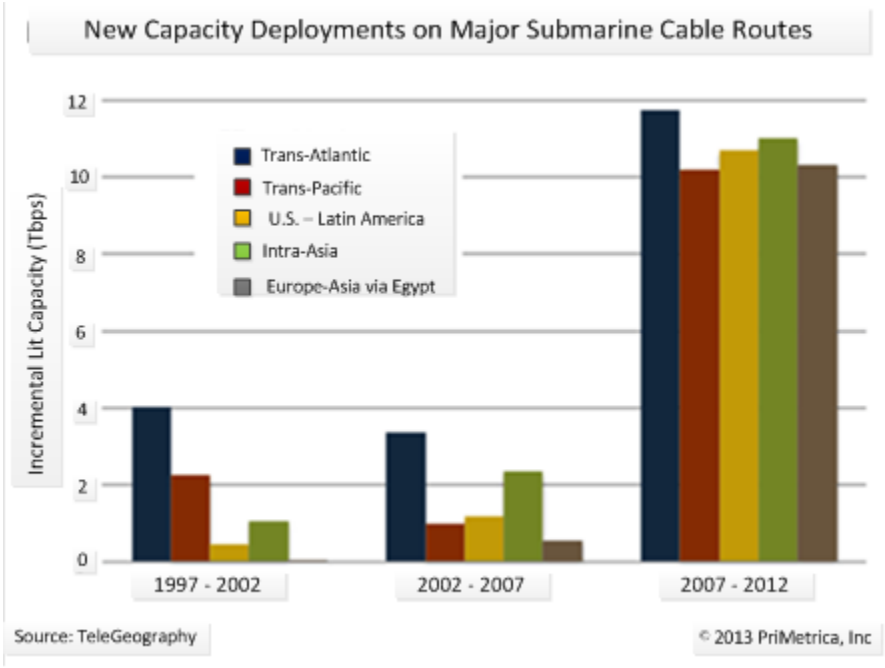

Figure 1.1 New capacity deployment on major submarine cable routes vs. year over year growth. Data according to TeleGeography [1].

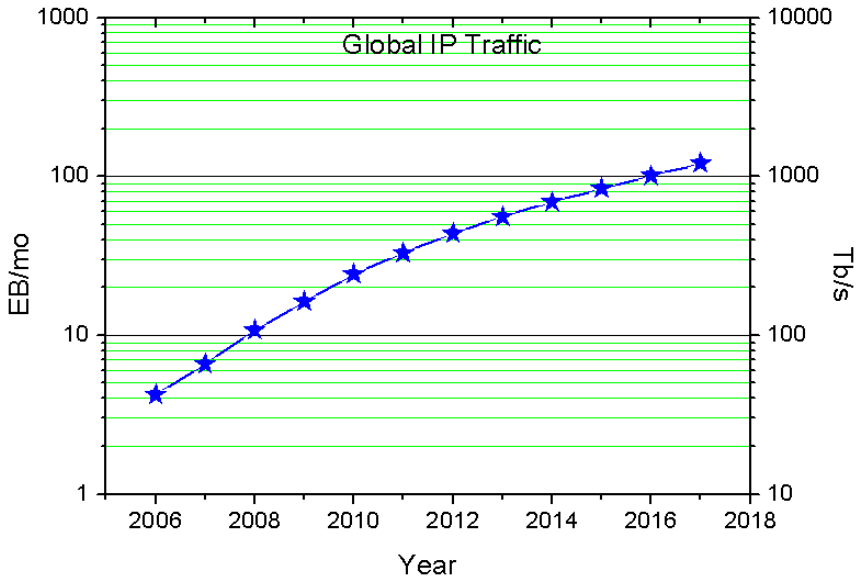

Figure 1.2 Global IP traffic in Extra-Bytes (EB = 10^{18} Bytes) per month vs. year over year growth. Data according to Cisco Visual Network Index [2]. 1 EB/s corresponds to a deployed capacity of 10 Tb/s assuming a peak to average factor of 3.3 in the variation of demand.

from > 1,000 dB/km in 1960 to < 20 dB/km in 1970 and eventually to < 0.2 dB/km now, due to the improved fabrication technologies [5, 6]. With the current deployed optical fiber, despite the other available transmission windows such as 850 nm and 1300 nm, the 1550 nm window alone can support up to 100 nm (~ 12.5 THz) transmission bandwidth. The theoretical limit to the fiber capacity of the current single-core single-mode fiber is predicted to be ~ 100 Tb/s due to a number of factors such as the Shannon limit, optical fiber nonlinearities, the fiber fuse effect, as well as optical fiber amplifier bandwidth [7].

In this chapter, a brief introduction of fiber optical communication systems is given in section 1.1 with a focus on the technologies being introduced for increasing the system capacity. Following the introduction section, the reason why we need to build high-speed optical sources and all-optical clock recovery circuits will be discussed in section 1.2. The main contribution of the thesis work will be presented later with associated published papers in section 1.3. A description of the organization of this dissertation will be given in the last section.

1.1 Fiber optical communication systems

There are three main challenges researchers and engineers have being working on during the development of modern fiber optical transport systems/networks in the past twenty years.

First, although optical fiber has tremendously huge bandwidth and significantly low loss compared with other transmission media, we have not used even half of the total available bandwidth in our commercial transmission systems. So the first challenge is how to fully utilize the huge bandwidth provided by optical fiber.

Second, with the advent of high-speed transmitters and receivers, the aggregate throughput of networking equipment may exceed Tb/s in the future, which may well exceed the maximum processing speed of the current and/or future electronic devices. Therefore, it is highly desirable to realize all-optical signal processing functions such as routing, switching and signal regeneration either in end-to-end terminal equipment or inline networking elements.

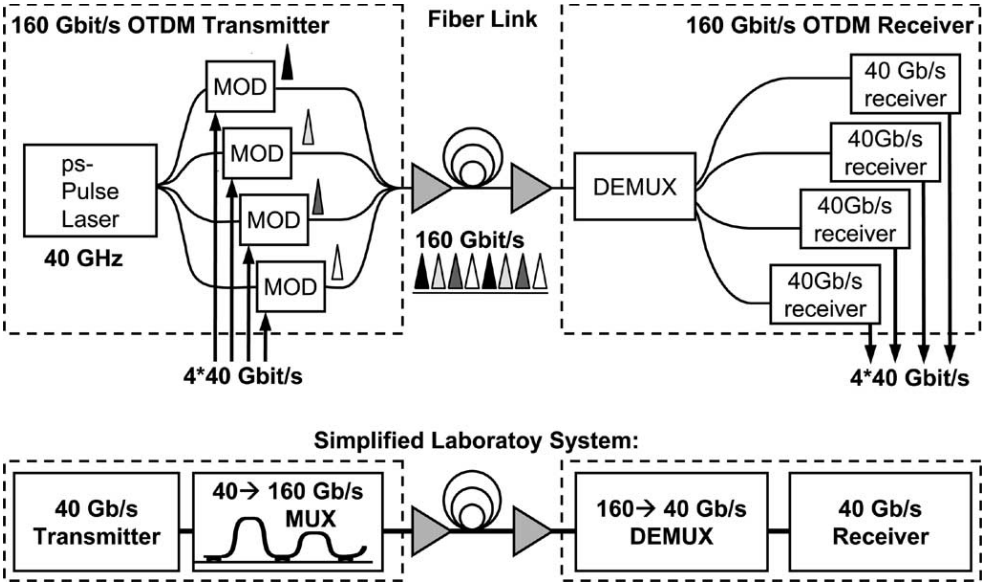

Figure 1.3 A typical OTDM system [8]. Copyright © 2006, IEEE. Reproduced with permission from IEEE.

Third, to deploy new equipment and systems in the real-world scenario, cost is always the number one concern. The third challenge is how to make agile optical components that are cost-effective and easy to be upgraded in the future.

Over the past years, researchers have developed many multiplexing methods to make efficient use of the existing bandwidth, in which the main technologies are optical time-division multiplexing (OTDM) and wavelength-division multiplexing (WDM). In OTDM systems, low-speed data signals are time-interleaved to form a high speed data stream, which will be de-multiplexed using time gating at the receiver end. A typical OTDM system is shown in Figure 1.3 [8]. In this setup, a 160 Gb/s signal is formed by time-interleaving four 40 Gb/s signals. There are several key components to form an OTDM system: (1) an optical pulse source which is capable of generating ultra-short, high-repetition-rate pulses, (2) high-speed external electro-optic modulators (EOMs), (3) high-speed all-optical signal processing such as multiplexing, de-multiplexing, and clock recovery. Among them, the optical pulse source and high-speed all-optical clock recovery are of particular importance. In general, an optical pulse source should have the ability to generate optical pulses with short pulse duration, low timing jitter, low amplitude noise, and little chirp. In addition, the wavelength of the pulse source should have the tunable or

switchable capability to accommodate a wide range of usage while reducing the cost of OTDM systems. For an all-optical clock recovery circuit, it is required that the recovered clock has low timing jitter, low amplitude noise and can be recovered with little latency. The circuit should be able to operate in high speed, robust against input signal quality degradations, and the wavelength of the recovered clock can be tunable. As one of the promising candidates for increasing the transmission capacity, OTDM has received considerable research interests in recent years [8-16].

However, for OTDM systems, a higher bit rate makes transmission systems more vulnerable to chromatic dispersion (CD) and polarization-mode dispersion (PMD), as well as creating the need for a higher optical signal-to-noise ratio (OSNR) in the wavelength channel. A higher OSNR requires a higher signal power which makes the system more sensitive to fiber nonlinearities. Compared with OTDM, WDM technology has the potential to meet the need for future ultra-broadband transport networks because it can transmit multiple wavelengths in a single fiber, as long as the wavelengths are in the transmission window of the standard single-mode fiber (SMF). The invention of the erbium-doped fiber amplifier (EDFA) further consolidates WDM as the predominant multiplexing technology nowadays. Besides, instead of simple point-to-point transmission, WDM can involve networking functions such as routing, switching using optical add/drop multiplexers (OADMs), and optical cross connects (OXCs) [17, 18], which make the transport networks more flexible, sustainable, robust, and cost-effective. High capacity WDM transmission systems have been widely reported in the past years [19-21]. Figure 1.4 shows a typical WDM based optical transport network [22]. It can be seen that several key components are required to form a WDM system: (1) multi-wavelength optical sources, (2) wavelength multiplexing and de-multiplexing, OADMs and OXCs, (3) all-optical signal processing (e.g., wavelength conversion, clock recovery, etc.). Among them, multi-wavelength optical sources and all-optical signal processing are of vital importance. Instead of using distributed feedback laser (DFB) arrays, a single multiwavelength optical source that can emit wavelengths in the whole wavelength range of interest with desired wavelength spacing can significantly reduce the cost and complexity of the transmitters. All-optical signal processing plays an important role in future all-optical networks which can avoid unnecessary optical-electrical-optical

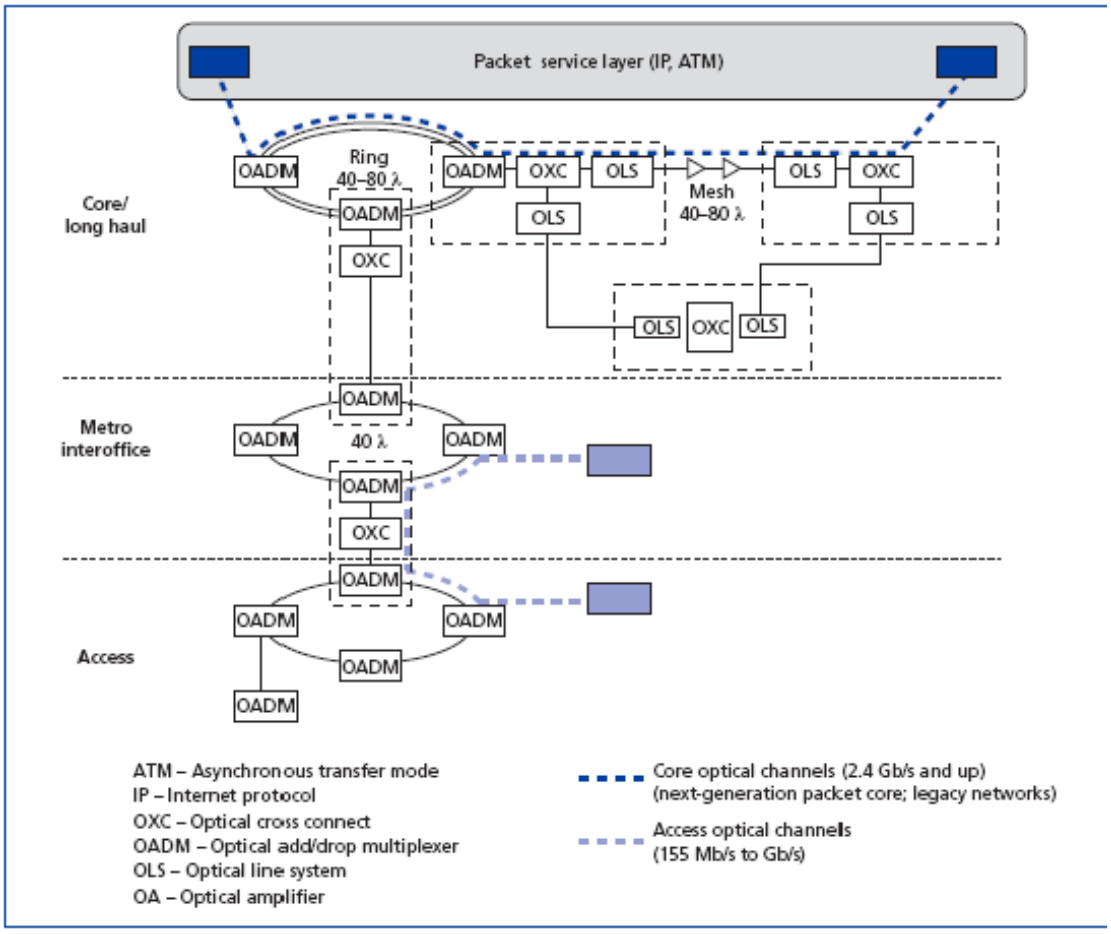

Figure 1.4 WDM based optical transport networks [22]. Copyright © 1999, Lucent Technologies Inc. Reproduced with permission from John Wiley & Sons.

conversions.

In the past few years, researchers and engineers switched their attention to the 'old' technique – coherent communication – which was used mostly in free-space applications. Advanced modulation formats, coherent detection, and digital signal processing (DSP) are the key words in this technology revolution, which are expected to increase the transmission speed significantly by increasing the spectral efficiency [23, 24]. For instance, the symbol rate can be reduced by a factor of 8 if polarization-division multiplexing (PDM) 16-ary quadrature-amplitude modulation (QAM) modulation format is exploited in digital coherent transponders. Digital coherent communication has been used in both OTDM and WDM communication systems. Most recently, up-to 10.2 Tb/s

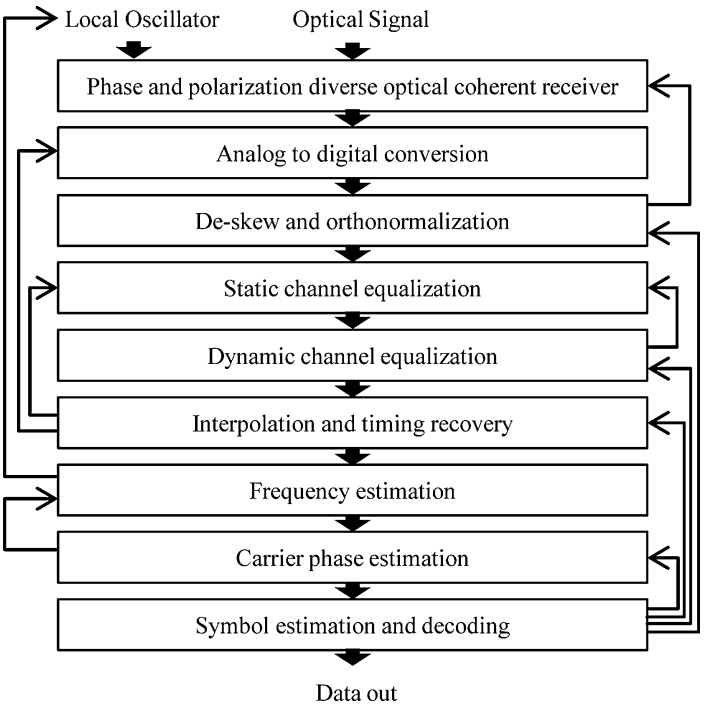

Figure 1.5 Subsystems in a digital coherent receiver [26]. Copyright © 2010, IEEE. Reproduced with permission from IEEE.

error-free serial data transmission and detection was achieved in one wavelength channel [16]. One of the key techniques is ultra-short pulse generation using a mode-locked laser and pulse compressor. Data signal with pulse duration as short as 300 fs was generated and multiplexed to 1.28 TBd with 128-fold OTDM. Dual-polarization 16QAM was exploited to achieve record high 10.2 Tb/s data rate. The signals were detected by an ultrafast digital coherent receiver based on a pulsed local oscillator. Moreover, a record-high 102.3 Tb/s transmission was achieved over 240 km of pure-silica-core fiber by employing 548 Gb/s PDM-64QAM single-carrier frequency-division-multiplexing (SC-FDM) signals with pilot tone [25]. 224 channels are wavelength multiplexed and amplified by ultra-wideband Raman amplification in the C- and L-bands. A spectral efficiency of 9.1 b/s/Hz was achieved in this demonstration.

Although digital coherent communication based OTDM/WDM systems have achieved transmission capacity several orders greater compare to their incoherent counterparts, sophisticated PDM-QAM modulators in the transmitter side, complicated coherent detectors and application-specific integrated circuits (ASICs) design in order to

handle massive required DSP functions in the receiver side (see Figure 1.5 [26]) make the coherent transponders rather cumbersome, expensive, and power-hungry. Moreover, it is reported that the spectral efficiencies achieved in research experiments have approached the nonlinear Shannon limit which is calculated according to the information theory, and spectral efficiency increases at a cost of reduced transmission distance because higher-order QAM signals suffer from a lower tolerance to various linear and nonlinear impairments such as amplifier noise, laser phase noise, fiber nonlinearities induced cross-talk, analog-to-digital conversion (ADC) resolution, etc. [27]. The need for increasing the transmission capacity while reducing the system cost remains a challenge. There is always a trade-off between the modulation format, the multiplexing scheme, the transmission capacity and reach, the system complexity, cost and the power consumption.

1.2 Motivation

The goal of this dissertation is not justifying the differences and the pros/cons among the above-mentioned technologies, but rather to seek for a potentially simple and cost-effective solution to address some of the common questions. For instance, lasers are one of the most important elements in all kinds of fiber optical communication systems. In OTDM systems, it is important that lasers can generate high-speed optical pulses with ultra-short pulse duration so that high-rate serial data signals can be created for transmission. In WDM systems, the cost of the transmitters can be significantly reduced if highly stable multi-wavelength sources can be implemented to replace the traditional DFB laser diode arrays. Moreover, in both systems the laser sources should be able to tune/switch the operating wavelengths to accommodate various configurations and needs. In particular, lasers that can be operated in non-conventional wavelength bands are highly desirable since new communication windows will be needed when the traditional C- and L-bands are filled with wavelength channels in the near future.

All-optical signal processing is another technique which is vital for the future ultra-high-speed optical transport networks. It is reported that historically quadrupling the serial line data has resulted in reducing the cost per bit by 40%, mostly due to the reduction in terminal equipment and related power consumption [28]. Electronic signal processing is likely to be limited to about 120 Gb/s as stated by the high-speed

electronics community itself [29]. Therefore, all-optical signal processing could be a cost-effective solution to the future ultra-high-rate serial data signals leveraged by the inherent ultra-fast response of many nonlinear optical phenomena. Among the various types of signal processing functions, optical clock recovery is of particular importance in all types of communication systems since it is essential for the decision circuits in the receivers and the optical regenerators.

In this dissertation, a type of laser – fiber optical parametric oscillators (FOPOs) will be analyzed and demonstrated as a simple and cost-effective solution to the many of the questions we discussed above. In particular, it will be shown that FOPOs can be configured to emit multiple wavelengths simultaneously with a large count of the wavelength (i.e., 129) and narrow wavelength spacing (i.e., 25 GHz); it can be mode-locked to generate optical pulses with high repetition rate (i.e., from 10 GHz up to 240 GHz) and short pulse duration (i.e., < 2 ps); and it can also be used to recover clock information from data streams with data rate up to 40 Gb/s. There are other features of FOPOs that are undiscovered by this dissertation. For example, FOPOs can potentially generate signals at arbitrary wavelength which only depends on the availability of the fiber and the pump source. Therefore, all the features presented in this dissertation might be able to apply to pulse generation and signal processing in the unconventional communication bands, which will make this type of laser a promising candidate as the versatile platform for the future optical communication systems.

1.3 Contributions

1.3.1 Significance of the work

FOPOs have become an interesting research topic in the recent years due to its unique features compared with other types of fiber lasers. Most of the features can be attributed to the properties of their amplification mechanism called optical parametric amplification. The physical origin of the amplification mechanism and a detailed introduction of the FOPOs will be given in section 2.3. Much research work has been done in a number of different aspects of FOPOs while this thesis is only focused on a few points: the multi-wavelength continuous-wave (CW) operation, high repetition-rate mode-locked

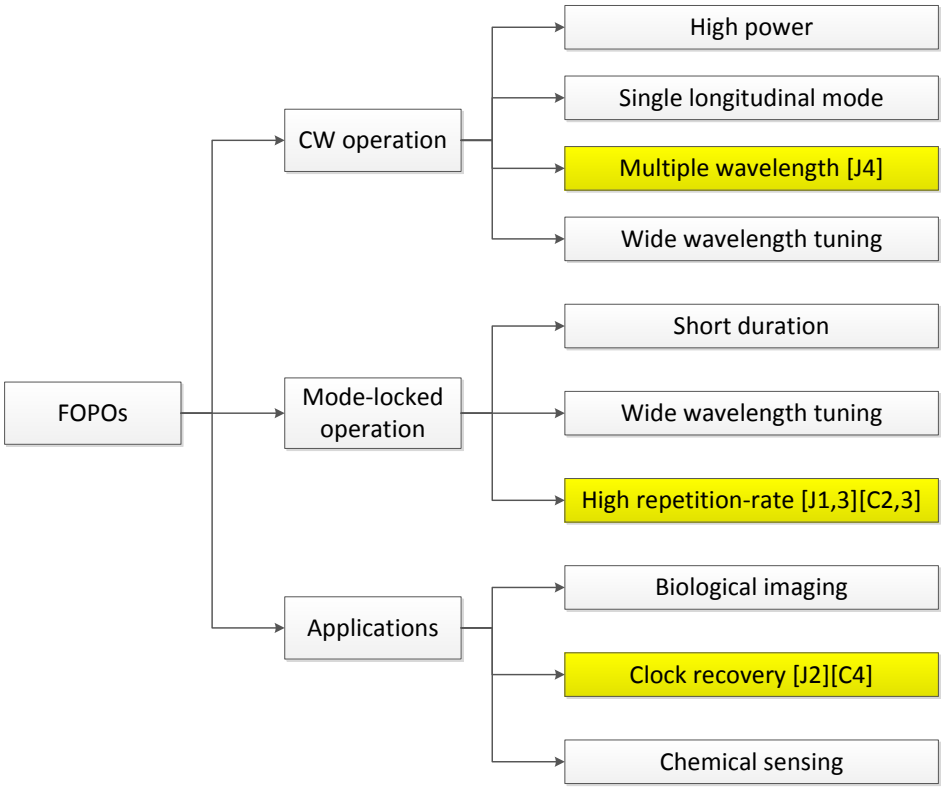

Figure 1.6 Example of various research work in FOPOs. Contributed research directions are highlighted with referenced journal and conference publications.

operation and its application to all-optical clock recovery. Figure 1.6 shows an example of various research work performed in FOPOs. The contributions from this thesis are highlighted and summarized briefly in the following paragraphs.

Multi-wavelength CW FOPOs: the first demonstration of a multi-wavelength FOPO covering the entire C-band, with the narrowest wavelength spacing, the largest number of lasing wavelengths, and the flattest spectrum. The spectral shape can be tunable and reconfigurable over the entire lasing spectrum. The laser configuration is simple and robust.

High repetition-rate mode-locked FOPOs: the first detailed analysis of an actively harmonically and rational harmonically mode-locked FOPO. The results provide a useful guideline for building a high performance FOPO with the desired requirements. Experimental results demonstrate that the proposed FOPO configuration can be used to produce optical pulses with various repetition rates from 10 GHz up to 240 GHz. This is the highest repetition rate that has ever been reported.

All-optical clock recovery using FOPOs: the first detailed analysis of all-optical clock recovery using a FOPO. The results provide a better understanding of the proposed approach in terms of its working range, and can be used as a reference for similar designs and applications in the future. 10 Gb/s to 40 Gb/s clock recovery are demonstrated in the experiments.

The results that are obtained in this thesis are based on detailed experimental characterizations. The experiments are limited to the availability of components and their specific properties, e.g., the HNLF. As such, the conclusions that are derived are specific to the properties of the components; nevertheless, they are useful for understanding general trends and provide some guidance for the design or optimization of the FOPO for the various applications.

1.3.2 List of published journal and conference papers

The following is a list of journal and conference papers summarizing research conducted during the Ph.D. program and my specific contributions in each case. Those that are related directly to the thesis topic are highlighted in section 1.3.1.

J1. **J. Li**, T. Huang, and L. R. Chen, "A comprehensive study of actively mode-locked fiber optical parametric oscillator for high-speed pulse generation," *IEEE/OSA Journal of Lightwave Technology*, vol. 31, no. 7, pp. 1120-1131, 2013.

I am the primary investigator of this work; I conceived the original idea and performed most of the experimental work, data analysis, and manuscript writing.

J2. **J**. **Li**, T. Huang, and L. R. Chen, "Detailed analysis of all-optical clock recovery at 10 Gb/s based on a fiber optical parametric oscillator," *IEEE Journal of Selected Topics in Quantum Electronics, Issue on Nonlinear Optical Signal Processing*, vol. 18. no. 2, pp. 701 - 708, 2012.

I am the primary investigator of this work; I conceived the original idea and performed most of the experimental work, data analysis, and manuscript writing.

J3. **J**. **Li**, T. Huang, and L. R. Chen, "Rational harmonic mode-locking of a fiber optical parametric oscillator at 30 GHz," *IEEE Photonics Journal*, vol. 3, no. 3, pp. 468- 475, 2011.

I am the primary investigator of this work; I conceived the original idea and performed most of the experimental work, data analysis, and manuscript writing.

J4. **J. Li** and L. R. Chen, "Tunable and reconfigurable multiwavelength fiber optical parametric oscillator with 25 GHz spacing," *Optics Letters*, vol. 35, no. 11, pp. 1872-1874, 2010.

I am the primary investigator of this work; I conceived the original idea and performed most of the experimental work, data analysis, and manuscript writing.

J5. L. R. Chen, **J. Li**, M. Spasojevic, and R. Adams, "Nanowires and sidewall Bragg gratings in silicon as enabling technology for microwave photonics," *Optics Express*, vol. 21, no. 17, pp. 19624-19633, 2013.

I contributed to the silicon waveguide design, performed the trial experiment of four-wave mixing on the silicon chip, and collaborated with the other researchers in characterizing the microwave photonic filter.

J6. T. Huang, S. Fu, **J. Li**, L. R. Chen, M. Tang, P. Shum, and D. Liu, "Reconfigurable UWB pulse generator based on pulse shaping in a nonlinear optical loop mirror and differential detection," *Optics Express*, vol. 21, no. 5, pp. 6401-6408, 2013.

I was involved in the discussion of the original ideas and provided feedback on the manuscript.

J7. T. Huang, J. Sun, **J. Li**, and L. R. Chen, "Comparison of nonlinear fiber-based approaches for all-optical clock recovery at 40 Gb/s," *Optics Communications*, vol. 298-299, pp. 213-221, 2013.

I was involved in the discussion of the original ideas, assisted in the experiments, and provided feedback on the manuscript.

J8. T. Huang, J. Sun, **J. Li**, and L. R. Chen, "40-Gb/s all-optical clock recovery based on mode-locked semiconductor fiber laser using nonlinear polarization rotation," *IEEE Photonics Technology Letters*, vol. 24, no. 8, pp. 682 – 684, 2012.

I was involved in the discussion of the original ideas, assisted in the experiments, and provided feedback on the manuscript.

J9. T. Huang, **J. Li**, J. Sun, and L. R. Chen, "Photonic generation of UWB pulses using a nonlinear optical loop mirror and its distribution over a fiber link," *IEEE Photonics Technology Letters*, vol. 23, no. 17, pp. 1255 -1257, 2011.

I was involved in the discussion of the original ideas, assisted in the experiments, and provided feedback on the manuscript.

J10. T. Huang, **J. Li**, J. Sun, and L. R. Chen, "All-optical UWB signal generation and multicasting using a nonlinear optical loop mirror," *Optics Express*, vol. 19, no. 17, pp. 15885 – 15890, 2011.

I was involved in the discussion of the original ideas, assisted in the experiments, and provided feedback on the manuscript.

C1. **J. Li**, R. Adams, Z. Sarac, D. Berardo, and L. R. Chen, "A reconfigurable microwave photonic filter based on four wave mixing in a silicon nanophotonic waveguide," *Photonics North*, 3-5 June 2013, Ottawa ON.

I contributed to the silicon waveguide design, performed the trial experiment of four-wave mixing on the silicon chip, and collaborated with the other researchers in characterizing the microwave photonic filter.

C2. **J. Li**, T. Huang, and L. R. Chen, "Analysis of fiber optical parametric oscillator for high-repetition-rate pulse generation," *IEEE Photonics Conference (IPC'12)*, 23-27 Sep. 2012, Burlingame, CA.

I am the primary investigator of this work; I conceived the original idea and performed most of the experimental work, data analysis, and manuscript writing.

C3. **J. Li**, T. Huang, and L. R. Chen, "40 - 200 GHz pulse train generation in a mode-locked fiber optical parametric oscillator," *IEEE Photonics Conference (IPC'11)*, paper ThAA 2, 9-13 Oct. 2011, Arlington, VA.

I am the primary investigator of this work; I conceived the original idea and performed most of the experimental work, data analysis, and manuscript writing.

C4. **J. Li**, T. Huang, and L. R. Chen, "Wavelength tunable all-optical clock recovery at 40 Gb/s based on a fiber optical parametric oscillator," *IEEE Photonics Conference (IPC'11)*, paper TuF 1, 9-13 Oct. 2011, Arlington, VA.

I am the primary investigator of this work; I conceived the original idea and performed most of the experimental work, data analysis, and manuscript writing.

C5. R. Adams, **J. Li**, Z. Sarac, D. Berardo, and L. R. Chen, "Comparing nonlinear fiber and a silicon nanophotonic waveguide for implementing a microwave photonic filter," *IEEE Photonics Conference (IPC'13)*, 8-12 September 2013, Bellevue, WA.

I contributed to the silicon waveguide design, performed the trial experiment of four-wave mixing on the silicon chip, and collaborated with the other researchers in characterizing the microwave photonic filter on the silicon chip.

C6. T. Huang, J. Sun, **J**. **Li**, and L. R. Chen, "40 Gb/s all-optical clock recovery using a semiconductor fiber laser and nonlinear optical loop mirror," *IEEE Photonics Conference (IPC'12)*, 23 – 27 Sep. 2012, Burlingame, CA.

I was involved in the discussion of the original ideas, assisted in the experiments, and provided feedback on the manuscript.

C7. T. Huang, **J**. **Li**, J. Sun, and L. R. Chen, "Photonic UWB signal generation and multicasting using a nonlinear optical loop mirror," *IEEE Photonics Conference (IPC'11)*, 9-13 Oct. 2011, Arlington, VA.

I was involved in the discussion of the original ideas, assisted in the experiments, and provided feedback on the manuscript.

C8. T. Huang, **J**. **Li**, and L. R. Chen, "40 GHz and 80 GHz mode-locked semiconductor fiber laser using nonlinear polarization rotation in a highly nonlinear fiber," *IEEE Photonics Conference (IPC'11)*, 9 – 13 Oct. 2011, Arlington, VA.

I was involved in the discussion of the original ideas, assisted in the experiments, and provided feedback on the manuscript.

1.4 Outline of the dissertation

In this chapter, some background knowledge of the fiber optical communication system such as OTDM, WDM, and coherent communication technologies are introduced. The motivation and the significance of the research work described in this dissertation are also discussed. The remainder of this thesis is organized as follows.

In chapter 2, various nonlinear phenomena that occur in silica fiber are reviewed such as the stimulated Brillouin scattering (SBS), stimulated Raman scattering (SRS), self-phase modulation (SPM), cross-phase modulation (XPM), and four-wave mixing (FWM). The theory of fiber optical parametric amplifier (FOPA) and its gain characteristics such as gain, bandwidth, and one-pump and dual-pump configuration are discussed later, together with a detailed performance review of the device. FOPO, which

is based on FOPA, is introduced in the following sections and its performance is also reviewed at end of the chapter.

Chapter 3 discusses how to generate multiple wavelengths simultaneously in a single-pump FOPO configuration. A detailed literature review of the multi-wavelength fiber lasers based on EDFA and semiconductor optical amplifier (SOA) is performed at the beginning of the chapter, followed by a description of the FOPO based multi-wavelength source and its operating principle. The experimental results are demonstrated and discussed in detail, which reveals the unique features of a FOPO based multi-wavelength source such as wide operating wavelengths range, narrow wavelength spacing, tunable and reconfigurable. Chapter 3, in part, is a reprint of the material as it appears in *Optics Letters* in the article authored by Jia Li and Lawrence. R. Chen, "Tunable and reconfigurable multiwavelength fiber optical parametric oscillator with 25 GHz spacing," vol. 35, no. 11, pp. 1872-1874, 2010. I am the primary investigator and author of this article.

Chapter 4 discusses actively mode-locked FOPO operating at 10 GHz. It starts with a review of actively mode-locked fiber ring lasers in terms of different gain media, mode-locking mechanisms, and wavelength selection methods. Then the unique characteristic of parametric amplifier based fiber laser is demonstrated and discussed in the following experiment which analyzes the performance of the proposed FOPO configuration in terms of many factors such as the pump pulse duty cycle, pump power, pulse chirp compensation, filter bandwidth, etc. The results are discussed and conclusions are presented at the end of this chapter. Chapter 4, in part, is a reprint of the material as it appears in *IEEE/OSA Journal of Lightwave Technology* in the article authored by Jia Li, Tianye Huang, and Lawrence R. Chen, "A comprehensive study of actively mode-locked fiber optical parametric oscillator for high-speed pulse generation," vol. 31, no. 7, pp. 1120-1131, 2013. I am the primary investigator and author of this article.

Chapter 5 investigates the possibility of multiplying the repetition rate of an actively mode-locked FOPO. Various repetition rate multiplication methods are reviewed at the beginning, and later two methods to increase the FOPO repetition rate are demonstrated and compared. Results show that rational harmonic mode-locking is superior to the nonlinear frequency doubling method, and finally up to 240 GHz

mode-locking of a FOPO was demonstrated based on rational harmonic mode-locking. Chapter 5, in part, is a reprint of the material as it appears in *IEEE/OSA Journal of Lightwave Technology* in the article authored by Jia Li, Tianye Huang, and Lawrence R. Chen, "A comprehensive study of actively mode-locked fiber optical parametric oscillator for high-speed pulse generation," vol. 31, no. 7, pp. 1120-1131, 2013, and in *IEEE Photonics Journal* in the article authored by Jia Li, Tianye Huang, and Lawrence R. Chen, "Rational harmonic mode-locking of a fiber optical parametric oscillator at 30 GHz," vol. 3, no. 3, pp. 468- 475, 2011. I am the primary investigator and author of these articles.

In chapter 6, all-optical clock recovery using actively mode-locked FOPO is discussed. Different all-optical clock recovery approaches are reviewed in the first section followed by a description of the basic setup for FOPO based all-optical clock recovery and its operating principle. Then a detailed analysis is performed for recovering the clock from a 10 Gb/s RZ-OOK signal in terms of investigating the impact of signal quality degradations, namely duty cycle, average power, extinction ratio, OSNR, residual dispersion, and DGD, on the performance of the clock recovery circuit. In the end, 40 Gb/s clock recovery is demonstrated using almost the same configuration. Chapter 6, in part, is a reprint of the material as it appears in *IEEE Journal of Selected Topics in Quantum Electronics* in the article authored by Jia Li, Tianye Huang, and Lawrence R. Chen, "Detailed analysis of all-optical clock recovery at 10 Gb/s based on a fiber optical parametric oscillator," vol. 18. no. 2, pp. 701 - 708, 2012. I am the primary investigator and author of this article.

Chapter 7 summarizes the work and the contributions that have been done in this dissertation, while several future directions are also discussed briefly at the end of the chapter.

Chapter 2 Nonlinear Effects in Optical Fiber

With unprecedented low loss feature compared with other media, optical fiber has been used as a linear medium for signal transmission for a long time. This 'linear' property is valid as long as the intensity of the light keeps relatively low inside the fiber core, while it can be disrupted when the intensity rises high. It is known that bound electrons of any dielectric are displaced from their equilibrium position forming electric dipoles under the influence of an applied electric field **E**. As a result, polarization field **P** induced by electric dipoles changes the electric flux **D** and the corresponding wave equations which govern the transmission properties of the electric field. The dependence of polarization **P** on electric field **E** can be expressed in a general relation [30]:

$$\boldsymbol{P} = \varepsilon_0\left(\chi^{(1)} \cdot \boldsymbol{E} + \chi^{(2)} : \boldsymbol{EE} + \chi^{(3)} \vdots \boldsymbol{EEE} + \cdots\right) \tag{2.1}$$

where ε_0 is the vacuum permittivity and $\chi^{(j)}$ (j = 1, 2, …) is jth order susceptibility. In general, $\chi^{(j)}$ is a tensor of rank j+1.

When incident electric field is small compared with the electric field generated by the nuclei, the response of the polarization field is largely linear with respect to the incident electric field. The linear relation between the polarization field and the stimulated electric field is related to the linear susceptibility $\chi^{(1)}$. $\chi^{(1)}$ is frequency dependent that affects the material properties such as the refractive index n and the attenuation coefficient α. The frequency dependent property of the refractive index gives rise to chromatic dispersion which plays an important role in the propagation of short optical pulses either in the linear or the nonlinear regime. To account for fiber dispersion, the mode propagation constant β is expanded in a Taylor series with respect to a reference frequency ω_0 at which the pulse spectrum is centered:

$$\beta(\omega) = n(\omega)\frac{\omega}{c} = \beta_0 + \beta_1(\omega - \omega_0) + \frac{1}{2}\beta_2(\omega - \omega_0)^2 + \cdots \tag{2.2}$$

where

$$\beta_m = \left(\frac{d^m\beta}{d\omega^m}\right)_{\omega=\omega_0} \tag{2.3}$$

Following the above convention, we can see that $\beta_1 = \frac{d\beta}{d\omega} = \frac{1}{c}\left(n + \omega\frac{dn}{d\omega}\right) = \frac{1}{v_g}$ represents the inverse of the group velocity of an optical pulse, and $\beta_2 = \frac{d^2\beta}{d\omega^2} = \frac{d\beta_1}{d\omega}$

represents dispersion of the group velocity which is denoted as the group-velocity dispersion (GVD) parameter. Alternatively, the GVD is commonly expressed in the wavelength domain in terms of dispersion parameter D. It is related to β_2 by the relation:

$$D = -\frac{2\pi c}{\lambda^2}\beta_2 \tag{2.4}$$

When the incident field is large compared with the electric field induced by nuclei, the response of the polarization field becomes nonlinear with respect to the incident field, which is characterized by higher-order susceptibility $\chi^{(2)}$, $\chi^{(3)}$, …etc. It is worth to note that optical fibers do not normally exhibit second-order nonlinear effects due to the fact that SiO_2 is a symmetric molecule and $\chi^{(2)}$ vanishes for silica glass. As a result, third-order nonlinear effects are the lowest-order nonlinear effects in optical fibers which originates from $\chi^{(3)}$ and are responsible for many nonlinear phenomena such as third-harmonic generation (THG), SPM, XPM, and FWM. Despite the fact that $\chi^{(3)}$ is small compared with other nonlinear media, the nonlinear effects are readily observable in optical fibers at relatively low power levels taking the advantages of the small core size and the low loss of optical fiber. However, the values of higher-order nonlinear susceptibility $\chi^{(j)}$ $(j > 3)$ are so small that their corresponding nonlinear effects are normally negligible.

A major feature of the nonlinear effects introduced above is that no energy is exchanged between the electromagnetic field and the dielectric medium, which is referred to as elastic process. Elastic processes are governed by the third-order nonlinear susceptibility $\chi^{(3)}$. Alternatively, there is a second class of nonlinear effects in which the optical fields transfer part of its energy to the dielectric medium, which are referred to as stimulated inelastic scattering. Stimulated inelastic scattering originates from the coupling between the incident electric field and the vibration in the lattice or nuclei. In optical fiber, two important nonlinear effects fall in this category which is known as SRS and SBS. From a quantum-mechanical point of view, for both SRS and SBS a photon of the incident field is annihilated to create a photon at a lower frequency and a phonon with the right energy and momentum so that the energy and momentum are conserved. A higher-energy photon can also be created as long as a phonon of right energy and momentum is available. The difference between the two effects is that optical phonons participate in SRS while acoustic phonons participate in SBS.

The mechanisms of the above mentioned nonlinear effects will be introduced in the following sections. They are among the most important nonlinear effects occurred in optical fiber and will be used to explain the principle and experimental results in this thesis. In particular, optical parametric amplification, a special nonlinear process which provides optical gain to signals, will be discussed in detail. It forms the foundation for the work that has been done in this thesis.

2.1 Stimulated inelastic scattering

2.1.1 Stimulated Brillouin scattering (SBS)

SBS is an inelastic nonlinear process that involves the coupling between the pump wave and the scattered Stokes wave through an acoustic wave. It originates from a phenomenon called electrostriction where the pump wave generates an acoustic wave in the dielectric medium. Then the pump wave is scattered by a moving index-grating in the same propagating direction as the pump wave which is induced by the refractive index change of the medium through the generation of acoustic wave. The frequency of the scattered light is downshifted compared with that of the pump wave because of the Doppler shift related to the moving grating.

From quantum-mechanical point of view, the SBS process involves the annihilation of a pump photon and the generation of a frequency downshifted Stokes photon and an acoustic phonon. The energy and the momentum of the interacting pump photons, Stokes photons and acoustic phonons must be conserved during each scattering for maximum efficiency. It is found that the Brillouin frequency shift depends on the scattering angle between the pump and Stokes waves. In the case of single-mode fiber, SBS occurs only in the backward direction with the maximum frequency shift (when the scattering angle is π) which is ~10 GHz at 1.55 μm. The spectral width of the Brillouin gain spectrum depends on the damping time of acoustic waves, Brillouin shift, and waveguide properties which is normally in the order of 10 MHz. Figure 2.1 shows a sample Brillouin gain spectrum obtained in 700 m of SMF, in which the experimental data (crosses) fit the hyperbolic cosine of a Lorenzian function; the frequency shift was 12.8 GHz and the gain bandwidth was 35.8 MHz [31].

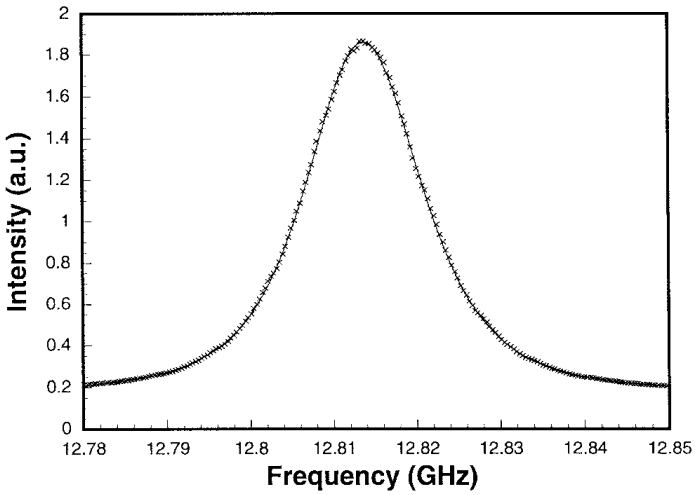

Figure 2.1 Brillouin gain spectrum of a 700-m single-mode fiber [31]. Copyright © 1997, IEEE. Reproduced with permission from IEEE.

SBS is generally harmful for fiber optical communications as it limits the channel power, and the back-propagating Stokes waves could degrade the line performance. It also impedes nonlinear processes which normally require high optical power levels. Thus it is important to estimate the SBS threshold. The SBS threshold P_{SBSth} is defined as the input pump power at which the backscattered Stokes wave power equals the transmitted power and is approximated by the following equation:

$$P_{SBSth} \approx \frac{21A_{eff}}{g_B L_{eff}} \tag{2.5}$$

where g_B is the peak value of the Brillouin gain which can be obtained at maximum frequency shift, L_{eff} is the effective interaction length which is defined as $L_{eff} = [1 - \exp(-\alpha L)]/\alpha$, and A_{eff} is the effective core area. If we use a narrow-linewidth laser as the pump and transmit it in a spool of 1 km fiber with high germanium concentration ($g_B = 2\times10^{-11}$ m/W) and effective core area of 10 μm^2, the corresponding SBS threshold will be 10 mW. Such low SBS threshold will impede various nonlinear phenomena from occurring in the similar type of fiber. Researchers have proposed and demonstrated many approaches to increase the SBS threshold such as changing the fiber core radius, applying a varying strain distribution along the fiber, adding an acoustic guiding layer to the fiber, and varying refractive index of the fiber along the span. One that is commonly used in the parametric amplification experiment is to broaden the CW pump linewidth through phase

dithering because Brillouin gain g_B can be significantly reduced if the spectral width of the pump is larger than the Brillouin gain bandwidth. Alternatively, one can increase the Brillouin threshold by using a pulsed-pump whose full-width half-maximum (FWHM) pulse duration is smaller than the phonon lifetime.

2.1.2 Stimulated Raman scattering (SRS)

SRS and SBS shares similar origins in which an intense pump wave is scattered when propagating in a dielectric medium. A fraction of its energy is transferred to another field whose frequency is downshifted while causing vibration of the molecules in the medium. From a quantum-mechanical point of view, one photon is annihilated through scattering with a molecule and another photon with lower frequency is generated while the molecule makes a transition to a higher-energy vibrational state. Different from SBS, an optical phonon is generated in the SRS as opposed to an acoustic phonon in the SBS case, which leads to different properties for the two phenomena.

SRS has much lower efficiency than SBS due to a much smaller Raman gain coefficient g_R which is related to the cross section of spontaneous Raman scattering and reaches its maximum value for the frequency component that is downshifted from the pump frequency by about 13.2 THz for pure silica. Figure 2.2 shows a sample Raman gain spectrum for both parallel and cross polarizations [32]. The broad Raman gain spectrum (up to 40 THz) sets it apart from SBS and makes it a good candidate as broadband optical amplifiers for WDM optical communication systems. Another advantage of SRS compared to SBS is that SRS occurs in both forward and backward directions with respect to that of the pump wave because of the isotropic nature of Raman process.

Raman threshold P_{SRSth} is defined as the input pump power at which the Stokes power becomes equal to the transmitted pump power at the fiber output which can be approximated by the following equation:

$$P_{SRSth} \approx \frac{16A_{eff}}{g_R L_{eff}} \tag{2.6}$$

It is worth to note that the above threshold condition is still valid for the backward SRS but the numerical factor 16 is replaced by 20 [30]. A simple calculation of the SRS

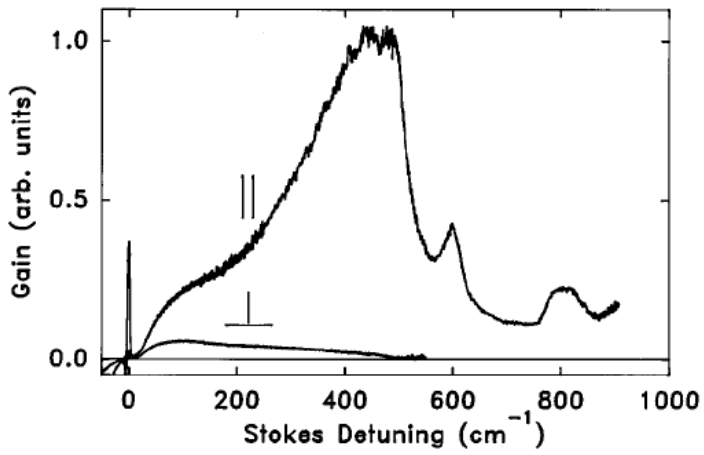

Figure 2.2 Parallel- and cross-polarized Raman gain spectra [32]. Copyright ©1995, OSA. Reproduced with permission from OSA.

threshold on a 1 km fiber with $A_{eff} = 10$ μm^2, $g_R = 1\times10^{-13}$ m/W (the same type of fiber as we used in section 2.1.1) shows that more than 1.6 W input pump power is required to reach the SRS threshold. Compared with 10 mW threshold power for SBS, SRS has a much higher threshold and thus SBS dominates and inhibits SRS in the case of CW pumping. As we discussed above, pump pulses with short duration (< 1 ns) can be used in order to suppress SBS.

2.2 Optical Kerr effect

2.2.1 Self-phase modulation (SPM) and cross-phase modulation (XPM)

Optical fiber plays an active role in the stimulated scattering processes in the sense that energy transition occurs between the fiber and the lightwaves via molecular vibrations or density variations of silica. However, optical fiber can play a passive role in a separate class of nonlinear phenomena which are referred as optical parametric process or optical Kerr effect, which include SPM, XPM, FWM, etc. In optical parametric processes, no energy transfer occurs between optical fiber and lightwaves; instead, optical fiber mediates the interaction among several optical waves through modulation of refractive index of the fiber. Phase-matching condition must be satisfied before some parametric process can be built up along the fiber.

SPM is a phenomenon where the spectrum of an intense optical pulse broadens through transmission along a length of optical fiber which is due to the intensity dependent refractive index change in the fiber. The refractive index $\tilde{n}$ of the fiber can be defined by the dielectric constant as the following:

$$\tilde{n} = n + n_2|E|^2 \tag{2.7}$$

$$n_2 = \frac{3}{8n} Re(\chi^{(3)}) \tag{2.8}$$

where the linear index n is related to the real part of $\chi^{(1)}$and n_2 is the nonlinear refractive index. SPM induced phase shift is proportional to fiber length and instantaneous optical power. As a result, phase shift varies with time which causes instantaneous optical frequency drifts over the entire pulse duration referred to as frequency chirping. Frequency chirp increases in magnitude with propagation distance, which broadens the pulse spectrum continuously. Depending on how the input pulse is chirped, SPM-induced chirp can cause spectral broadening or narrowing. For an unchirped input pulse, SPM always induces spectral broadening.

The interplay between the SPM and GVD gives rise to new features. Especially, when optical pulse propagates in the anomalous dispersion regime of the fiber, GVD and SPM cooperate with each other in a way such that the positive chirp induced by SPM and the negative chirp induced by GVD nearly cancel each other to maintain a chirp-free pulse. However, when pulse propagates in the normal dispersion, optical wave breaking occurs which results in pulse broadening like a rectangular shape with sharp leading and trailing edges with rapid oscillation near the pulse edges. The temporal oscillation is due to the nonlinear nature of the SPM induced chirp near the pulse edges and the corresponding interference between two different frequency components. Spectral side lobes always come with the temporal oscillation which is a result of nonlinear FWM between two different frequencies.

XPM occurs in the case where two pulses at different wavelengths propagate along the same fiber. XPM has the same origin as self-phase modulation, although phase variation of optical pulses applies to both wavelengths due to intensity dependent refractive index change. Spectral broadening occurs as a result of time variant phase of the pulses. However, asymmetric spectral broadening may occur if there is a group velocity mismatch between the two wavelengths and/or there is an initial relative time

delay between the two wavelengths. When GVD is not negligible, the combination of XPM and GVD will result in oscillation over the pulse tails due to the interference between different frequency components, which is similar to the case of optical wave breaking when both SPM and GVD are presented.

2.2.2 Four-wave mixing

The origin of FWM lies in the nonlinear response of bound electrons of a material to an electromagnetic field whose magnitude is governed by the nonlinear susceptibility. In quantum mechanical point of view, FWM occurs when two photons from one or two waves are annihilated and new photons are created at different frequencies. Efficient FWM occurs only when phase-matching condition is nearly achieved which requires the matching of the interacting frequencies as well as the wave vectors. Therefore, a specific choice of wavelengths and fiber parameters is required to achieve high efficient FWM. The most commonly observed case is when the two photons at frequencies ω_1 and ω_2 are annihilated while two photons at frequencies ω_3 and ω_4 are generated simultaneously in the way that the following relation is satisfied:

$$\omega_3 + \omega_4 = \omega_1 + \omega_2 \tag{2.9}$$

The phase-matching requirement for this process is:

$$\Delta k = \beta_3 + \beta_4 - \beta_1 - \beta_2 = 0 \tag{2.10}$$

A special case is the degenerate FWM in which the two pump frequencies cannot be distinguished (i.e., $\omega_1 = \omega_2$). In this case the low-frequency sideband and the high-frequency sideband, referred to as the Stokes and anti-Stokes bands correspondingly, can be generated from noise when phase-matching requirement is nearly satisfied. On the other hand, if a weak signal at ω_3 is launched into the fiber with a strong pump wave, the signal is amplified by the pump while a new frequency at ω_4 is generated simultaneously which is referred to as the idler wave.

Assuming the intensity of the pump waves are much higher than that of the other waves and are considered as un-depleted, the pump waves only acquire a phase shift due to the SPM and XPM. The signal and idler waves would experience parametric gain which is dependent on the effective phase mismatch expressed as:

$$\kappa = \Delta k + \gamma(P_1 + P_2) \tag{2.11}$$

where γ is the nonlinear coefficient of the fiber and is defined as

$$\gamma = \frac{n_2 \omega}{c A_{eff}} \tag{2.12}$$

The parametric gain g is defined as:

$$g = \sqrt{(\gamma P_0 r)^2 - (\kappa/2)^2} \tag{2.13}$$

where

$$r = 2(P_1 P_2)^{1/2}/P_0 \tag{2.14}$$

$$P_0 = P_1 + P_2 \tag{2.15}$$

The maximum parametric gain is obtained when $\kappa = 0$, or $\Delta k = -\gamma(P_1 + P_2)$. The shift of the gain peak from $\Delta k = 0$ in (2.10) is due to the contribution of XPM from the pump waves to the phase mismatch term.

As can be seen, phase mismatch term κ comprises a linear term and a nonlinear term. The linear term originates mainly from the material dispersion and can be expressed in terms of the frequency shift of the signal frequency away from the pump frequency denoted as Ω_s:

$$\Delta k = \beta_2 \Omega_s^2 + (\beta_4/12)\Omega_s^4 \tag{2.16}$$

where β_2 and β_4 are the second-order and fourth-order dispersion parameters at the pump frequency ω_1. β_4 is generally much smaller than β_2, and can be neglected if the pump wavelength is not very close to the fiber zero-dispersion wavelength λ_0. It can be seen from the above equations that phase-matching can be realized if the pump wavelength exceeds λ_0 and Δk becomes negative.

2.3 Fiber optical parametric amplifiers and oscillators

2.3.1 FOPA gain

The dual-pump FWM process is governed by the four coupled nonlinear Schrodinger equations (NLSE) as shown below:

$$\frac{\partial A_1}{\partial z} = i\gamma A_1[|A_1|^2 + 2(|A_2|^2 + |A_3|^2 + |A_4|^2)] + 2i\gamma A_2^* A_3 A_4 e^{i\Delta kz} \tag{2.17}$$

$$\frac{\partial A_2}{\partial z} = i\gamma A_2[|A_2|^2 + 2(|A_1|^2 + |A_3|^2 + |A_4|^2)] + 2i\gamma A_1^* A_3 A_4 e^{i\Delta kz} \tag{2.18}$$

$$\frac{\partial A_3}{\partial z} = i\gamma A_3[|A_3|^2 + 2(|A_1|^2 + |A_2|^2 + |A_4|^2)] + 2i\gamma A_4^* A_1 A_2 e^{i\Delta kz} \tag{2.19}$$

$$\frac{\partial A_4}{\partial z} = i\gamma A_4[|A_4|^2 + 2(|A_1|^2 + |A_2|^2 + |A_3|^2)] + 2i\gamma A_3^* A_1 A_2 e^{i\Delta kz} \quad (2.20)$$

where A_j (j=1,2,3,4) is the slowly varying envelopes of the four waves along the propagation direction z, and γ is the nonlinear coefficient of the fiber. In this set of equations, A_1 and A_2 correspond to the complex amplitude of the pump waves, A_3 and A_4 correspond to the complex amplitude of the signal and the idler waves. Δk is the linear phase mismatch as defined in (2.10).

Under the assumption that the pumps are undepleted and only the signal is present with the pumps at the fiber input, analytic solution of the set of NLSEs can be derived, and the parametric amplifier gain for the signal G_s and the idler G_i can be written as:

$$G_s = 1 + (\gamma P_0 r/g)^2 \sinh^2(gL) \quad (2.21)$$

$$G_i = G_s - 1 \quad (2.22)$$

From the solution it can be found that the idler wave can acquire nearly the same gain/power as the signal at the output of the fiber. The parametric gain g depends on the phase mismatch $\kappa = \Delta k + \gamma(P_1 + P_2)$. Δk is the linear phase mismatch which is related to many factors such as the pump frequencies, signal frequency, and the dispersion property of the optical fiber. $\gamma(P_1 + P_2)$ is the nonlinear phase mismatch which is proportional to the fiber nonlinearity and the pump powers. Therefore, the gain and the gain bandwidth of the FOPA can be controlled by choosing the pump frequency, power, and by tailoring the fiber dispersion. Under the perfect phase-matching condition and $gL \gg 1$, the amplifier gain G_s increases exponentially with P_0 as:

$$G_s \approx \frac{1}{4}\exp(2\gamma P_0 rL) \quad (2.23)$$

The amplifier bandwidth is defined as the frequency range over which the amplifier gain exceeds 50% of the peak gain value, which is dependent on many factors such as the pump peak power P_0, fiber length L, and the pumping configuration (i.e., one-pump or dual-pump configuration). The gain peak occurs at signal frequency at which κ = 0 (i.e., the phase-matching condition is perfectly satisfied). In the case of single pump, $\kappa = \Delta k + 2\gamma P_0$ with $\Delta k = \beta_2 \Omega_s^2$ where $\Omega_s = |\omega_1 - \omega_3|$ is the frequency detuning of the signal with respect to the pump. Therefore, the gain peak occurs at:

$$\Omega_s = (2\gamma P_0/|\beta_2|)^{1/2} \quad (2.24)$$

In the case of long fibers, the gain bandwidth $\Delta\Omega_A$ is set by the fiber length which is calculated as:

$$\Delta\Omega_A = \frac{\pi}{L}(2\gamma P_0|\beta_2|)^{1/2} \tag{2.25}$$

In the case of short fibers, the gain bandwidth is limited by the nonlinear effect which can be approximately given by:

$$\Delta\Omega_A \approx (\frac{\gamma P_0}{2|\beta_2|})^{1/2} \tag{2.26}$$

It is obvious from the above equation that for a given pump power, the amplifier gain bandwidth can be increased by employing fibers with higher nonlinear coefficient and moving the pump wavelength closer to the fiber zero-dispersion wavelength.

It is worth to note that distinct parametric gain characteristics can be obtained if the pump wavelength is in the normal dispersion regime of the fiber and is away from the fiber zero-dispersion wavelength. This is still related to the phase mismatch term in the parametric gain expression (2.13). It has been discussed that phase-mismatch needs to be zero so that maximum parametric gain can be obtained. From (2.11) and (2.16) it can be derived that:

$$\begin{aligned}\kappa &= \Delta k + \gamma(P_1 + P_2) \\ &= \beta_2\Omega_s^2 + (\beta_4/12)\Omega_s^4 + \gamma(P_1 + P_2) \\ &= 0\end{aligned} \tag{2.27}$$

In the case that the pump wavelength is in the normal dispersion regime, β_2 becomes positive, and the nonlinear phase mismatch term is always positive, so β_4 needs to be negative to compensate the positive terms. Since β_4 is generally much smaller than β_2, large signal wavelength detuning is required to meet the phase-matching condition. By tuning the pump wavelength further from the fiber zero-dispersion wavelength, β_2 increases in magnitude and therefore shifts the phase-matched signal wavelength even further away. Narrowband parametric gain can be obtained in this case which could be several hundred nanometers away from the pump wave, which is on contrary to the broadband gain obtained when pumping at the anomalous dispersion regime. While this could be useful for wavelength conversion, tunable narrowband amplification/filtering, it is not in the scope of this dissertation since broadband gain is always required in the actively mode-locked fiber lasers and the associated optical clock recovery application.

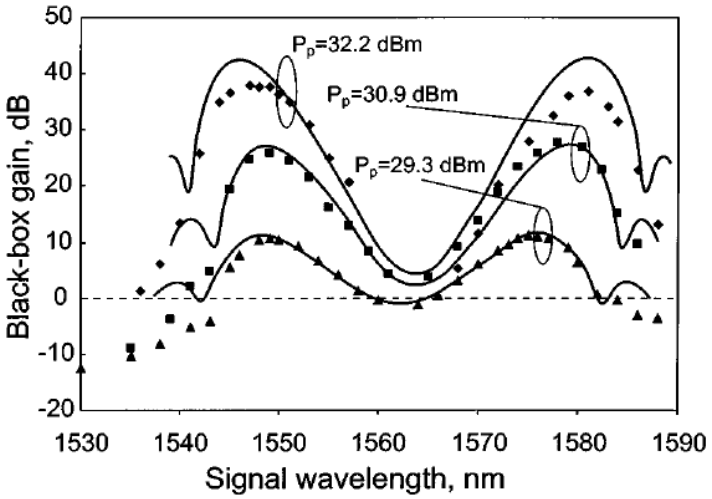

Figure 2.3 Measured and calculated net "black-box" gain for three different pump powers [33].

2.3.2 One-pump and dual-pump FOPAs

In the single-pump FOPA configuration, the pump wavelength is chosen to be close to the zero-dispersion wavelength of the fiber. As mentioned above, linear phase mismatch Δk can be expanded in a Taylor series around the pump frequency and only even-order dispersion parameters contribute to the linear phase mismatch. In general, Δk is dominated by β_2 although higher-order dispersion needs to be taken into account when the signal deviates far from the pump. In practice, the pump wavelength is chosen such that β_2 is slightly negative so that Δk is negative to balance the nonlinear phase mismatch $2\gamma P_0$. In conventional optical fibers, pump waves are placed in the anomalous GVD regime to realize phase-matching and high gain. As a result, the maximum gain is usually achieved when the signal wavelength is detuned relatively far away from the pump wavelength in order to compensate the nonlinear phase mismatch contribution. Figure 2.3 shows sample one-pump FOPA gain spectra for different pump powers [33].

From (2.23), one can see that high parametric gain can be achieved by increasing $\gamma P_0 L$. However, from (2.25) it can be seen that gain bandwidth scales inversely with L when $L \gg L_{NL}$. Therefore, in order to maximize both the peak gain and the gain bandwidth one must use a fiber as short as possible while increasing the value of γP_0.

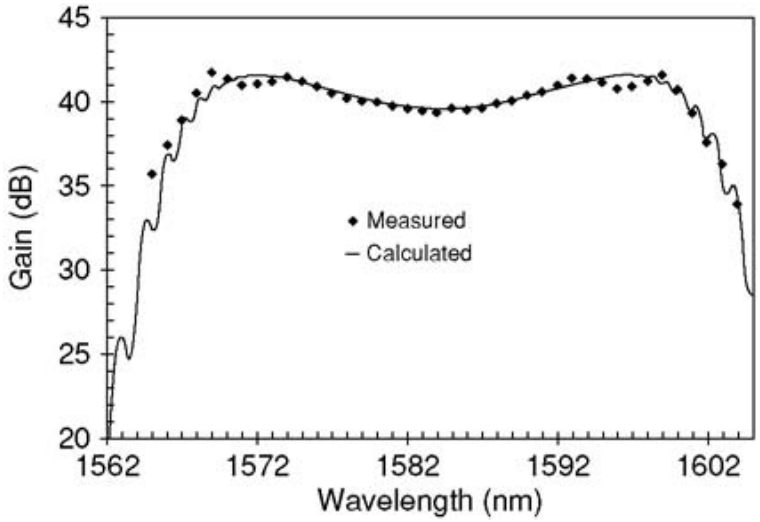

Figure 2.4 Measured and calculated gain spectra for a dual-pump FOPA [34]. Copyright © 2003, IET. Reproduced with permission from IET.

The performance of the FOPAs is affected by many factors that must be considered in the design. Noise figure is one of the most important evaluation factors for an optical amplifier. In FOPAs, the noise mainly comes from two sources: pump power fluctuation and ASE noise from EDFAs. Pump power fluctuation can be transferred to signals and idlers almost instantaneously due to the ultrafast nonlinear response of silica. ASE noise from the EDFAs (i.e., used to amplify the pump waves) can degrade the FOPA performance considerably. Moreover, phase dithering of the pump waves, which is usually required for SBS suppression, could be transferred to signals and idlers as phase noise and consequently be converted into amplitude noise by fiber dispersion.

Uniform gain spectrum is hard to be achieved using the single-pump configuration since phase-matching is difficult to be maintained over a broad wavelength range. This problem can be solved by using a dual-pump configuration. In the most commonly used configuration, the two pump wavelengths are located on the opposite sides of the zero-dispersion wavelength in a symmetric fashion, so that phase-matching can be achieved over a wide range of wavelength. By properly setting the pump wavelengths and spacing, wide and flat gain spectrum can be achieved in the dual-pump FOPA. Figure 2.4 shows sample gain spectra for a dual-pump FOPA [34].

2.3.3 Performance of FOPAs

2.3.3.1 FOPA gain

As discussed above, under the perfect phase-matching condition and $gL \gg 1$, the parametric gain is exponentially proportional to $\gamma P_0 L$. So in theory one can simply use long fibers with high nonlinear coefficient and high pump power to achieve high gain. However, the amount of pump power that can be launched into the fiber in practice is limited by the SBS, whose threshold is usually very small in long lengths of fiber. Therefore, highly efficient SBS suppression must be employed in order to achieve high parametric gain. In [35], two PMs were cascaded, one of which was driven by a 10 GHz wave while the other one was driven by the sum of four RF tones at 105, 325, 1,000, and 3,110 MHz. Peak parametric gain of 70 dB was achieved by launching 1.9 W pump power into the fiber. In [36], to further improve the SBS suppression ratio, the nonlinear fiber was cut in half and an isolator was inserted in between the two fiber segments. The isolator can prevent the light from reflecting back by SBS and thus can increase the SBS threshold power by a factor of 2. The correspondent gain in dB can be increased by almost a factor of 2 as well, which was confirmed in the experiment. 60 dB maximum gain was achieved with an isolator compared with 30 dB maximum gain without an isolator.

2.3.3.2 *FOPA gain bandwidth*

From the previous discussion it is known that broad parametric gain bandwidth can be obtained with short fiber length L, high pump power P_0, and small fiber dispersion (i.e., β_2 and β_4). In [37], a 100 nm bandwidth was achieved using a single CW-pump. The fiber used in this experiment was 100 m long and had a nonlinear coefficient of 10 $W^{-1}km^{-1}$ and $\beta_4 = 1 \times 10^{-56} s^4 m^{-1}$. The pump power used was 4 W. Generally the ability of generating high power CW pump in the C-band is limited by the EDFA used to amplify the pump wave. However, high peak power can be generated if a pulsed pump is used. In [38], the pump wave was modulated by a pulse train with 4 ns period and 1/256 duty cycle, and was amplified to a peak power of 20 W by two EDFAs. The nonlinear fiber used was only 30 m long and has a nonlinear coefficient of 18 $W^{-1}km^{-1}$, and $\beta_3 = 0.49 \times 10^{-40} s^3 m^{-1}$, and $\beta_4 = -5.8 \times 10^{-56} s^4 m^{-1}$. A fiber Bragg grating (FBG) and a

circulator were used to filter out the EDFA ASE noise from the pump. 400 nm gain bandwidth was achieved in this FOPA. Although the gain spectrum obtained in the one-pump FOPA is not flat since phase-matching is hard to be maintained over a broad range of wavelength, two-pump FOPA can provide flatter gain spectrum under appropriate design. In [39], parametric gain with 95 nm gain bandwidth and less than 2 dB of ripple was obtained in a two-pump configuration.

2.3.3.3 FOPA noise figure

Noise figure is an important factor to consider when designing optical amplifiers. Theoretically, non-degenerate FOPAs have the potential to approach the 3 dB noise figure quantum limit, but in actual situations it is limited by many factors such as the ASE noise generated by the EDFAs during the pump amplification stage. The higher the pump power is required, the higher the ASE noise would be introduced, which could degrade the amplifier noise figure considerably. Therefore, it is necessary to filter out the ASE noise at the output of the pump EDFAs before being coupled into the fiber. Thin film filters, FBGs and circulators can be used, however at the expense of increased insertion loss in the pump branch. In [40], a CW-pump configuration was exploited and a FBG was used to greatly reduce the EDFA ASE noise. As a result, a constant noise figure of 4.2 dB was obtained over the gain spectrum. Similarly, the noise figure performance of a pulsed-pump FOPA was measured by a photon-counting technique and about 3.7 dB noise figure was obtained [41].

2.3.4 FOPOs

FOPOs can be constructed by providing an optical feedback loop to the FOPAs. In normal configurations, the FOPO is pumped by a single laser source with no seed such as signals or idlers. The signal and idler waves are built up from quantum noise at frequencies defined by the intra-cavity filter wavelength and/or the phase-matching condition. The signal and idler waves are subsequently amplified by the parametric gain when circulating inside the cavity, although in most configurations only one wave is allowed to circulate inside the cavity.

There are a number of ways to design the feedback system, including a FP linear cavity with mirrors such as FBGs at both ends, a unidirectional fiber ring structure with

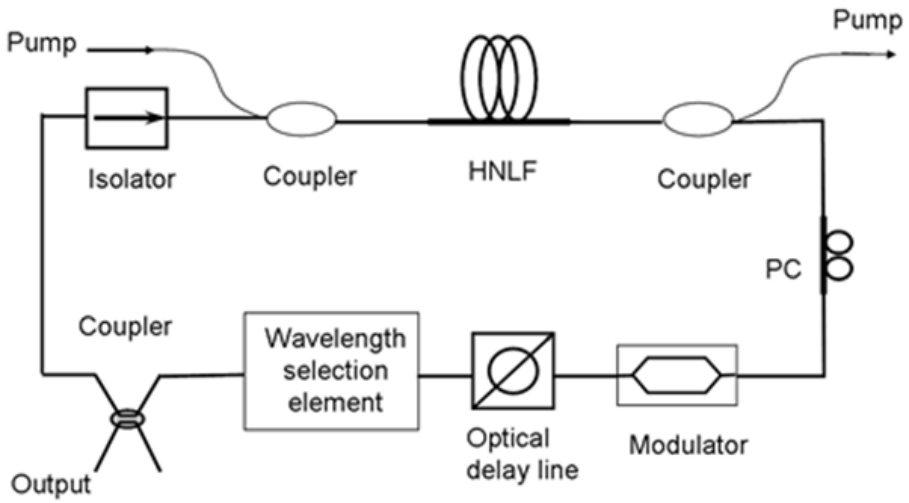

Figure 2.5 A typical configuration of an actively mode-locked FOPO.

couplers and filters to couple and split interacting waves, and a bidirectional loop mirror configuration which can separate the pump and the signal, idler in different fiber branches. In typical configurations, the pump wave is usually supplied externally, passes through the FOPO in one direction, and interacts with the signal and idler within the nonlinear medium.

A typical configuration of an actively mode-locked FOPO in a ring structure is shown in Figure 2.5, which is similar to the generic actively mode-locked fiber ring laser configuration shown in Figure 4.1 except that the gain medium is the HNLF. The HNLF needs to be pumped by an external laser source using appropriate optical couplers (OCs). The cavity configuration could be quite different depending on the types of pump sources. The pump can be a CW laser source and the resultant parametric gain keeps constant with time, which is similar to conventional optical amplifiers such as EDFAs and SOAs. Opto-electronic modulators (OEMs) could be employed as a way of achieving mode-locking in such configuration. Alternatively, the pump can be a periodic pulse train and the cavity gain is modulated periodically with the same pattern as the pump due to the ultra-fast response nature of the parametric process. Therefore, mode-locking can be achieved without an intra-cavity modulator in this configuration. The latter configuration is also referred to as synchronously-pumped FOPO. More benefits can be found using this configuration as we will discuss in the later chapters. It is worth noting that the

parametric process is polarization sensitive and requires precise alignment of the polarization states of the pump and the signal waves to maximize efficiency. Polarization-maintaining cavities can be used to improve stability for practical applications. Alternatively, polarization insensitive operation is also possible, and has been demonstrated in both one-pump and two-pump configurations [42, 43].

2.3.5 Performance of FOPOs

2.3.5.1 CW FOPOs

A CW FOPO was demonstrated in [44] with different lengths of HNLF. A threshold of 240 mW was achieved using a spool of 100 m long HNLF in which the output idler could be tuned over 80 nm. A maximum output idler power of 100 mW was obtained by using 1 km long HNLF, which corresponds to an internal conversion efficiency of 30%. In [45], a CW FOPO based on holey fiber was demonstrated. The oscillator was also operated at 1550 nm, however with a threshold of 1.28 W and a saturation pump power of 1.6 W. The signal linewidth is about 10 pm with extinction ratio of 30 dB.

Since the FOPO has a long cavity length compared with bulk OPOs, frequency spacing between multiple longitudinal modes is very small (i.e., in the order of megahertz or even kilohertz) making it very difficult to design an intra-cavity optical filter to select a single frequency. The phases of the multiple longitudinal modes have random relationship in normal circumstances and as a result the combined CW oscillation wave shows random time variant noise due to the beating between different modes. In [46], a single-longitudinal-mode FOPO was achieved by resonating both the signal and idler in two separate cavities assisted with another subring cavity inserted in the cavity. The threshold pump power can be reduced by oscillating the signal and idler waves together. Mode restriction is realized since only certain frequencies that satisfy the resonant conditions of all the three cavities simultaneously can oscillate. Another technique was demonstrated in [47], in which the single longitudinal mode operating was achieved by inserting a coupled subring cavity with a short cavity length and a fiber loop mirror with an unpumped EDF inside the loop. The loop mirror functions as an ultra-narrow-bandwidth self-induced FBG due to the spatial-hole burning in the EDF.

2.3.5.2 Actively mode-locked FOPOs based on CW pumps

Actively mode-locked FOPOs based on a CW pump were achieved by inserting an intensity modulator in the FOPO cavity [48]. 10 GHz pulse train with pulse duration of 24 ps was generated by modulating the intensity modulator with a 10 GHz sinusoidal wave. The cavity length was carefully adjusted so that the cavity resonance frequency matched with the modulation frequency of the RF driving source. The wavelength can be tunable over 21 nm by tuning the intra-cavity tunable optical filter. Wavelength tuning can also be achieved by simply inserting a length of dispersive fiber in the cavity and without any kinds of optical filters [49]. The oscillating signal can adjust its wavelength automatically such that the pulses can center itself in the modulation transmission window. The wavelength can be simply tuned by changing the modulation frequency of the RF source.

2.3.5.3 Pulsed-pump FOPOs in anomalous dispersion regime

Instead of using an intra-cavity EOM as the mode-locker, an alternative approach is using a pulsed-pump FOPO configuration which is also referred to as synchronous pumping. Since the parametric process in optical fiber has ultrafast response, the intensity variation of the pump wave can be transferred to the signal/idler gain instantaneously which is exponentially proportional to the pump intensity if phase-matching is satisfied. The cavity gain can therefore be modulated periodically in time if the pump wave is a periodic pulsed source. The pump wavelength is usually allocated in the anomalous dispersion regime such that a broadband FOPA gain could be obtained.

An early experiment was demonstrated based on a nonlinear fiber Sagnac interferometer (NFSI) in a degenerate operation [50]. NFSI enables the separation of the pump and signal, and output pulse with 0.83 ps duration was achieved with input pulse duration of 3.9 ps indicating the device acting as a pulse compressor. In addition, the output pulse exhibits improved spectral symmetry and a reduced time-bandwidth (TBW) product compared with the pump pulses. However, careful control of the signal phase via fiber length was necessary as degenerate FOPO is phase sensitive. A non-degenerate operating FOPO was also demonstrated based on the same configuration [51]. The gain medium was a 105 m long dispersion-shifted fiber (DSF). Since the FOPO was operated in non-degenerate configuration, the signal wavelength could be tunable over a broad

range of wavelength as long as the parametric gain was sufficiently large to compensate the cavity loss. As a result, this FOPO can emit pulses with pulse duration of 1.7 ps out of 7.7 ps pump pulses and can be tunable over 40 nm in the C-band. The repetition rate was only 100 MHz.

There is an increasing interest of using microstructure fiber (MF) as the nonlinear medium for FOPOs since MF offers more flexibility in terms of fiber design such as arbitrary zero-dispersion wavelength, high nonlinear coefficient, very flat dispersion curve, uniform zero-dispersion wavelength, endless single-mode, etc. FWM in the MF was first demonstrated in [52], in which parametric gain of 13 dB was obtained in 6.1 m long MF with a pump peak power of 6 W. A FOPO based on FWM in MF was later demonstrated in a 2.1 m long MF for the first time [53]. 40 nm tuning range was achieved in this device with a pump peak power of 34.4 W. It was shown later that decreasing the length of fiber can dramatically increase of the phase-matching bandwidth, and the overall output power also improves with decreasing the fiber length. In the experimental work conducted in [54], 570 fs pulses was generated from 1.6 ps pump pulses with average output power of 50 mW and peak power of 1.2 kW. The MF used in this experiment had 3 cm length and over 200 nm tuning range was achieved in this FOPO. In a separate experiment, more than 120 nm broad gain spectrum was demonstrated in a synchronously-pumped FOPO using a 12.5 m long MF, which was a result of super-continuum generation (SCG) stimulated by SRS [55]. However, only 30 nm tunable range was demonstrated due to the limited optical filter operating wavelength. One of the advantages of using FOPO compared with the approach of using SCG followed by spectral slicing is that optical pulses with good coherence can be generated.

2.3.5.4 Pulsed-pump FOPOs in normal dispersion regime

When the pump is located in the normal dispersion regime of the optical fiber, a distinct parametric gain characteristic can be obtained compared with the occasion in the anomalous dispersion regime. Specifically, narrowband parametric gain is formed which can be shifted several hundreds of nanometers away from the pump determined by the phase-matching condition and the higher-order dispersion parameter β_4. We have discussed this special operation regime briefly in Section 2.3.1. If a synchronously-pumped FOPO works in this regime, no intra-cavity optical filter is

required and the output lasing pulses can be tuned over a broad range of the wavelength by simply tuning the pump wavelength. Considerable attention must be paid to the FOPO design, such as the choice of nonlinear fiber, pump source, and the cavity constituent components. In particular, the characteristics of the nonlinear fiber are the most important since the phase-matching condition and the parametric gain are extremely sensitive to the fiber dispersion, length, zero-dispersion wavelength fluctuation, fiber birefringence, etc. FOPOs that operate in normal dispersion regime have been widely demonstrated in the past few years. These devices can be classified in terms of their operating wavelength. Considerable amount of work has been done in the 1 μm regime where the generated pulse train can be useful in pump-probe measurements such as probing the carrier lifetime in semiconductors, spectroscopically resolving fast chemical or biological reactions, and in settings where multi-photon excitation is used [56-59]. Spectral bands near the 1.55 μm communication window are also attractive as these non-conventional bands can be utilized to make a full use of the fiber bandwidth [60-63]. Another wavelength band of interest is the 2 μm which has wide applications in biomedical imaging, chemical sensing, etc. [64, 65]. However, this type of FOPO is out of the scope of this thesis and will not be discussed in the following chapters.

2.4 Summary

An overview of various nonlinear optical phenomena in optical fiber is given in this chapter, including the origins and the properties of each phenomenon and their impact on the optical signals such as phase variation, frequency chirping, optical gain, etc. Although many of these nonlinear phenomena are generally harmful to fiber optical communication systems, some are beneficial and have been used to demonstrate important optical signal processing functions. Raman gain and parametric gain are essentially broadband when certain requirements are satisfied, and have been used to make optical amplifiers and lasers. The Kerr effect has an ultra-short response time due to the fast electronic vibrations and have been used to process high-speed optical signals directly in the optical domain. Despite the numerous possible applications these nonlinear phenomena can offer, this dissertation will focus on the parametric amplification which is the fundamental of FOPAs and FOPOs. In theory, these parametric devices can provide high gain, broad gain bandwidth in any wavelength of interest, and are able to process optical signals at Tb/s data rate, and therefore are considered as good candidate for the future ultra-broadband optical transport networks. In the next few chapters, high performance FOPOs will be

demonstrated as a versatile platform for many of the functionalities such as CW lasing, mode-locking, and signal processing.

Chapter 3 Multi-wavelength CW-FOPO

3.1 Introduction

Optical sources that can emit multiple wavelengths simultaneously are cost-effective solution to the WDM optical communication systems [66]. Besides, they can find applications in a wide range of areas such as fiber optical sensor systems [67], optical instrumental test and measurement [68], microwave photonics [69], etc.

Conventionally, this is implemented by using multi-wavelength semiconductor lasers which consist of physically separated laser cavities and gain media [70, 71]. The demand of squeezing the size and reducing the complexity and hence the cost of the laser sources has led to the development of multi-wavelength lasers. Multiple wavelengths share the same laser cavity and gain medium in multi-wavelength laser sources, and therefore complexity and cost can be reduced. However, the performance of this kind of laser must be critically evaluated in order to compete with existing technologies. In particular, it should be capable of emitting a large number of wavelengths simultaneously over a broad range of wavelength with narrow wavelength spacing, equal optical power distribution on individual wavelengths, tunable emitting wavelength, reconfigurable emitting spectral shape and stable operation in both power and wavelength.

3.1.1 EDFA based multi-wavelength fiber lasers

Previously, much research has been done in multi-wavelength fiber lasers with EDFAs or semiconductor optical amplifiers (SOAs) as the gain medium. EDFA is very attractive for its low cost, high saturation power and low polarization dependent gain. However, EDF has the problem of homogeneous gain broadening at room temperature. The gain broadening linewidth is typically larger than a few nanometers, which limits the minimum wavelength spacing that can be achieved between adjacent lasing frequencies.

It was reported in [72] that spectral hole width could be reduced to 1 nm by immersing the EDF fiber spool in liquid nitrogen (i.e., at 77 K) and multi-wavelength operation is promoted. Birefringence was introduced at the same time to diversify the polarization states of different wavelengths in the EDF. By exploiting spectral hole

burning (SHB) and polarization hole-burning (PHB) in the EDF, up to 24 wavelengths simultaneous lasing was achieved.

Although straightforward and effective, cooling EDF in liquid nitrogen is not practical in many applications. Other methods such as linear phase modulation of the cavity oscillating frequencies and nonlinear phenomena based inhomogeneous loss mechanisms were demonstrated, which aimed at multi-wavelength lasing at room temperatures. For example, in [66] an acousto-optic frequency shifter (AOFS) was used in a feedback loop to translate the light frequency by 100 MHz to a neighboring frequency, and therefore homogeneous gain broadening was suppressed and single-wavelength steady-state lasing was prevented. Similarly, other phase modulation based methods have been demonstrated such as using an electro-optic PM or an all-fiber PM driven by a piezoelectric transducer (PZT) [73], and using an SOA as a PM by biasing the SOA below the transparent point and modulated with a low-voltage sinusoidal signal [74].

In addition, nonlinear phenomena based inhomogeneous loss mechanisms were demonstrated. For example, In [75], FWM and bandwidth limiting optical filter worked together as the nonlinear loss mechanism. FWM between the intra-channel longitudinal modes caused broadening of the emission spectrum which was followed by a FP filter with appropriate bandwidth. In the case of multi-wavelength operation, a channel with higher power would experience a larger amount of spectral broadening in the HNLF and would see higher loss in the bandwidth limited FPF. As a result, the powers between the lasing wavelengths were automatically balanced and the gain competition in the EDF was greatly reduced. Similarly, in [76] nonlinear polarization rotation (NPR) in the HNLF followed by a polarizer forms the nonlinear loss mechanism. Intensity dependent inhomogeneous loss could be introduced by carefully adjusting the state of polarization (SOP) of the lasing wavelengths before the polarizer such that the transitivity decreases with increasing signal power. Recently, researchers found that FWM is also helpful for reducing gain competition between the modes due to a self-stabilization mechanism. It has been theoretically analyzed by an un-depleted approximation and a perturbation method [77], and also been experimentally demonstrated in many references [78-80]. In a recent study, both wavelength dependent loss and intensity dependent loss mechanisms

were exploited in a nonlinear high-birefringence fiber loop mirror to implement a multi-wavelength laser with more than 100 wavelengths and 0.14 nm wavelength spacing [81].

3.1.2 SOA based multi-wavelength fiber lasers

Although various methods have been demonstrated to overcome the homogeneous linewidth broadening of EDF based fiber lasers, they inevitably increase the complexity of the lasers and the cost. On the other hand, SOAs have inhomogeneous linewidth broadening, which allows SOA based fiber lasers to lase multiple wavelengths simultaneously with narrow wavelength spacing. For example, a triple-wavelength SOA fiber laser with 50 pm wavelength spacing was reported, in which three π-phase shifts are introduced in one FBG structure to realize a triple-transmission-band with ultra-narrow wavelength spacing [82]. In addition, SOA fiber lasers with different numbers of simultaneous lasing wavelengths and wavelength spacing were demonstrated. In [83], simultaneous lasing of 52 wavelengths spaced at 50 GHz was achieved by using two cascaded SOAs to broaden the gain spectrum and a single-pass optical feedback was used as a saturation signal to equalize the power distribution of the oscillating wavelengths. In [84], SOA fiber lasers with three different configurations (i.e., single-SOA linear cavity, single-SOA ring cavity, and double-SOA ring cavity) were compared. Up to 41 wavelengths were obtained in a double-SOA ring laser with a wavelength spacing of 25 GHz and a wavelength tunability of 10 nm. In [85], simultaneous lasing of 126 wavelengths with 0.08 nm wavelength spacing was demonstrated with 20.2 nm wavelength tuning range. Nonlinear polarization rotation based intensity dependent loss mechanism was used to reduce the wavelength competition and to help stabilize multi-wavelength operation.

Different wavelength selecting elements were used in various approaches which included delay interferometers, arrayed waveguide gratings, serial and parallel arrays of FBGs, FPF [83], PMF loop mirrors [86], sampled high-birefringence (Hi-Bi) fiber gratings [87], superimposed chirped FBGs [84], and Sagnac loop mirrors [85, 88]. In particular, wavelength switchability and tunability can be obtained by changing the phase

plates in the PMF loop mirrors [86], the SOP of the input to Hi-Bi sampled FBGs [87], and the SOP inside the Hi-Bi loop filter [84] or the Sagnac loop filter [85, 88].

3.1.3 FOPA based multi-wavelength fiber lasers

With the features inherited from FOPAs such as large optical gain, broad gain bandwidth, and ultra-short response time, FOPOs have attracted considerable interests as multi-wavelength laser sources. Indeed, a multi-wavelength FOPO was demonstrated before the work described in this chapter was performed [89]. In [89], the laser cavity was comprised of a spool of HNLF and two optical pumps as the gain medium, and a superimposed chirped FBG as the comb-like filter. Seven wavelengths with a spacing of 125 GHz (i.e., 1 nm) could oscillate simultaneously in this FOPO cavity. However, the results shown in [89] are not competitive with those demonstrated in EDFA or SOA based approaches, especially in terms of the number of wavelengths or narrow wavelength spacing. In addition, a two-pump structure was used to flatten the parametric gain, which adds complexity compared with the one-pump approach as will be discussed in the next section. Later, a multi-wavelength FOPO with a tunable wavelength-spacing feature based on a tunable Mach-Zehnder interferometer (MZI) was demonstrated [90, 91]. With the MZI as a comb filter, multi-wavelength lasing with 10 GHz (i.e., 0.08 nm at 1550 nm) spacing was demonstrated. Since the MZI is a combination of several discrete fiber-pigtail components (i.e., two 3-dB couplers, an optical variable delay line, a polarization controller (PC)), it suffers from poor stability due to environmental perturbations. A peak power fluctuation of 0.8 dB was observed within half an hour. It was shown that the two-pump configuration [91] had a better power uniformity of the lasing wavelengths than the one-pump based configuration [90]. However, the number of simultaneous lasing wavelengths is still not large compared with other approaches. Besides, wavelength tunability and reconfigurability were not addressed in these references [89-91].

In this work, we present a multi-wavelength FOPO that can generate 129 wavelengths simultaneously with 25 GHz (i.e., 0.2 nm at 1550 nm) spacing, using only one pump and operating stably at room temperature. The laser configuration is quite simple because only one spool of nonlinear fiber is required in the cavity, which

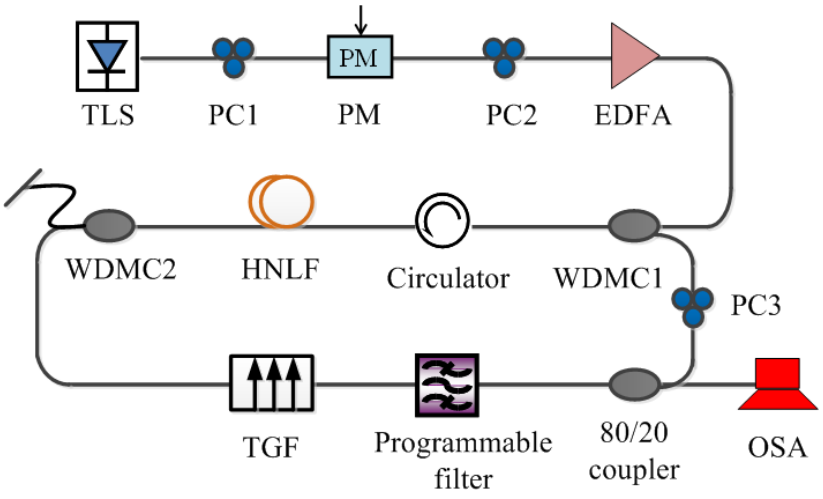

Figure 3.1 Experimental setup of a multiwavelength FOPO.

functions as the gain medium as well as to eliminate mode competition through FWM. Stable operation has been achieved in terms of wavelength and power fluctuations. Wavelength tunability and reconfigurability are also demonstrated.

3.2 Experimental setup and principle of operation

The experimental setup of the proposed multi-wavelength FOPO is shown in Figure 3.1. A continuous-wave tunable laser source (TLS) with a wavelength of 1558 nm is used as the pump source. It is phased modulated by a 10 GHz PRBS signal with a PM to suppress the SBS. After phase dithering, the pump wave is then amplified by a high-power EDFA before being coupled into a WDM coupler (WDMC1). WDMCs are used to couple the pump wave and the oscillating signal wave, which has a transmission band of 1554.89 nm - 1563.89 nm, and a reflection band of 1510 nm - 1551.39 nm and 1567.39 nm - 1600 nm. A circulator is used to ensure unidirectional operation of the laser cavity and to avoid any reflecting light from damaging the EDFA. The pump wave is launched into a 1 km spool of highly-nonlinear fiber (HNLF) with a nominal zero-dispersion wavelength of 1552 nm and nonlinear coefficient of 10 $W^{-1}km^{-1}$. After parametric amplification, the

pump is discarded using WDMC2, which has the same spectral properties as WDMC1, while the ASE noise is allowed to recirculate in the cavity.

A transmission grating filter (TGF), formed by superimposing two linearly chirped FBGs acting as a distributed FP cavity [92], is used as a comb filter. The two chirped gratings comprising the TGF were written in hydrogen-loaded photosensitive fiber using 244 nm CW UV laser. The longitudinal shift between the two gratings was induced by displacing the phase mask by the required amount between successive exposures. The phase mask used had a central period of 1064.05 nm and a chirp of 2.5 nm/cm; for a free spectral range (FSR) of 25 GHz; the required displacement is about 4.1 mm. The TGF spans the whole *C* band, with a nominal FSR of 25 GHz. The 3 dB bandwidth of the transmission spectral peaks is approximately 27 pm, and the extinction ratio (ER) is about 18 dB.

A programmable filter (Peleton QTM) is used to define the spectral range and the corresponding optical power of the lasing wavelengths. It allows multiple transmission channels in the *C*-band; each channel is anchored on the ITU frequency grid and has a 3 dB bandwidth of 0.8 nm. The channels can be switched ON or OFF separately and the attenuation of each channel can be adjusted independently. In this experiment, all the channels of the programmable filter were ON (i.e., open) for multi-wavelength oscillation with a high count of wavelength number, while some of them were OFF (i.e., closed) or attenuated for tunable or reconfigurable laser operation.

Then the spectrally sliced ASE noise passes through an 80/20 OCs; 20% of the total power is coupled out of the cavity while 80% remains circulating in the cavity by injecting into the WDMC1. Polarization controllers (PC) PC2 and PC3 are used to optimize the SOP of the signals with that of the pump so that maximum parametric gain can be achieved. If the parametric gain is larger than the round-trip cavity loss, stable multi-wavelength lasing will occur after multiple circulations in the cavity. The optical spectra were measured using an OSA with a resolution bandwidth (RBW) of 0.06 nm.

3.3 Experimental results and discussions

First, the small-signal gain spectrum of the FOPA was characterized in an open-loop pump-probe configuration. A second TLS was used as the probe (not shown in Figure 3.1)

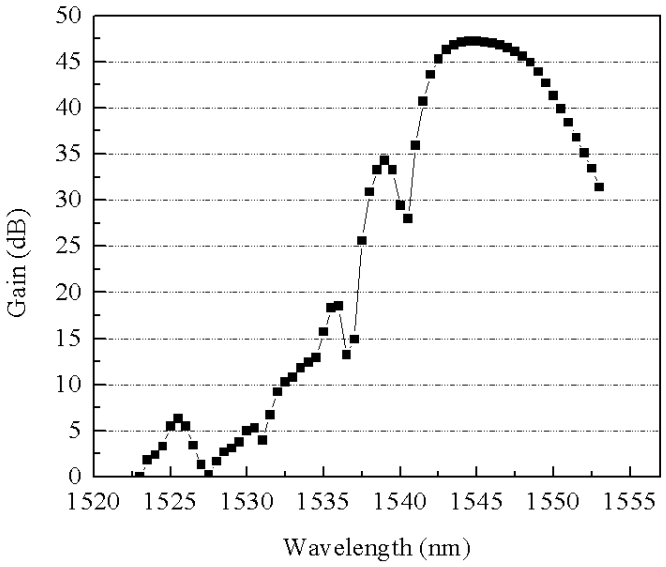

Figure 3.2 Gain spectrum of the FOPA in the anti-Stokes band.

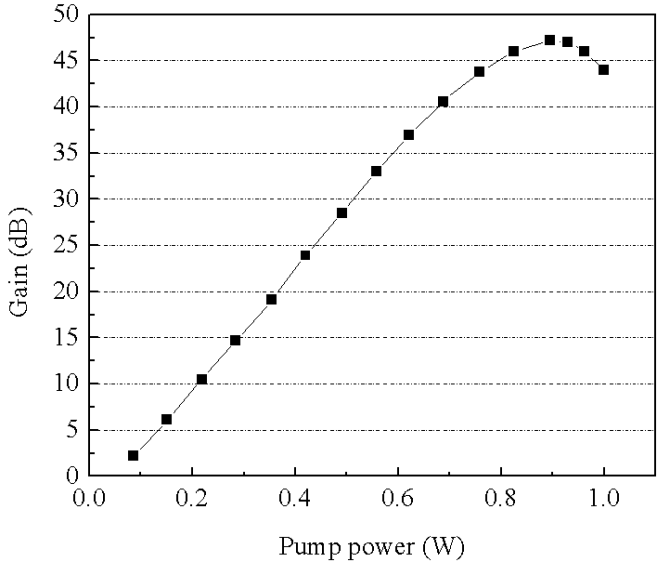

Figure 3.3 The dependence of the FOPA gain on the pump peak power.

which was scanned over the anti-Stokes band of this FOPA with a constant optical power of -30 dBm. The pump wavelength was set at 1558 nm with a constant optical power of 29.4 dBm. Then the amplified probe power ws monitored by an optical spectrum analyzer (OSA), and the corresponding FOPA gain spectrum was measured which is shown in Figure 3.2. From the plot it can be seen that maximum FOPA gain of 47.2 dB

can be achieved when the probe wavelength is 1545 nm. Substantial gain (i.e., over 20 dB) can be obtained over 16 nm spectral range from 1537 nm to 1553 nm. Since the round-trip cavity loss was measured to be 13.2 dB; as such, the FOPA gain can compensate for the cavity loss from 1535 nm to 1553 nm, assuming no significant pump depletion. However, the measured gain bandwidth is limited by the available bandwidth of the WDMC1, which has a cutoff wavelength at around 1553 nm. As we have mention in section 2.3 that the achievable gain bandwidth is largely dependent on the length of the nonlinear fiber and the peak pump power. Since the length of the HNLF is fixed, we can only change the peak pump power to vary the FOPA gain.

Figure 3.3 shows the dependency of FOPA gain on the peak pump power. It can be seen that FOPA gain (in dB) increases almost linearly with increasing peak pump power when FOPA gain is less than 37 dB. The slope of this linear curve is 65.5 dB/W. However, increased SBS and spurious FWMs will prevent the gain from increasing in a linear fashion at a very high pump power, and that is why the gain curve starts to saturate. After characterizing the FOPA gain, the cavity is closed and the evolution of the FOPO spectral output was monitored in the OSA as the input pump power increases gradually, which is shown in Figure 3.4. Note that a wavelength is defined to lase if its power exceeds -30 dBm in our case. It can be observed that no wavelength starts to lase until the pump power was increased to 0.3 W, when a wavelength at 1549.6 nm appeared abruptly in the spectrum. So it can be determined that the threshold of this FOPO is 0.3 W. Considering the cavity loss and FOPA gain without pump depletion under the perfect phase-matching condition, the theoretical threshold of this FOPO is calculated to be 0.26 W, which agrees well with the measured value. The discrepancy can be attributed to the nonideal FOPA gain obtained in the experiment due to various factors such as pump depletion, zero-dispersion wavelength fluctuation and random birefringence of the HNLF. As the pump power increases beyond the laser threshold, more wavelengths start to oscillate in the cavity. However, the power distribution of these wavelengths is not equal and the lasing spectrum varies a lot when we change the cavity polarization. This is due to the severe gain competition occurring among different lasing wavelengths. As the pump power increases further, the lasing spectrum becomes flatter in power. Moreover,

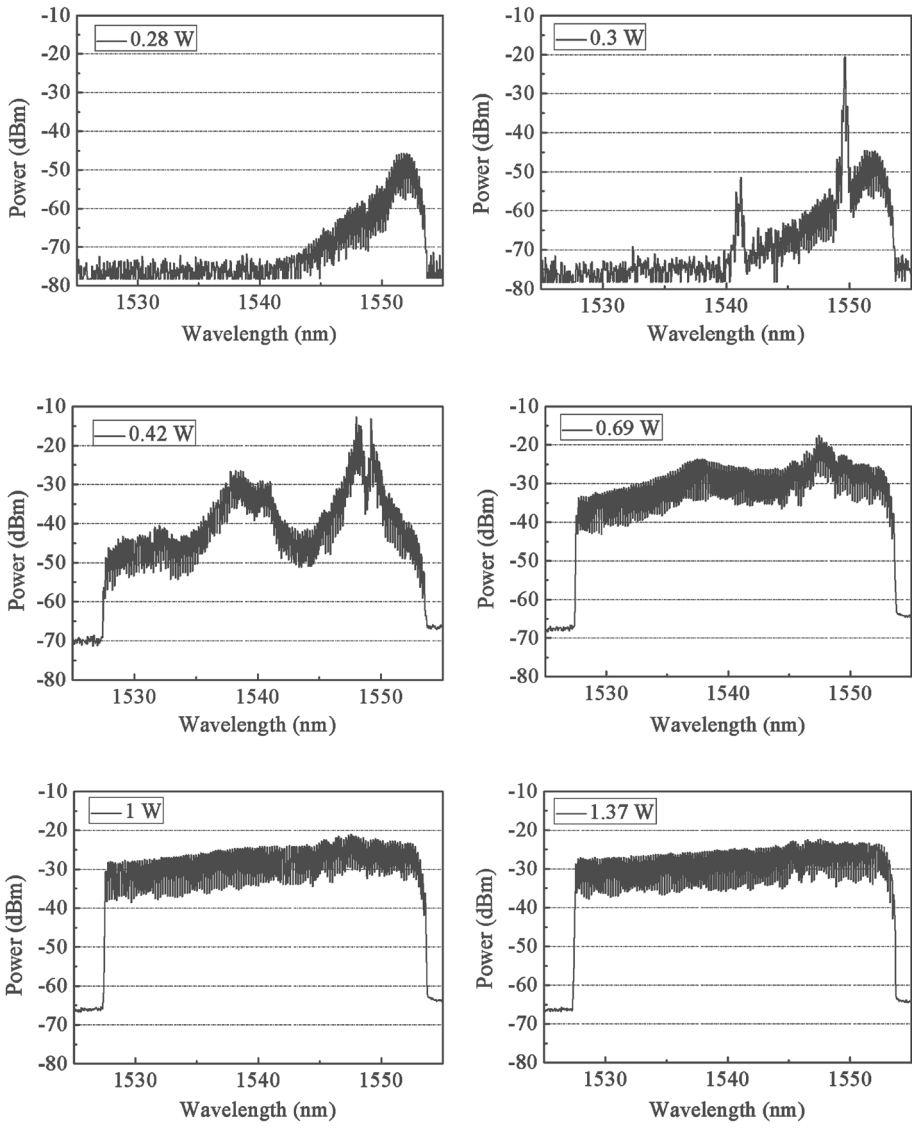

Figure 3.4 Evolution of FOPO lasing spectrum at different pump powers. OSA RBW: 0.06 nm.

the spectrum is observed to be quite stable even when we vary PC3 on purpose. The wavelength spacing between adjacent wavelengths is 0.2 nm (i.e., 25 GHz).

Figure 3.5 summarizes the dependence of the number of output wavelengths and power nonuniformity on the input power. Power nonuniformity is defined as the power difference between the two spectral peaks that have the maximum and minimum power. From Figure 3.5 it can be observed that the power nonuniformity of the lasing spectrum decreases from 18.4 dB to 6.5 dB as the pump power increases from 0.35 W to 1.37 W without varying the cavity polarization, and 129 lasing wavelengths can be obtained

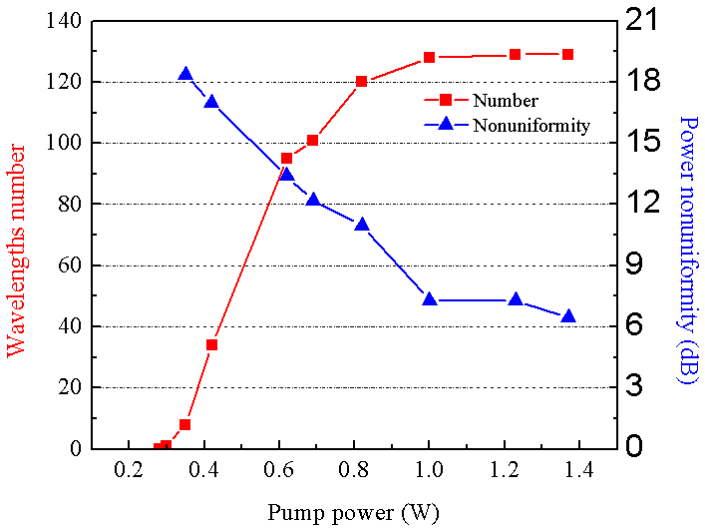

Figure 3.5 Output wavelength number and power nonuniformity vs. input pump power.

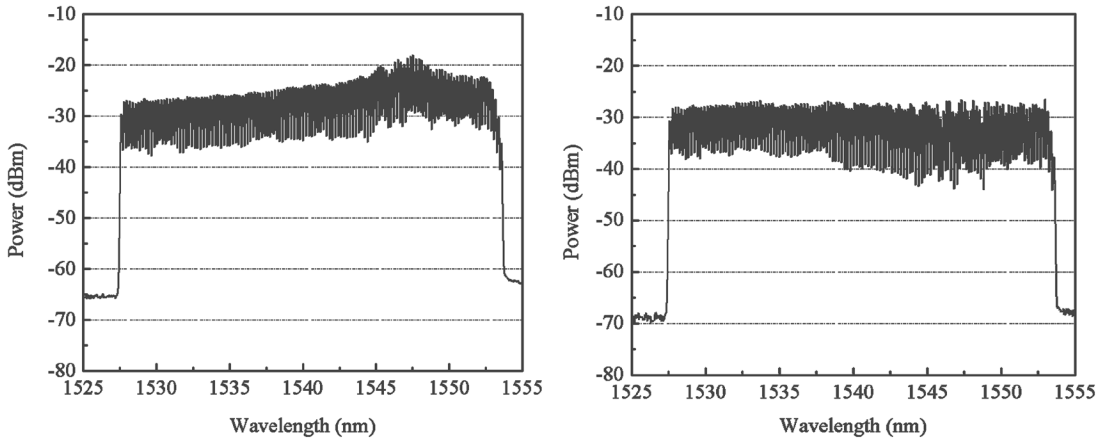

Figure 3.6 FOPO spectrum at 1 W pump power (a) without flattening, and (b) with flattening. OSA RBW: 0.06 nm.

when the pump power is larger than 1.23 W. This is because, when the pump power increases, each oscillating wavelength levies more power from the pump due to the higher gain obtained. It is known that FWM efficiency also increases with increasing powers of the interacting wavelengths, which introduces a dynamic gain flattening mechanism that leads to a flattened lasing spectrum [77].

We demonstrated that 129 wavelengths with 25 GHz spacing could be achieved in our proposed multiwavelength FOPO configuration. We also found that the flatness of the lasing spectrum depends on the input pump power due to a dynamic gain flatterning mechanism. However, the pump power required to achieve a flat spectrum is a bit high, which might not be useful in some applications. We show below that by programming the attenuation of individual channels in the programmable filter, an output spectrum with a flat top can be achieved at relatively low pump powers. Figure 3.6 shows a comparison between the FOPO lasing spectrum with and without using the programmable filter for spectrum flattening. In both cases, 129 wavelengths can lase simultaneously with 0.2 nm (i.e., 25 GHz) wavelength spacing. However, the power nonuniformity of the 129 wavelengths without spectral flattening is 11.6 dB, while that with spectral flattening is only 4.5 dB. An improvement of 7.1 dB can be obtained. In the case of with spectral flattening, the lasing spectrum spans over 25.6 nm from 1527.58 nm to 1553.18 nm.

The optical signal to noise ratio (OSNR) of the laser is defined as the ratio of the optical power of each lasing wavelength to that of the noise within its corresponding linewidth. The linewidth was measured to be 0.019 nm (in a separate experiment as discussed below), and a RBW of 0.06 nm was chosen to measure the signal power. The in-band noise power was estimated by measuring the out-band noise power at the same RBW (i.e., 0.06 nm) as the signal. As the visibility of the inter-wavelength noise floor was obstructed by the limited OSA resolution at the time when this measurement was performed, the noise power out of the lasing bandwidth was measured instead. Note that this was a blind measurement by assuming the in-band noise power was the same as the out-band noise power, which may not be true. Using this method, the measured OSNR was more than 36 dB. The total output power of the laser is -5.2 dBm. The per wavelength power is relatively low for certain applications, e.g., as a transmitter for optical communications. While the output power can be increased by increasing the pump power, this will be eventually limited by the SBS imposed on the pump wave. However, the per wavelength power can be increased by reducing the total number of lasing wavelengths (which in turn depends on the requirements of the specific application).

The 3 dB linewidth of the laser was measured using an OSA with 0.16 pm resolution (Apex Complex OSA, 2443B). The linewidth is actually broadened by FWM, since a separate measurement made when only two wavelengths oscillate and no FWM was observed shows that the linewidth was less than 2 pm. Such a significant linewidth broadening is due to the combined effect of FWM between the multiple longitudinal modes within each wavelength and the multiple oscillating wavelengths of the laser in the frequency range in which phase matching is satisfied. It is worth to note that, for wavelengths less than 1535 nm, the FOPA gain is less than the round-trip cavity loss and therefore, in principle no wavelengths should oscillate. Nevertheless, output wavelengths are indeed obtained in this region because of the strong FWM that occurs among the spectral peaks. Since the lasing wavelength are in the vicinity of the zero-dispersion wavelength (i.e., ~1552 nm) of the fiber and the dispersion slope around 1552 nm is very flat (i.e., ~0.02 ps/nm^2/km), the phase-matching condition can still be satisfied over a large frequency range. As the optical power of each lasing wavelength is not high, the output spectrum can be flat even if the fiber length is as long as 1 km [93].

Figure 3.7 shows the repeated scans of the output spectrum from 1538 nm to 1539 nm taken in at 2 min intervals over a 20 min period. It can be observed that the output spectrum is very stable both in power and wavelength. A measurement of the optical powers at four wavelengths (i.e., 1538.5 nm, 1539.9 nm, 1541.5 nm, 1542.7 nm) shows that the maximum power fluctuation is less than 0.1 dB over this 20 min period. Wavelength fluctuations are not observed within the OSA resolution (i.e., 0.06 nm). Stable operation over a longer period of time is expected but was not tested since the high pump power might damage the optical components inside the laser cavity (which were not designed to sustain high power.

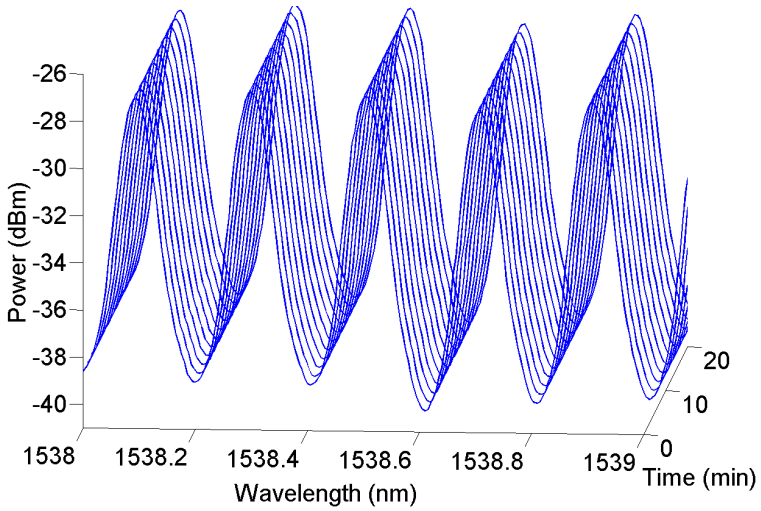

Figure 3.7 Repeated scans of the FOPO output spectrum in 20 min period. OSA RBW: 0.06 nm.

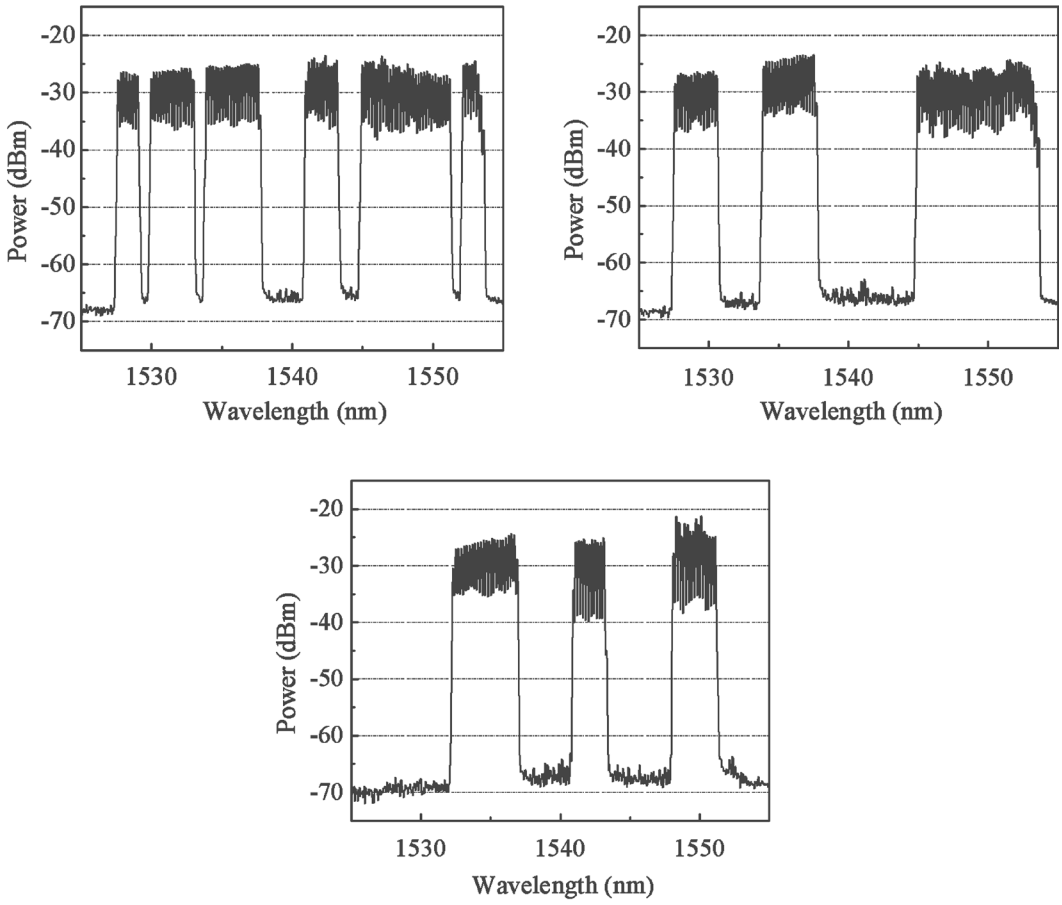

Figure 3.8 Multiwavelength FOPO with arbitrary lasing spectrum. OSA RBW: 0.06 nm.

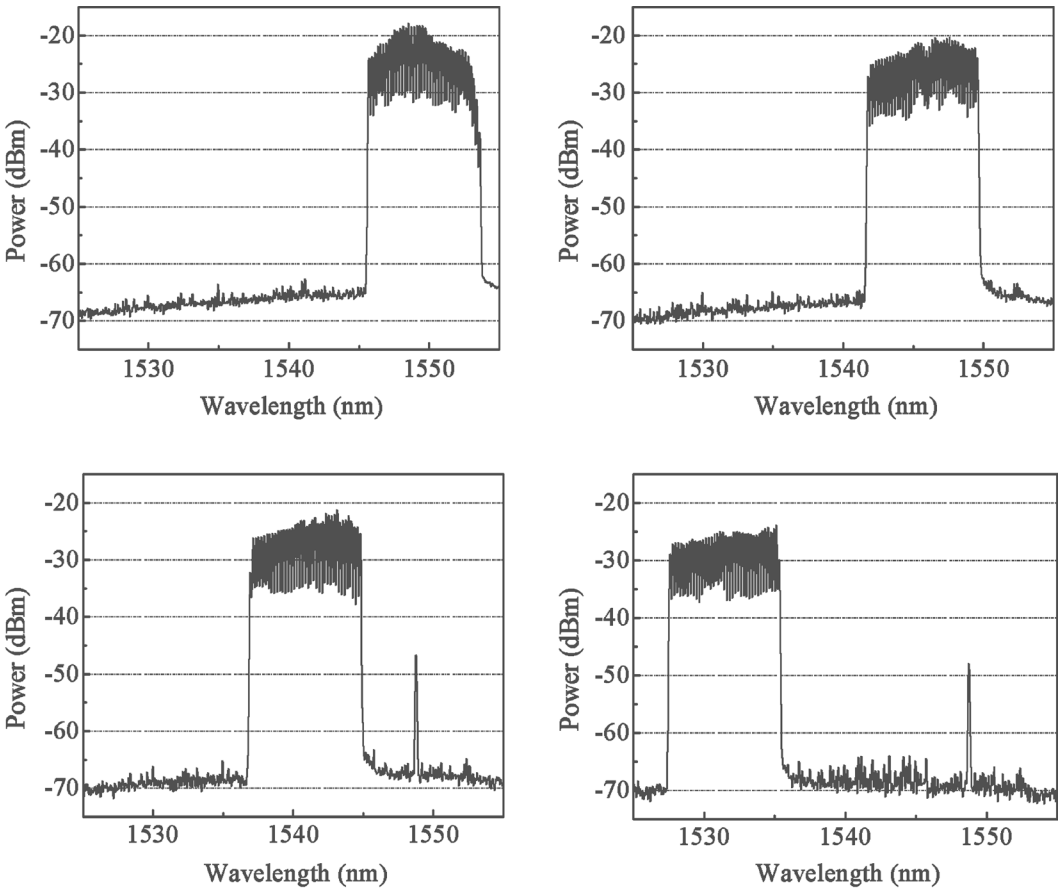

Figure 3.9 Multiwavelength FOPO with tunable wavelength range over the entire lasing spectrum. OSA RBW: 0.06 nm.

In addition to flatten the FOPO output spectrum, the use of programmable filter adds additional functionalities to this laser by shaping its spectrum to arbitrary shape, and by tuning the wavelengths over the entire lasing spectrum. Figure 3.8 shows the emission spectrum when different channels are open or closed by programming the filter. We can easily tailor the output spectrum with only small power nonuniformity. Figure 3.9 shows that this multiwavelength FOPO can be tunable over the whole lasing spectral range without much change in the power spectrum. The small peak at 1548.7 nm is due to leakage from the programmable filter at that wavelength.

Table 3.1 Comparison of various types of multi-wavelength lasers discussed in this chapter

Approach	Spacing (nm)	Number of wavelength	Tunability	Reconfigurability	References
EDFA-based	1.1	24	No	Yes	[72]
	0.19	26	No	Yes	[74]
	0.2	70	No	No	[75]
	0.14	>100	Yes	No	[81]
SOA-based	0.05	3	No	No	[82]
	0.4	52	No	No	[83]
	0.2	41	Yes	No	[84]
	0.08	126	Yes	No	[85]
FOPO	1	7	No	No	[89]
	0.08 – 0.8 (tunable)	24	No	Yes	[91]
	0.2	129	Yes	Yes	Our approach

3.4 Conclusions

In this chapter, we first introduce the importance of multiwavelength laser sources. Then EDFA and SOA based fiber lasers are discussed and compared. EDFA based fiber lasers suffer from homogeneous linewidth broadening and thus additional mechanisms must be used to overcome this problem. SOA based fiber laser has inhomogeneous linewidth broadening and therefore can support multi-wavelength lasing with narrow wavelength spacing. Various approaches have been demonstrated to build a broadband comb filter with narrow wavelength spacing, wavelength tunability and switchability. Table 3.1 shows a comparison among different approaches discussed in this chapter. Later, we demonstrate a stable multi-wavelength FOPO based on a single-pump configuration with a TGF and a programmable filter as the wavelength selection element. Single-pump configuration simplifies the laser structure significantly while still provides enough gain

over a broad wavelength range. Inherent FWM in the parametric amplification helps to stabilize the power distribution of the lasing wavelengths by reducing the gain competition, therefore relatively flat lasing spectrum can be obtained. TGF serves as a narrow-band comb filter which is more stable than MZI or Sagnac loop based filter structures. Programming filter further tailors the emission spectrum to arbitrary shape or to realize wavelengths tunability. This approach demonstrates the largest number of wavelength, the narrowest wavelength spacing, the widest spectral range, the flattest power distribution in all demonstrated lasers of this type at the time when this work was published. The maximum number of wavelengths that is possible in this type of laser depends on the parametric gain and FWM bandwidth, and in principle it can be increased further by increasing the pump power. Another factor which may impose limitations is the optical filter bandwidth. For instance, the number of wavelengths achievable in our experiment was limited by the bandwidth of the WDMCs and the programmable filter. Moreover, stable operation could be more challenging at smaller wavelength spacing because of increased gain competition between the narrowly-spaced oscillating wavelengths. Multi-wavelength FOPO with 0.08 nm spacing has been demonstrated which is the narrowest spacing demonstrated to date [91].

It is worth noting that the lasing wavelengths of the demonstrated FOPO contain multiple longitudinal modes due to the fact that FOPO cavity is 1 km long. There are several demonstrations of single wavelength, single longitudinal mode operation by using subring cavities [46] and unpumped erbium-doped fiber [47]. However, these approaches may not work for multi-wavelength operation. Although the multi-longitudinal mode nature of the demonstrated FOPO prevents its use as a transmitter in WDM communications, it can find applications in other areas such as optical instrumentation and optical sensing where single longitudinal mode operation is not required.

Chapter 4 Actively Harmonically Mode-Locked FOPO

Optical pulse sources which can generate wavelength tunable high-speed short-duration pulses play an important role in OTDM and WDM communication systems. Early demonstrations include but not limited to gain-switching DFB laser diodes [94], mode-locked external-cavity semiconductor laser diodes [95], DFB laser diodes integrated with electro-absorption modulators (EAMs) [96], and passively mode-locked lasers. Actively mode-locked lasers have attracted great research interest nowadays, due to their ability of generating high-repetition-rate ultra-short pulses which are of special importance for ultra-high-speed optical communication systems and networks. In particular, in OTDM systems, low-speed data is encoded in the form of ultra-short optical pulses and time-interleaved to form a high-speed data stream. Besides, actively mode-locked lasers can find wide applications in optical packet switching, optical sampling, and frequency comb generation [97-99].

Among the various types of mode-locked lasers, fiber based ones are especially attractive due to their light weight, no need for optical alignment, ease of coupling into fiber transmission systems, and flexibility for inclusion of intra-cavity elements. Beyond these, fiber based mode-locked lasers have the ability of generating high-repetition-rate ultra-short optical pulses with low timing jitter and wide wavelength tuning range. A typical fiber based actively mode-locked ring lasers consist EDFAs or SOAs as gain media, EOMs such as amplitude modulators (AMs) or phase modulators (PMs) as mode-lockers, and tunable optical filters as wavelength selective elements. Optical pulses can be generated by AM mode-locking and FM mode-locking. However, AM mode-locking is preferred due to its ability to generate more stable optical pulses compared to those generated by FM mode-locking. This is because optical pulses have the tendency to switch randomly between the two phase maxima (i.e., 180° apart relative to the modulated signal) in FM mode-locking, which result in the increased pulse instability [100]. Only actively mode-locked fiber ring lasers based on AM mode-locking will be discussed in this dissertation.

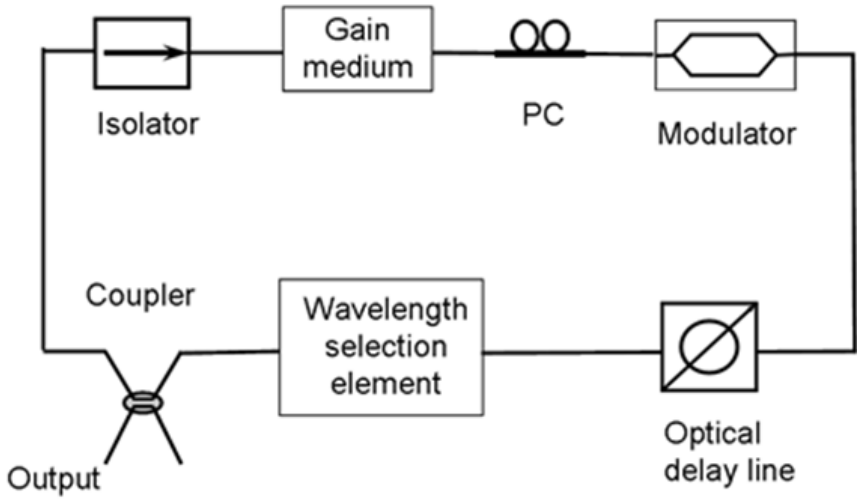

Figure 4.1 A typical configuration of an actively mode-locked fiber ring laser.

4.1 Introduction

4.1.1 Fiber ring laser basics

The typical structure of an actively mode-locked fiber ring laser is shown in Figure 4.1. The gain medium is used to compensate the cavity loss which can be an EDFA, an SOA, a FOPA, etc. The modulator is employed to lock the phase of the multiple longitudinal modes of the oscillator, which can be an EOM, an EAM, a PM, or even all-optical modulators like a nonlinear optical loop mirror (NOLM), cross-gain modulation (XGM) in an SOA, cross-absorption modulation (XAM) in an EAM, phase modulation using the Kerr effect in a length of optical fiber, passive mode-locking using a linear optical amplifier and a semiconductor saturable absorber. The optical delay line (ODL) is used to adjust the cavity length so that the modulation frequency applied to the modulator is an integer number of the mode-spacing of the cavity. The wavelength selection element is used to select the required wavelength of this laser, which can be a tunable bandpass filters (BPF), a FBG, or even other mechanisms like self-adjusting wavelength in a dispersive cavity or tuanble narrow-band optical amplification. The isolator is used to ensure the unidirectional operation of the laser.

As can be seen from Figure 4.1, the key component for active mode-locking is the modulator. Let us assume this is an intensity modulator. By applying a periodical electrical signal such as a sinusoidal RF signal to the intensity modulator, the light can pass the modulator periodically; in another word, the cavity loss is changed periodically. Only in the time duration when the modulator is 'on' the pulse shall be allowed to pass through. From the temporal perspective, the period of the pulse train should be equal to the round-trip time that one pulse needs to travel in the cavity. From the spectral perspective, only the modes having the same phase can oscillate in the cavity. So after traveling more and more round trips, the phase of the modes are locked and periodical short pulses are formed in the time domain. The theory of active mode-locking in fiber lasers has been discussed extensively [101]. However, it can be simply explained as follows [102].

Let us assume the cavity length is $2d$, the speed of light in the medium is c, so the mode spacing of the cavity is $c/2d$. Assume multiple modes are phase locked, and each mode can be represented by a uniform planar wave traveling in the z direction with speed $c=c_0/n$ where n is the refractive index of optical fiber. So the combined electromagnetic field equation of all the phase-locked modes can be represented as:

$$U(z,t) = \sum_q A_q \exp[j2\pi\nu_q(t-\tfrac{z}{c})] \tag{4.1}$$

where

$$\nu_q = \nu_0 + q\nu_F, \quad q = 0, \pm1, \pm2, \ldots \tag{4.2}$$

and ν_q is the frequency of mode q. Substituting (4.2) into (4.1) and assigning ν_0 as the central frequency of the laser lineshape at q=0, (4.1) can be written as:

$$U(z,t) = A\left(t-\tfrac{z}{c}\right)\exp[j2\pi\nu_0(t-\tfrac{z}{c})] \tag{4.3}$$

where

$$A(t) = \sum_q A_q \exp(\tfrac{jq2\pi t}{T_F}) \tag{4.4}$$

$$T_F = \frac{1}{\nu_F} = \frac{2d}{c} \tag{4.5}$$

The complex amplitude $A(t)$ in (4.4) is a periodic function of period T and $A(t-z/c)$ is a periodic function of z with period $cT = 2d$. Consider M modes ($q = 0, \pm1, \pm2, \ldots \pm$

S, so that $M = 2S + 1$), whose complex coefficient are all equal, $A_q = A, q = 0, \pm 1, \pm 2, \ldots \pm S$. Then the optical intensity can be expressed as:

$$I(t,z) = |A|^2 \frac{\sin^2 |M\pi(t-\frac{z}{c})T|}{\sin^2 |\pi(t-\frac{z}{c})T|} \tag{4.6}$$

where m is the number of modes. Figure 4.2 shows the frequency distribution and the temporal distribution of the intensity of M waves of equal phase. The results of the waveform are summarized in Table 4.1.

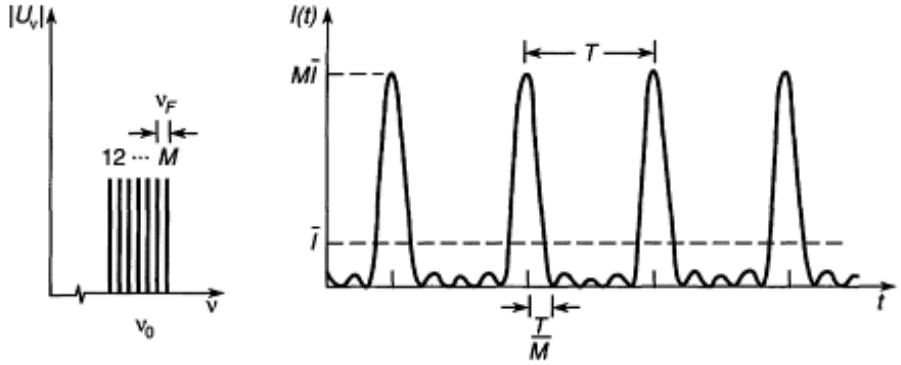

Figure 4.2 (a) Frequency distribution of M waves of equal intensity and phase. (b) Temporal distribution of M waves in mode-locking condition [102].

Table 4.1 Waveform results of the mode-locked lasers.

Temporal period	$T = 2d/c$
Pulse width	$\tau_{pulse} = \frac{T}{M}$
Spatial period	$2d$
Pulse length	$d_{pulse} = 2d/M$
Mean intensity	$\bar{I}$
Peak intensity	$I_p = MI$

From the results we can see that the mode-locked lasers can produce a train of periodically spaced short pulses in the form of one dominated short pulse and some weaker side pulses in a period. The pulsewidth of the mode-locked laser will become shorter with an increasing number of mode-locked modes, at the same time the mean

intensity as well as the peak intensity of the pulses will increase too. If there is an all-optical modulator in the cavity, such as a NOLM, a SOA, or an EAM, the actively mode-locked fiber ring laser can be used for all-optical clock recovery.

4.1.2 EDFRLs and SFRLs

EDFA based fiber ring lasers or EDFRLs operating at various repetition rates with different configurations have been demonstrated in the past decades [103-110]. Despite the numerous advantages that EDFRLs have such as simple and cost-effective laser cavity configuration, broad gain bandwidth in the C-band and ability of generating nearly transform-limited pulses, they face a severe challenge of long-term stability. Unlike semiconductor lasers, EDFRLs are composed of fiber-pigtailed optical components and fiber cavities which range from tens of meters up to hundreds of meters. Laser instability arising from the long fiber cavity is primarily due to three reasons: change of light polarization in the cavity, cavity length drift, and supermode noise.

Changes of the SOP can be solved by using all polarization-maintaining fiber laser cavities and stable laser operation was successfully demonstrated [103, 104]. Active cavity control was widely exploited to compensate random cavity length drift due to temperature variations and mechanical perturbations. For example, a stabilization scheme based on phase-locked loop (PLL) which relies on locking the optical pulse phase with that of the electric drive source was reported [107, 111]. Another stabilization method was demonstrated by observing the relaxation oscillation RF power of the detected output pulses as the index of instability and controlling the cavity length to minimize the RF power [105]. A similar method was used to stabilize an EDFRL by detecting the differential noise increase at different RF frequencies (i.e., corresponding to relaxation oscillation and beating between supermodes) when there are cavity length drifts [106]. Regenerative mode-locking is also an effective way to stabilize the EDFRLs which is accomplished by feeding back the longitudinal self-beat signal which is detected with a high-speed photodetector (PD) and a high Q filter [107, 112]. The phase between the optical pulses and the electric driving signal is automatically adjusted which can reflect instantaneous phase change between the longitudinal beats. Lasing is initiated by the

noise through the use of artificial loss modulation, and modulation frequency is automatically adjusted according to the cavity length drift.

Supermode noise, which arise from beating between different subsets of the cavity resonance modes which are phase-locked and separated by the modulation frequency, is the main source of amplitude noise of mode-locked pulses. It originates from the fact that the relaxation time of the erbium gain medium is much longer than the pulse spacing which can be suppressed in several ways. For example, nonlinear pulse limiting approaches have been demonstrated to stabilize pulse intensity by using either NRP or SPM in the highly-nonlinear fiber [113, 114]. The laser cavity is set such that optical pulses with higher intensity suffer from higher loss when passing through the pulse limiting mechanism. In [113], this is achieved by adjusting the birefringent elements and the polarizer. In [114], however, this is achieved by properly adjusting the amount of SPM and the limiting filter bandwidth. A much simpler way to suppress supermode noise is to introduce a high-finesse fiber Fabry-Perot (FP) etalon filter inside the laser cavity whose FSR is the same as the modulation frequency of the laser [115]. In this way, only supermodes whose frequencies match the peaks of the pulse-rate etalon filter can lase while all the other unmatched modes will be suppressed. From a temporal perspective, each pulse that emerges from the etalon filter represents a weighted average of many input pulses, so pulse amplitude fluctuation can be well suppressed. Lastly, it is also reported that SOAs can be added into the cavity to suppress supermode noise because of the fast gain saturation feature of the SOAs [110, 116].

SOA fiber ring lasers or SFRLs have attracted great interests as well. Compared with EDFRLs, SFRLs have shorter cavity length and thus are more robust to temperature changes and environmental perturbations. Besides, SOAs have a shorter carrier lifetime compared with EDFAs, therefore are usually included in fiber lasers where EAMs are used as the mode-locker to prevent high optical energy due to Q-switching which can potentially damage EAMs [117, 118]. Typically, EAMs can be modulated by either applying a RF drive signal [117] or by applying a modulated optical signal which can cross modulate the loss of EAMs [118]. Another advantage of this configuration is that SOAs can be monolithically integrated with EAMs to build compact optical pulse sources. Noting that EDFAs are usually limited in the C-band, SOAs with a broad gain bandwidth

can be made which are helpful to implement broadband fiber lasers. In [119], ~100 nm tuning range has been achieved by using a broadband SOA together with a birefringence loop mirror filter which is used to spectrally shift the gain peak of the SOA by controlling the transmission ratio.

On top of all the features of SFRLs mentioned above, SOAs can be used not only as the gain medium but also as the mode-locking element, which is realized through a nonlinear phenomenon referred to as the XGM. In this type of laser, an external optical pulse source is injected into the SOAs to saturate the gain and therefore imposes gain modulation over the lasing wavelength. This configuration provides many advantages over the conventional SFRLs. First, a single element is used as both the gain medium and the mode-locker which reduces complexity and cost. Second, polarization-insensitive SOAs can be used to replace polarization-sensitive EOMs. Third, high-speed mode-locking can be achieved due to fast gain saturation of SOAs. Since it is based on all-optical mode-locking, the SFRLs can also be used for all-optical clock recovery applications. SFRLs using SOAs as mode-lockers have been widely investigated [116, 120-123]. In [121, 123], up to 40 GHz repetition-rate single-wavelength optical pulses were achieved by using rational harmonic mode-locking in the SOA, and 30 GHz repetition-rate 48 oscillation wavelengths could be achieved taking advantage of the inhomogeneous linewidth broadening of the SOAs. In [116], an SOA was used as both the mode-locker and supermode noise suppressor while an EDFA was introduced in the cavity to complement the SOA gain. 28 dB supermode noise suppression ratio was achieved. Nearly linearly chirped pulses were generated and compressed to less than 4 ps when the cavity dispersion was anomalous while 11 ps nearly transform-limited pulses were generated without compression when the intracavity dispersion was normal.

In addition to optical gain media, mode-locking elements are another key component in fiber ring lasers. In traditional systems electro-optic amplitude or phase modulators driven by RF signals are used as mode-locking elements. However, the operating speed of this kind of mode-locker is limited by the available bandwidth of the EOMs and that of the RF driving source. On the other hand, it is also possible to achieve mode-locking using all-optical methods. In addition to XGM in SOAs and XAM in EAMs that have been discussed in previous sections, SOA based MZI [124, 125], XPM

in NOLM [126-128], and cross-polarization modulation (XPolM) in the HNLF [129] were also demonstrated. Taking advantage of the fast linear/nonlinear response from semiconductor based or fiber based media, mode-locking can be achieved at a higher frequency otherwise is difficult to be achieved by conventional methods. Moreover, it is possible to use all-optical mode-locked fiber ring lasers in optical signal processing functions such as synchronization to an external optical signal at a high repetition rate for applications in ultrafast all-optical logic operations [124], or all-optical clock recovery applications [118, 126, 129].

Passive optical filters are commonly used in mode-locked fiber ring lasers where the wavelengths of the lasing signals are selected by tuning the center wavelength of the optical filter. Cavity length or modulation frequency needs to be adjusted correspondingly to match with the new wavelength. In order to make wavelength tuning smoothly without interrupting the lasing signal, dispersion tuning has been demonstrated [119, 130-133]. A dispersive medium such as a linearly chirped FBG or a length of fiber can be introduced into the laser cavity and different wavelengths see distinct cavity lengths. Once the modulation frequency or the cavity length is changed, the lasing wavelength can be tuned automatically to match with this change. Continuous wavelength tuning is possible with this approach while the lasing signal keeps uninterrupted. Multi-wavelength operation is also possible with dispersion tuning when the cavity dispersion and gain bandwidth satisfy certain conditions [132].

4.1.3 Mode-locked FOPOs

Various types of actively mode-locked fiber ring lasers have been discussed above, in which EDFAs or SOAs are commonly used as the gain media and electro-optic amplitude or phase modulators as the mode-lockers. However, the amplification mechanism of EDFAs and SOAs relies on the energy transition between different energy states, which limits the available gain bandwidth and the wavelength regime achievable in this type of amplifiers. Mode-locking is realized by modulating the oscillating cavity modes by driving the EOMs with periodical RF signals such that the phases of the oscillating modes are forced to maintain their relative value. However, as the operating speed of this type of mode-locked fiber lasers is limited by the available bandwidth of the EOMs, the

need for higher bandwidth EOMs or novel ways to increase the repetition rate while keeping the small-bandwidth electronic increases.

FOPAs have attracted great interest in recent years due to the demand for amplification and lasing in unconventional optical bands [134]. The underlying parametric process is based on highly efficient four-photon mixing relying on the relative phase between the four interaction photons [33], and thus can provide large flat gain and broad gain bandwidth in any wavelength of interest under proper design. Besides, since parametric process is based on the Kerr effect which has ultrafast response and has been widely used in many ultra-high-speed optical signal processing applications [33, 134]. As one of the examples, parametric amplification can be used as an ultra-high-speed optical modulator in synchronously pumped actively mode-locked FOPOs. It has been reported that actively mode-locked FOPOs [56] can offer lasing wavelengths from the visible band to the short-wave infrared (SWIR) using either a pulsed-pump or a CW-pump [38, 54, 56-65, 135-139]. Moreover, ultra-short optical pulses (i.e., sub 50 fs) generation was also demonstrated [140].

Although a large number of papers have reported widely-tunable ultra-short pulse generation in FOPOs, very few have analyzed pulse generation with high repetition-rate. When using a synchronous-pumping scheme, parametric amplification can be used as a high-speed all-optical mode-locker taking advantage of its ultra-fast response time. Indeed, actively mode-locked FOPO at 10 GHz has been demonstrated using either an intra-cavity loss modulation [48, 49], or an external cavity synchronous-pumping (i.e., parametric gain) modulation [55, 141, 142]. However, they lack detailed analysis of the laser designs such as the pump requirements and the cavity settings which are essential for high-quality pulse generation.

In the following sections, the implementation of a synchronously-pumped actively mode-locked FOPO working at 10 GHz will be presented, and the effect of the pump and the cavity settings on the characteristics of the pulses will be studied in detail. Compared with the intra-cavity loss modulation method, synchronous-pumping scheme is found to provide many advantages in terms of reducing the total cavity loss, increasing the mode locking frequency, enabling ultra-high-speed pulses generation using RHML, and

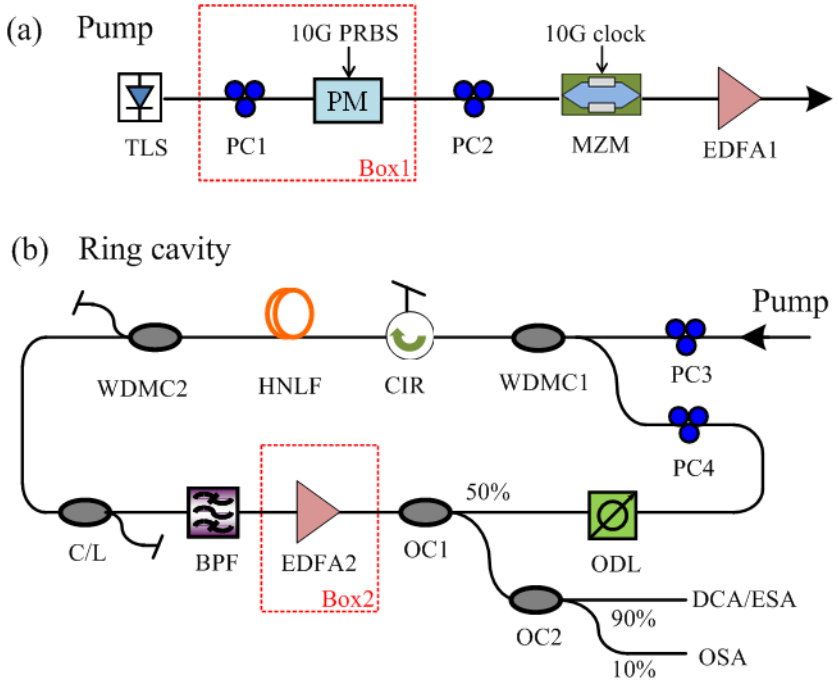

Figure 4.3 Experimental setup for an actively mode-locked FOPO working at 10 GHz.

application to all-optical clock recovery. The results and conclusions from this study form a foundation of designing mode-locked FOPOs with a higher repetition rate.

4.2 Operating principle and experimental setup

There are a number of ways to build a FOPO. One of the simplest is to build a ring structure. A typical setup for an actively mode-locked FOPO consists of two parts: a periodically modulated lightwave as the pump/seed signal (shown in Figure 4.1(a)) and a ring cavity (shown in Figure 4.1(b)) built with a gain medium, a mode-locking device, a wavelength selection element, and several fibers and couplers. The pump branch is comprised of a TLS, a PM, a MZM, and a high-power EDFA. To achieve a broader and flatter gain, the wavelength of the TLS should be set near the zero-dispersion wavelength in the anomalous dispersion regime of the fiber gain medium, here a length of HNLF. Since the linewidth from the TLS is narrow, phase modulation/dithering may be required to increase the threshold the SBS, depending on the nonlinear gain medium and the pump power required for amplification and/or mode-locking. It is reported that the SBS can be

suppressed by 32 dB by phase modulation of the pump using a 10 Gb/s pseudo-random binary sequence (PRBS) signal [48]. A periodic pump signal is generated by intensity modulation in a MZM driven by a 10 GHz clock signal. A PC is used to align the SOP of the incident light with the axis of the modulator. Then it is amplified by an EDFA before being launched into the ring cavity.

In the ring cavity, the key component is the HNLF where parametric amplification occurs. Since parametric gain is proportional to the instantaneous power of the pump signal and has a fast response [30], if the pump is a CW signal, parametric gain is kept constant over time if we ignore gain saturation, and the output will be CW light at the defined wavelength by the intra-cavity optical filter. On the other hand, if it is a periodically modulated pulse train as in this case, the parametric gain changes periodically in time in the same manner as that of the pump signal. By properly setting the cavity loss, the modulated gain can be higher or lower than the cavity loss so that mode-locking can be realized. Different from [48, 49] where mode-locking is realized by modulating the cavity loss using an intra-cavity MZM, it is achieved by modulating the cavity gain associated with synchronous-pumping in this case. There are several advantages of using this structure: first, it can reduce the cavity loss by removing the modulator; second, only a single mechanism is required to function as both the gain medium and the mode-locking device; third, higher modulation frequency can be applied to the all-optical mode-locker since the parametric process in the fiber has a very short response time; and finally, it is essential for RHML and all-optical clock recovery applications as will be discussed in later chapters. On the other hand, a complementary gain medium (e.g., an EDFA or an SOA) can be used to compensate part of the cavity loss, where the power budget for the pump would be less stringent and phase modulation might not be necessary. This is extremely helpful to reduce the root-mean square (RMS) timing jitter of the generated pulses and sustain RHML. In addition to the HNLF, a pair of WDMCs is included to couple/split the incident pump and the oscillating signal. In particular, the pump is discarded after passing through WDMC2. A C/L band coupler is also included to suppress unwanted wavelengths to prevent excess optical power from damaging the BPF. A BPF (i.e., Peleton filter which can be tunable in both wavelength and bandwidth) is used as the wavelength selection element which can be tunable over

C-band. An ODL is used to adjust the cavity length so that the condition for harmonic mode-locking (i.e., the modulation frequency of the pump equals a multiple integer of the cavity resonance frequency) can be achieved. Besides, a 3 dB OC is used to couple part of the light out of the cavity while the rest remains inside. PC3 and PC4 are used to align the SOP of the pump and the signal in order to achieve maximum gain efficiency.

The output signal is monitored in an optical sampling module (Agilent 86116C) with 65 GHz optical bandwidth connected to a digital communication analyzer (DCA, Agilent 86100). The nominal impulse response is 7.4 ps (though waveforms with a pulsewidth < 7 ps can be measured). The optical spectra were measured using an OSA with a minimum RBW of 0.06 nm. The supermode noise suppression ratio (SNSR) is measured using a broad-bandwidth photodiode connected to an electrical spectrum analyzer (ESA) with 40 GHz bandwidth and 10 kHz RBW. Timing jitter measurements are made by measuring the histogram of the optical pulses in the time domain using the DCA triggered with a precision timebase module (Agilent 86107A) operating in sample mode with a persistence time of 300 ms. The typical RMS jitter is < 100 fs. It is worth noting that this measurement technique is less accurate in cases where the timing jitter of the measured pulse is close to the jitter noise floor of the DCA, or when the measured pulses exhibit amplitude fluctuations. In these circumstances, a more accurate measurement technique, such as integrating the single sideband phase noise of the signal obtained in the electrical domain using a phase noise spectrum analyzer, should be used [143].

Table 4.2 and Table 4.3 show the specifications of the HNLF used and the default operating conditions of the mode-locked FOPO in the experiment. Note that by default, phase modulation is required (box 1 is ON) and an intra-cavity EDFA is not needed (box 2 is OFF).

Table 4.2 Specifications of the HNLF

Parameter	Value
Length	1001 m
Dispersion@1550 nm	-0.04 ps/nm/km
Dispersion slope@1550 nm	0.02 ps/nm^2/km
Loss	1.7 dB
Nonlinear coefficient	10 W^{-1}km^{-1}

Table 4.3 Default operation condition of the mode-locked FOPO

Parameter	Value
Pump wavelength	1556.5 nm
Pump duty cycle	33%
Pump power	0.35 W
Pump phase modulation (box 1)	ON
Intra-cavity EDFA (box 2)	OFF
Signal wavelength	1546.1 nm
Filter bandwidth	1.6 nm
Cavity dispersion management	No

4.3 Experimental results and analysis

4.3.1 Pump pulse duty cycle

First, we investigate the impact of the pump pulse duty cycle on the mode-locked pulse performance in terms of pulse width and root-mean square (RMS) timing jitter. The pump peak power keeps constant for different duty cycles. The results are shown in Figure 4.4. It is quite obvious that the output pulse width decreases from 14.7 ps to 8.8 ps with decreasing pump duty cycle. On the other hand, the RMS timing jitter also decreases

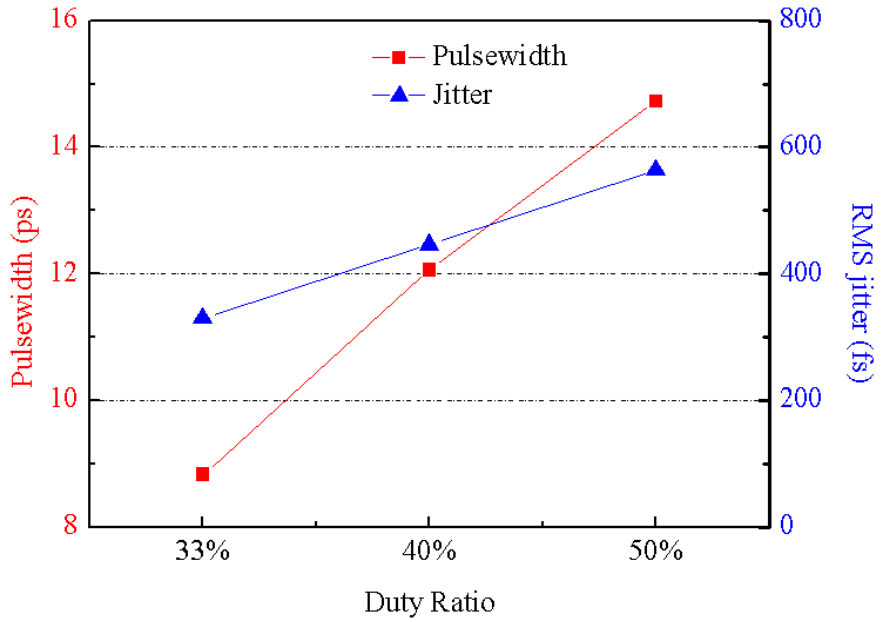

Figure 4.4 Impact of pump pulse duty cycle on the mode-locked pulse.

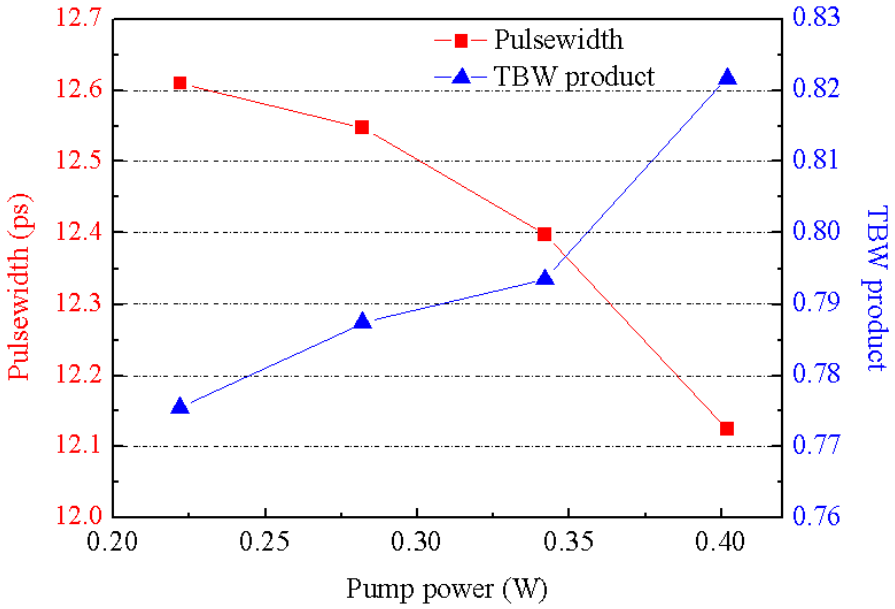

Figure 4.5 Impact of pump power on the mode-locked pulse. (Filter BW=0.8 nm).

with a reduced duty cycle. Specifically, it reduces from 563 fs to 329 fs when the duty cycle decreases from 50% to 33%. The results demonstrated that stable mode-locking can be achieved in a FOPO with shorter pump pulses. This is very helpful when we want to

generate high-repetition-rate pulse trains with very short pulse width using a commercialized pulsed source (we will discuss this further in later sections). However, it is worth noting that for ultra-short pulse generation (< 1 ps) walk-off between the pump and the signal will broaden the output pulse and limit the tuning range of the signal wavelength [63, 140]. Therefore, a careful design of the FOPO cavity is necessary.

4.3.2 Pump power

A high pump power gives larger parametric gain and therefore more output power. Besides, it also affects the pulse quality. Under perfect phase-matching conditions, parametric gain is exponentially proportional to the instantaneous pump power, and therefore the signal pulse duration can be effectively shortened compared with that of the pump. This feature has been used to produce short pulses in a FOPA [144]. In the case of a FOPO, we also find similar behavior as shown in Figure 4.5. In this measurement, the filter bandwidth (BW) is chosen to be 0.8 nm instead of 1.6 nm in order to prevent wavelength hopping due to the shift in the parametric gain spectrum under high pump power. However, the results should also apply to the case with 1.6 nm filter BW. From Figure 4.5, it can be observed that when the pump power is increased from 0.22 W to 0.4 W, the corresponding pulse duration decreases from 12.6 ps to 12.1 ps. Nonetheless, this decrease of pulse duration is at the expense of an increase in TBW product which rises from 0.77 to 0.82. The TBW product is defined as the product of the FWHM pulse duration and the 3 dB bandwidth of its optical spectrum. The TBW product of a chirp free pulse is 0.441 for Gaussian pulse shape and 0.315 for sech^2 pulse shape. The 3 dB bandwidth was measured in an OSA with 0.2 nm RBW and the center wavelength was measured in the middle of the filter passband. The relative large TBW product indicates that the output pulse is chirped, which is mainly due to XPM between the pump and the signal [63, 145]. This can be confirmed from the fact that the TBW product/frequency chirp increases with increasing pump power. We will see in the next section that this nonlinear frequency chirp can be partially compensated by intra-cavity dispersion management.

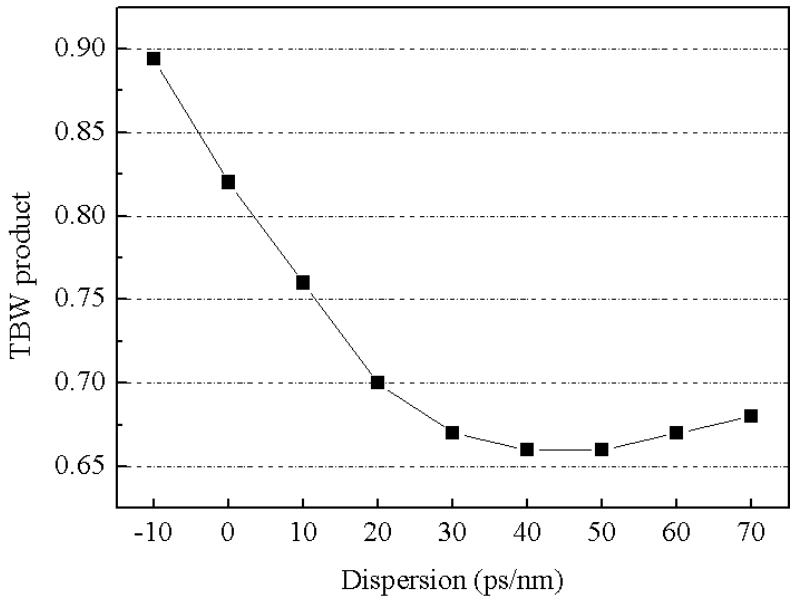

Figure 4.6 Impact of intra-cavity dispersion management on the mode-locked pulse. (Filter BW=0.8 nm)

4.3.3 Pulse chirp compensation

We have discussed that the large TBW product of the generated pulse is due to the frequency chirp induced by XPM. It is observed in our experiment that this nonlinear chirp can be partially compensated using intra-cavity dispersion management. We use a tunable dispersion compensator (TDC) which has a 3 dB bandwidth of 0.8 nm. Therefore, the filter BW is also set as 0.8 nm. The results are shown in Figure 4.6. The cavity dispersion without the TDC is 0.13 ps/nm. So when TDC is set at -10 ps/nm, the lasing wavelength is in the normal dispersion regime ($D < 0$). As we know that XPM will cause a quasi-positive chirp similar to the case when the pulse is propagating in the normal dispersion medium [30], the combination of these two effects causes a large positive chirp to the pulse. This is confirmed by the fact that the TBW product rises from 0.82 to 0.89 when the dispersion decreases from 0 to -10 ps/nm. On the contrary, when the TDC is set in the anomalous dispersion regime ($D > 0$), the TBW product decreases because XPM induced quasi-positive chirp is partially canceled out with anomalous dispersion induced negative chirp. The minimum TBW product is obtained when the TDC is set at

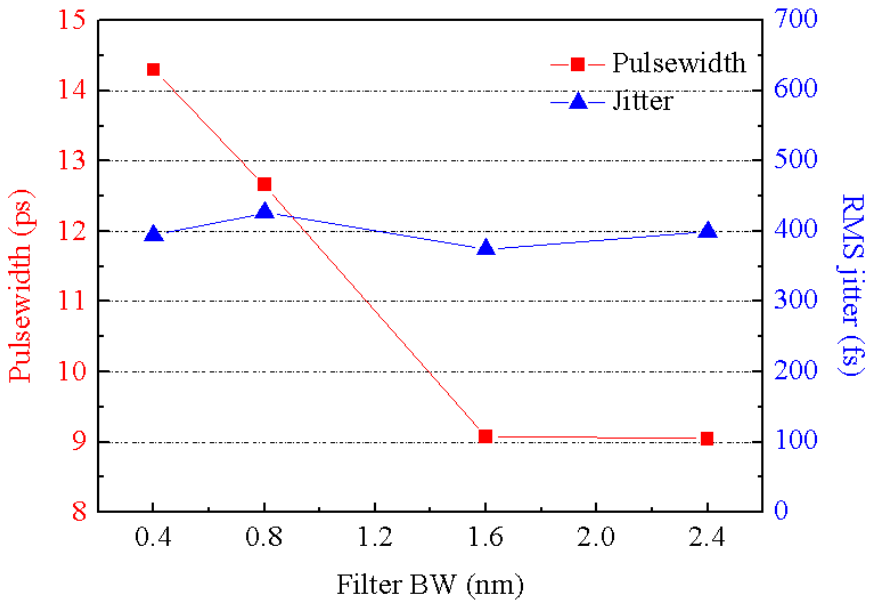

Figure 4.7 Impact of intra-cavity FBW on the mode-locked pulse.

40 ps/nm. The pulse is still not transform limited because this linear chromatic dispersion cannot cancel out entirely the nonlinear phase modulation from XPM.

4.3.4 Filter bandwidth (FBW)

The bandwidth of the BPF affects the output pulse duration directly. In order to choose the BPF with a suitable bandwidth, we change the filter BW from 0.4 nm to 2.4 nm and see its impact on the output pulse. As can be seen from Figure 4.7, the shortest pulses (9.1 ps) are obtained when filter BW is 1.6 nm. When the filter BW is smaller than 1.6 nm, a portion of the spectral sidebands is cut off by the filter and thus increases the pulse duration. On the other hand, when the filter BW is greater than 1.6 nm, the pulse width remains almost the same. In terms of RMS timing jitter, the best case is obtained at a filter BW of 1.6 nm. This indicates that the most stable mode-locking can be achieved with 1.6 nm FBW. A larger bandwidth will introduce more noise and therefore larger jitter to the mode-locked pulse. Although 1.6 nm is the optimum optical filter bandwidth to achieve the best performance for mode-locked pulse generation, we used 0.8 nm for some of our analysis (e.g., pump power and pulse chirp compensation) due to restrictions

such as the limited bandwidth of the tunable dispersion compensator or the high pump power induced wavelength drift.

4.3.5 Wavelength tuning characteristics

Wavelength tuning range is one of the most important parameters for a laser source. Tunability of the proposed mode-locked FOPO is achieved by adjusting the central wavelength of the intra-cavity BPF. A sample waveform of the input pump pulses is shown in Figure 4.8 (a). Note that the pump power is different for different lasing wavelengths (e.g., higher pump power is required for lasing at shorter wavelengths). A sample waveform of the mode-locked pulses at the output of the FOPO is shown in Figure 4.8 (b). A sample lasing spectra of this FOPO is shown in Figure 4.8 (e). The characteristics of the output pulses (i.e., pulse width, TBW product, and RMS timing jitter) are also characterized and the results are shown in Figure 4.8 (c, d). It is observed that the mode-locked FOPO can be tuned from 1529.9 nm to 1552.2 nm, which is 22.3 nm. The same tuning range is expected in the Stokes-band because of the symmetric property of the parametric gain with respect to the pump frequency. However, we could not verify this experimentally since the BPF used in our experiments only operates in the C-band. By taking into account both the Stokes- and anti-Stokes bands, the combined tuning of the FOPO is over 44.6 nm. The tuning range is limited by the available bandwidth of the BPF (C-band) and WDMCs (3 dB attenuation point is 1551.4 nm). In addition, it is also limited by the parametric gain bandwidth which depends on the characteristics of the HNLF (e.g., fiber length, nonlinearity, dispersion, birefringence, etc.) and pump peak power [54].

In the wavelength range from 1535 nm to 1552 nm, the pulse duration and the TBW product of the mode-locked pulses keep almost constant – around 9 ps and 0.8, respectively. The RMS timing jitter is around 400 fs. However, when the wavelength is below 1535 nm, the pulse width starts to increase as does the TBW product. This is because the parametric gain at shorter wavelength is smaller than that at the central wavelength, so a higher pump power is required to compensate the loss. Therefore, more ASE noise is added into the cavity which reduces the mode-locking strength. This leads to increased pulse width and worse jitter performance. In the meantime, the TBW product

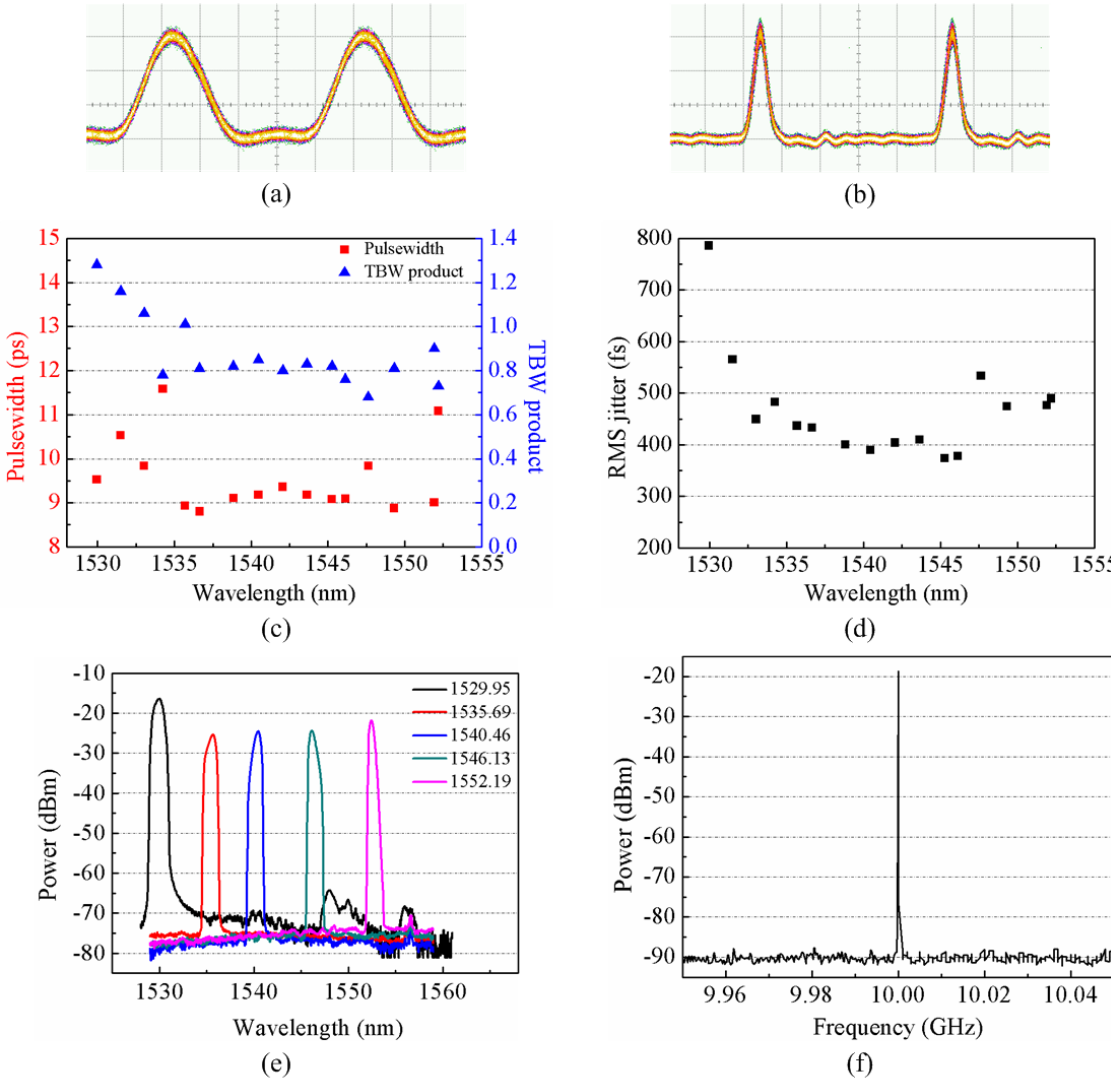

Figure 4.8 Characteristics of a 10 GHz harmonically mode-locked FOPO. (a) Waveform of the input pump pulses with 33% duty cycle. 20 ps/div. (b) Waveform of the output mode-locked pulses. 20 ps/div (c) Pulsewidth and TBW product characteristics vs. tunable wavelength. (d) RSM timing jitter performance vs. tuning wavelength. (e) Tunable lasing spectra of the FOPO. RBW = 0.06 nm. (f) Electrical spectrum of the mode-locked pulses (waveform shown in figure (b)) from the FOPO. RBW= 10 kHz.

is increased because of the spectral broadening induced by a higher pump power. We note that in most cases, the RMS timing jitter of the output pulses is less than that of the pump pulses. This can be attributed to three possible reasons. First, it has been reported that for the same pulse energy, shorter pulses come with less timing jitter in mode-locked lasers [146]. This is in accordance with the results we obtained in section 4.3.1. Second, pulse regeneration occurs due to the nonlinear transfer function of the saturated

parametric amplifier [147]. Finally, the combined effect of spectral broadening due to SPM and spectral filtering by the intra-cavity filter helps to alleviate mode hopping in the FOPO [114]. In addition, we also characterize the output power of the FOPO. The maximum average power is obtained at 1542.2 nm which is 3.1 mW. Thus the peak power can be calculated to be 33.3 mW. The average output power is around 2 mW. Compared with the results obtained using a 0.8 nm BPF (i.e., pulse width: 12.5 ps, TBW product: 0.8, RMS jitter: 450 fs), using a BPF with 1.6 nm FBW can produce much better mode-locked pulses in terms of shorter pulse duration and less RMS timing jitter.

We also show a typical RF spectrum of the signal from the mode-locked FOPO in Figure 4.8 (f). Since the cavity resonance frequency is ~ 200 kHz, the RF spectrum is measured with a RBW of 10 kHz over a frequency span of 100 MHz. It can be observed that the SNSR is ~70 dB which means that the generated pulses are very stable in amplitude. A very important reason for the high SNSR in a FOPO is attributed to the ultrafast response of the parametric process in optical fiber. The individual pulse energy is well equalized because of the instantaneous parametric gain as opposed to the slow gain recovery in erbium-doped fiber lasers in which the SNSR is usually low. The other reason for the high SNSR is due to the combined effect of spectral broadening of the signal due to SPM and spectral filtering by the intra-cavity filter [114]. We have performed a separate experiment to verify this effect. We observed that for a specific filter bandwidth, e.g., 0.8 nm or 1.6 nm, the SNSR increases with increasing pump power and reaches a maximum value at a particular pump power (360 mW and 390 mW corresponding to filter bandwidths of 0.8 nm and 1.6 nm, respectively, see Figure 4.9). This is because the larger the pump power is, the larger the parametric gain will be, and so will be the signal power in the cavity. Therefore, more spectral broadening of the signal occurs due to SPM. At a certain point when the spectral broadening matches the filter cutoff bandwidth, the combined effect of SPM and spectral filtering functions as an amplitude limiter that reduces amplitude fluctuation of the mode-locked pulses. However, if the pump power increases beyond the optimal point, the amount of spectral broadening exceeds the filter bandwidth and the SNSR starts to decrease. Furthermore, the oscillating modes become unstable because of excessive gain in the cavity.

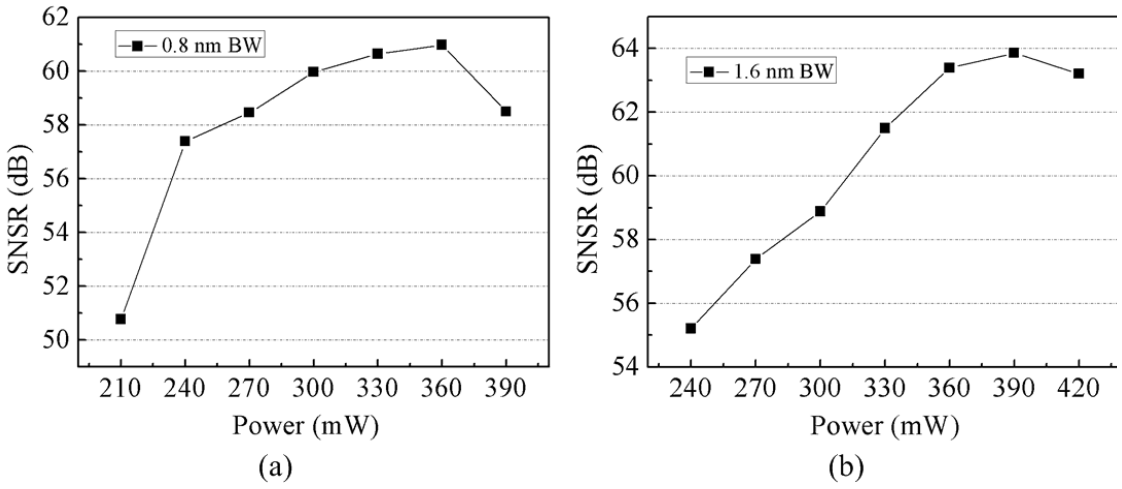

Figure 4.9 Dependence of SNSR on average pump power for different values of filter bandwidth.

4.3.6 Pump phase modulation

Phase modulation of the pump can be eliminated if a complimentary EDFA is incorporated in the cavity (i.e., in Figure 4.3, box 1 OFF and box 2 ON). This is because the EDFA gain can help compensate part of the cavity loss rather than the parametric gain itself. Therefore, lower pump power (i.e., below the SBS threshold) is required and no phase modulation is needed. We have tested the performance of this FOPO structure (i.e., with an intra-cavity EDFA and without pump phase modulation) under almost the same experimental setup/conditions, except that the pump power is only 0.07 W and an intra-cavity EDFA is inserted which provides an open-loop small-signal gain of 14 dB. The characteristics of the output pulses are shown in Figure 4.10.

The tested tuning range of this configuration is 23.8 nm (from 1528.7 nm to 1552.5 nm). Together with the same tuning range expected in the Stokes band, the total tuning range is 47.6 nm which is slightly larger than the previous configuration (i.e., box 1 ON and box 2 OFF). The pulse width is around 9 ps over most of the tuning range. The pulse duration becomes larger at the edge of the tuning region because the mode-locking strength becomes weaker due to the smaller parametric gain and larger cavity loss in this region. This agrees with the results obtained in the previous configuration. However, the

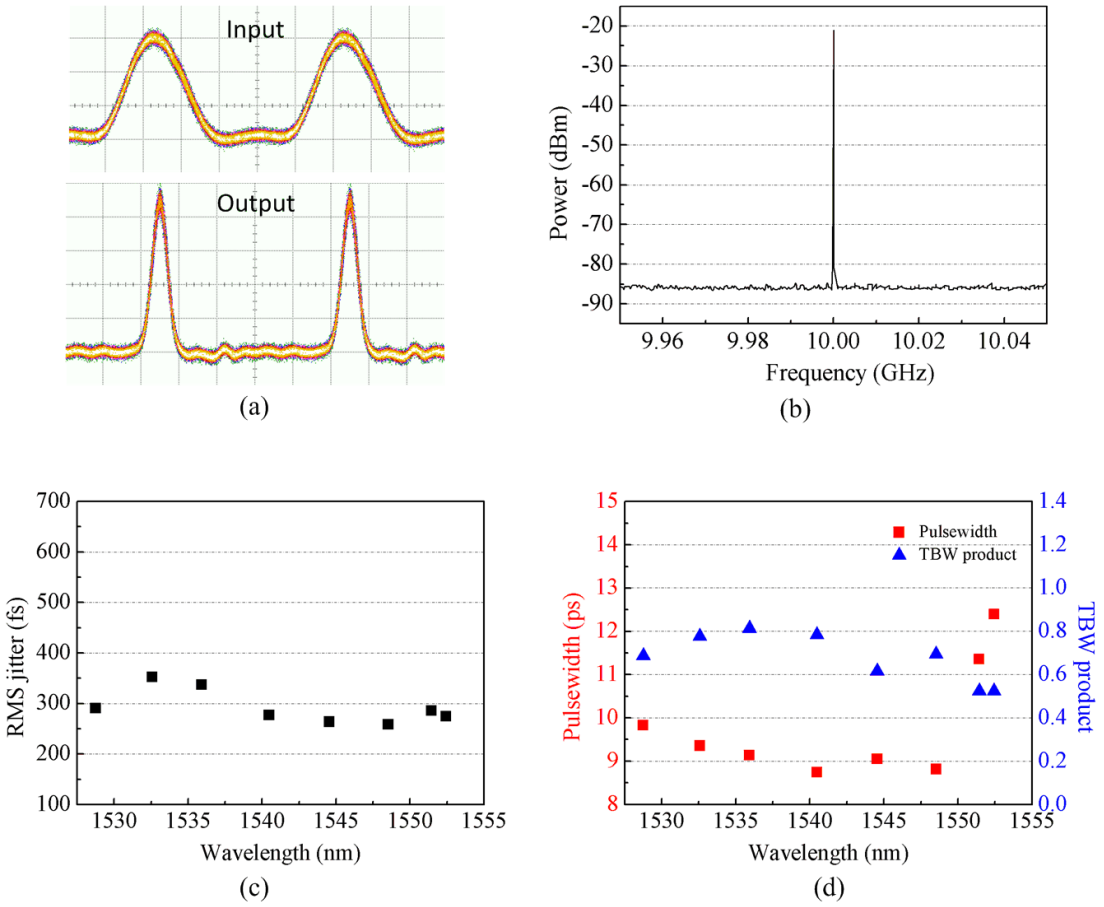

Figure 4.10 Characteristics of the mode-locked pulses when no PPM is applied. (a) Waveforms of the input pump pulses and the output mode-locked pulses. 20ps/div. (b) Electrical spectrum of the mode-locked pulses. RWB: 10 kHz. (c, d) RMS timing jittr, pulsewidth, and TBW product vs. tuning wavelength.

TBW product is a bit different. In this case, since the EDFA can provide gain over the entire C-band, especially larger gain at shorter wavelengths, the requirement for parametric gain in this regime can be relieved. Therefore, there is no need to increase the pump power dramatically as in the previous configuration. This leads to a smaller and flatter TBW product (~ 0.7) over the entire tuning range.

Moreover, the RMS timing jitter is measured to be around 300 fs, which is much lower than that in the previous configuration (i.e., without the EDFA and with pump phase modulation). It is reported that pump phase modulation can cause parametric gain modulation in a FOPA [148] which can cause instability of the oscillating modes in the FOPO. This results in a larger RMS timing jitter when pump phase modulation is applied.

In order to verify if the intra-cavity EDFA also contributes to the reduction of timing jitter, we placed the EDFA in the cavity while still applying pump phase modulation. In this case, the RMS timing jitter was measured to be ~ 600 fs, which is even worse than before. Therefore, we confirm that the reduction of timing jitter is largely due to the elimination of pump phase modulation. It is worth noting that the minimum RMS timing jitter is measured to be 258 fs at a wavelength of 1548.5 nm. The result is comparable with that obtained using a regenerative feedback loop configuration which is 230 fs [141], however without using an expensive ultra-low-jitter self-starting EAM based optoelectronic oscillator (EAM-OEO). The RF spectrum shows that the SNSR is ~ 64 dB. This is a little lower than the previous case (i.e., ~ 70 dB SNSR without an intra-cavity EDFA) which indicates the hybrid gain of EDFA and parametric gain can cause more amplitude fluctuations than parametric gain itself. This is because the relaxation time of the erbium ions in the EDFA is much longer than the cavity mode-spacing so that the energy distribution among different modes is not uniform. This leads to the oscillation of supermodes that cause amplitude fluctuations of the mode-locked pulses. The results show that in general the FOPO configuration without pump phase modulation is very promising in terms of generating high quality mode-locked pulses with low cost. However, drawbacks such as degraded SNSR and limited tuning range caused by the intra-cavity EDFA (or any other gain medium) must also be considered.

4.4 Discussion and conclusion

In this chapter, various kinds of fiber based actively mode-locked lasers are reviewed and compared. As conventional gain media, EDFAs and SOAs provides limited gain bandwidth and wavelength regime due to their amplification mechanism which is based on energy transition among different energy states. On the contrary, FOPA based gain provides broad gain bandwidth and arbitrary wavelength regime since it only relies on the phase matching between the interacting wavelengths. However, the results demonstrated in this chapter are limited by the performance of available components such as the HNLF when the experiments were performed. Better results may be obtained if the HNLF parameters such as dispersion, length, nonlinear coefficient, zero-dispersion wavelength fluctuation are optimized. In addition, the fast parametric gain response brings the unique

feature of very high SNSR compared with EDFA or SOA based fiber lasers. Following the discussion of gain media, active mode-locking schemes are also reviewed and concluded that all-optical mode-locker provides additional features than conventional EOMs such as higher modulation bandwidth, possibility of direct injection of optical drive signals, realization of both amplification and mode-locking in one device, and potential to be used for all-optical clock recovery. Parametric amplification provides gain modulation in the mode-locked laser which can be potentially very fast. Although only 10 GHz operation is demonstrated in this chapter, its performance with a higher repetition rate will be discussed in the next chapter.

We investigated a harmonically mode-locked FOPO working at 10 GHz in detail in terms of analyzing the impact of pump pulse duty cycle, pump power, intra-cavity dispersion management, intra-cavity filter bandwidth, and pump phase modulation on the characteristics of the mode-locked pulse quality. The results show that by properly configuring the experimental setups and parameters (e.g., pump pulse with smaller duty cycle, higher pump power, with intra-cavity dispersion management, without pump phase modulation, and with a proper FBW), mode-locked pulses with shorter duration, less RMS timing jitter, less TBW product and high SNSR can be generated. The wavelength tuning range and the corresponding pulse characteristics were also discussed.

Chapter 5 Rational Harmonically Mode-locked FOPO

Harmonically mode-locked fiber ring lasers have been discussed in the previous chapter, where the pulse repetition rates (i.e., f_{rep}) equal the modulation frequencies (i.e., f_{mod}) of the mode-locker. Modulation frequencies are integer multiplies of the cavity resonance frequencies (i.e., $f_{mod} = m \times f_{cav}$) and mode-locking enforces a constant phase relation between the multiple cavity lasing modes. As a result, repetition rates of harmonically mode-locked fiber ring lasers are limited to the modulation speed of the mode-lockers and the bandwidth of the driving electrical or optical signals. However, the demand for building mode-locked lasers with higher repetition rates while remaining the usage of cost-effective low-speed electronics is growing due to the increasing importance in high-speed optical communication systems, ultra-high-speed all-optical signal processing, microwave photonics, etc.

In response to the demand for mode-locked lasers with high repetition rates, various methods have been proposed and demonstrated by researchers in which the repetition rates of the mode-locked lasers were multiplied from several GHz to tens of GHz, and even to sub-THz. These methods can be broadly divided into two categories: nonlinear methods and linear methods. For example, in [149] optical pulses with repetition rate as high as 0.3 THz was generated by using modulation instability in optical fiber. As opposed to nonlinear methods, predominant ways for pulse repetition rate multiplication are using linear methods which include amplitude and/or phase spectral filtering, temporal Talbot effect, biasing the MZM in the nonlinear regime, rational harmonic mode-locking, etc. In this chapter, rational harmonic mode-locking is exploited in an actively mode-locked FOPO to achieve repetition rate multiplication. The results will be compared with those obtained by biasing the MZM in the nonlinear regime.

The rest of this chapter will be organized as follows: section 5.1 is devoted to review and compare different pulse repetition rate multiplication approaches. The technique of doubling the repetition rate in a FOPO by biasing the MZM at the minimum transmission point will be demonstrated and discussed in section 5.2. In contrast, rational

harmonic mode-locking of a FOPO will be described subsequently in section 5.3 and will be compared with the previous method. Finally, high-speed mode-locking of a FOPO from 40 GHz up to 240 GHz by RHML will be demonstrated in section 5.4. The chapter will be concluded in the last section.

5.1 Pulse repetition rate multiplication methods

5.1.1 Amplitude-only spectral filtering

The optical spectrum of a periodic optical pulse train contains periodic features which include not only its fundamental modes but also higher-order modes. These modes are separated by an amount equal to the pulse repetition rate. The relative amplitude and phase of each mode are determined by the pulse shape. It is straight forward to achieve pulse repetition rate multiplication by using an intra-cavity filter to select higher-order longitudinal modes while filtering out the intermediate modes. This method has been demonstrated using a fiber FP filter in both FM and AM mode-locked fiber lasers [150, 151]. Very stable optical pulses with low amplitude fluctuation and timing jitter can be generated using this method since only those longitudinal modes with frequency spacing equal to the FSR of the FPF are enhanced while all the other modes are suppressed in the mode-locking process. However, FP filters with high finesse must be used in order to prevent amplitude modulation of the optical pulse trains, which can result in high sensitivity to line-rate detuning due to the narrow bandwidth. It is also demonstrated that low finesses FPF can still be used without inducing much amplitude modulation by using a double-passing FPF structure since the decay time of the impulse response of the FPF is extended while a larger bandwidth is still maintained [152].

Instead of using an intra-cavity optical filter, external filtering is also possible with various devices, among which FBGs are the most attractive devices due to their compact size and low insertion loss. In [153], four uniform FBGs with low reflection were used to introduce a relative time delay between the three replicas of the original optical pulses. However, a positioning accuracy of 1 um is required in the grating-writing system. Similarly, a sinc-sampled FBG was designed to filter out the intermediate longitudinal modes and pulse repetition rate multiplication was achieved from 10 GHz to

40 GHz [154]. It is worth to note that periodical spectral response with narrow passbands, a square envelop amplitude response and a periodic phase response are required for FBGs. In addition, FBGs and optical pulses must be carefully adjusted so that the center frequencies of the passbands of the FBGs must match with the higher-order modulation sidebands of the optical pulses. In the real cases, deviations from the ideal cases are expected which are due to the grating-writing inaccuracies. Since the repetition rate of the generated optical pulses is determined by the spacing between individual maxima in the grating's spatial profile, it turns out that a shorter spacing between the maxima is required to achieve a higher repetition rate, and therefore the fabrication complexity increases for higher repetition-rate pulse generation [155]. To solve this problem, superimposed FBGs operating in reflection are used to achieve amplitude/phase spectral filtering, in which shorter gratings are necessary and the maximum repetition rate is only limited by the bandwidth of the original pulse [155, 156].

5.1.2 Phase-only spectral filtering

An alternative approach to multiply the repetition rate of an existing pulse source or to build a burst pulse source is spectral phase filtering. Both spectral amplitude and phase filtering process the optical pulses in the frequency domain. But opposed to spectral amplitude filtering, in which periodical set of the frequency components of the optical pulses are selected while the rest are filtered out, almost no energy of the frequency components are lost during the process of spectral phase filtering (i.e., the insertion loss of the pulse shaping device is not taken into account). In spectral phase filtering, the phase response of the filter changes periodically with frequency, but the amplitude response remains the same. The repetition rate of the filtered pulse train is equal to the frequency periodicity of the filter, while the amplitude of the pulse train depends on the pattern of the phase response within a single period.

Using a home designed femtosecond pulse shaping apparatus, in which the optical frequency components of the pulses were spatially dispersed using a lens and grating apparatus and were spatially filtered with a phase mask fabricated on fused silica substrates, repetition rates up to 6 THz are achieved in [157]. It is also reported that a phase response with an autocorrelation that consists of a series of isolated spectral peaks

must be chosen to obtain a burst of pulses under a smooth envelope by using a phase filter. The phase masking approach was observed to exhibit overall amplitude ~15 times higher than that of the amplitude masking. It was also reported that two-to-five-times repetition-rate multiplication of a 9 GHz source was achieved by using phase-only line-by-line pulse shaping [158]. With an ~ 18mm diameter input optical beam, a 1200 grooves/mm diffraction grating, and a 2 × 128 pixel liquid crystal modulator (LCM) array, independent control of both amplitude and phase of individual spectral lines can be achieved with 2.6 GHz resolution. Different from a burst pulse train generation in [157] which is limited by the filter spectral resolution, a real pulse repetition rate multiplication can be achieved by controlling the amplitude and phase of individual spectral lines. By controlling the phase of the discrete spectral components of the input pulses so that the so-called Talbot condition is satisfied, pulse rate multiplication can be achieved.

5.1.3 Temporal fractional Talbot effect

The Talbot effect [159] is referred to as a self-imaging effect. Under appropriate conditions, a beam of coherent light is reflected from an object with periodical structures, and the exact images of the object or a multiple of the original images are formed at specific distances from the object, which are referred to as integer Talbot effect and fractional Talbot effect, correspondingly. Similar effect is observed in the temporal domain as well when a signal with periodical temporal pattern (i.e., a pulse train) propagates along a dispersive medium under first-order dispersive condition. Reproduction of the original periodical signal pattern or repetition rate multiplication of the original signal occurs at specific locations of the dispersive medium. This can be understood as follows. After transmission in the dispersive medium, different spectral components of the pulse train acquires different amount of phase shift. Under specific dispersion conditions, when the spectral components which are spaced by some integer multiple of the repetition rate of the original pulse train are in-phase while phases of the intermediate spectral components are mismatched, a pulse train with multiplied repetition rate is generated. Up to THz repetition rates have been reported using both SMF and LCFBG as the dispersive medium [159-162].

Temporal fractional Talbot effect is essentially a phase-only spectral filter. Different from the pulse shaper based spectral filter described in the previous section where bulky optical components with high spectral resolution are required, a simple dispersive medium such as SMF or LCFBG can be used in the temporal fractional Talbot effect based pulse rate multiplier. However, this approach is very sensitive to the spectral phase applied to the spectral modes of the signal as any deviation from the Talbot condition would degrade the quality of the multiplied pulse train such as peak-to-peak pulse intensity variation. Therefore, delicate control of the length of the SMF and fabrication of long LCFBG with very low group delay ripple are required. Moreover, only pseudo-multiplication is achieved since not all the pulses have the same phase.

5.1.4 Rational harmonic mode-locking

The methods described above (i.e., spectral amplitude filtering, spectral phase filtering, and temporal fractional Talbot effect) are passive approaches that are able to multiple the repetition rate of the optical pulse train external to the laser cavity. On the other hand, rational harmonic mode-locking seeks to multiply the pulse repetition rate actively inside the laser cavity. It was first demonstrated by Onodera *et al*. that pulse repetition rate doubling could be achieved by modulating the laser at a frequency between the two harmonics of the cavity resonance frequency [163]. Later, the phenomenon was qualitatively explained in [164] that pulse repetition rate multiplication in an actively mode-locked laser is a result of interaction between the circulating pulses and the cavity loss modulation. Briefly speaking, a pulse circulating in the cavity experiences minimum modulator loss in every second round-trip of the cavity if the modulation frequency is offset by half of the cavity resonance frequency away from the harmonic mode-locking frequency. Therefore, the repetition rate of the laser will be doubled if this applies to every pulse that is generated. Generally speaking, optical pulse train with repetition rate of $(np + 1)f_{cav}$ can be produced when the modulation frequency is set at $(p \pm 1/n)\, f_{cav}$, where f_{cav} is the cavity resonance frequency, and p and n are integers. 80 – 200 GHz pulse train generation was reported in an EDFA-based fiber laser using rational harmonic mode-locking where a multiplication factor of 2-5 times the fundamental modulation frequency was achieved [165]. It was also reported that the 22nd order of rational

harmonic mode-locking was achieved when the fundamental modulation frequency was 1 GHz, although severe pulse amplitude variation was observed for such a high-order repetition-rate multiplication [166]. In addition to MZMs which are conventionally used as loss modulators, FP laser diodes were reported to be used in loss modulation mode by properly adjusting the DC current and RF power. Up to 40 GHz rational harmonic mode-locked pulses were generated at repetition rate of 1 GHz [167]. Moreover, rational harmonic mode-locking is demonstrated in SFRLs where SOAs served as both the gain media and mode-lockers through XGM, and repetition rate multiplication could be achieved over several wavelengths simultaneously [121, 123].

An inherent problem that comes with the technique of rational harmonic mode-locking is pulse amplitude fluctuation, which originates from the fact that the modulation frequency of the laser doesn't match with the cavity resonance frequency. This is an intrinsic problem that exists in rational harmonic mode-locking with order larger than two [165]. Various approaches have been proposed and demonstrated in order to equalize the pulse amplitude which include using a NOLM based fiber ring laser external to the mode-locked laser [168], using a nonlinear amplifying loop mirror (NALM) based fiber ring laser [169], using an SOA loop mirror [170], using NPR effect in optical fiber as an artificial saturable transmitter [171], adding an optical feedback loop to equalize the SOA gain [172], using a dual-drive intra-cavity MZM in which each pulse experiences the same transmission coefficient in the transmission curve of the modulator [173], and using a saturated SOA followed by an optical bandpass filter [174].

5.2 Nonlinear frequency doubling using MZMs in a FOPO

Nonlinear transfer function of MZMs has been exploited to achieve frequency multiplication in mode-locked fiber lasers [104]. In this approach, the DC bias of the MZMs is set at the transmission minimum point of the transfer function and even-order modulation sidebands including the optical carrier are suppressed. Therefore a double-sideband suppressed-carrier modulation is performed, and the beating between the two first-order modulation sidebands creates a frequency doubled tone in the PD. The same experimental setup is used in this case as in Figure 4.3, except that the bias of the MZM is changed to the minimum transmission point. The RF driving signal is still a

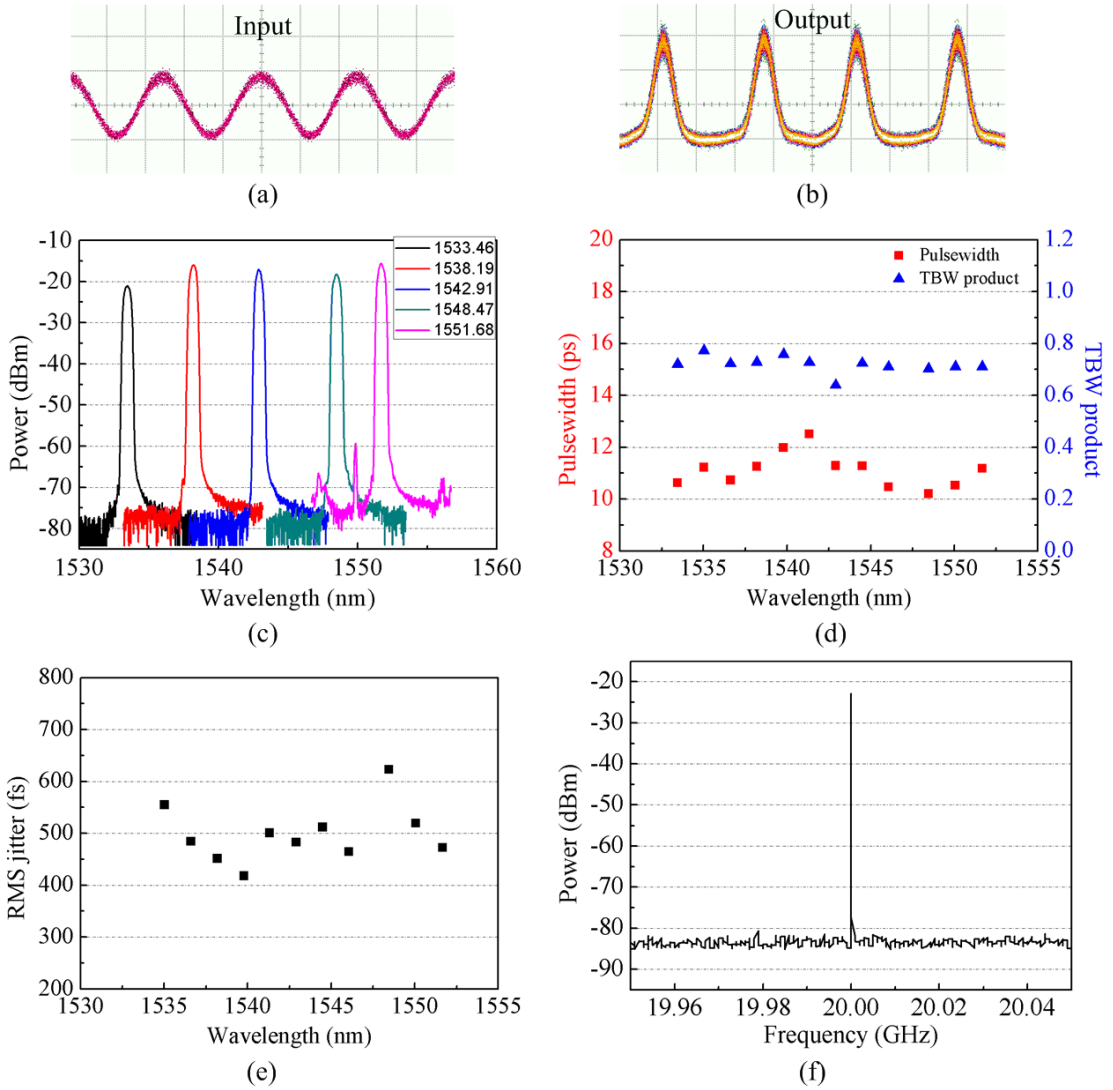

Figure 5.1 (a) Waveform of the input pump pulses with 20 GH repetition rate and 50% duty cycle. (b) Waveform of the output mode-locked pulses. (c) Lasing spectra of the 20 GHz harmonically mode-locked FOPO. RBW = 0.06 nm. (d, e) Pulsewidth, TBW product and RMS timing jitter vs. tuning wavelength. (f) Electrical spectrum of the mode-locked pulses.

10 GHz sine wave. Sample waveforms of the frequency doubled pump pulses with 50% duty cycle and the corresponding mode-locked pulses are shown in Figure 5.1 (a, b). Since the voltage swing of the applied radio-frequency signal in our experiment remains to be V_π, a 3 dB extra loss is introduced compared with the linear modulation case (i.e., the bias is set at the quadrature point of the transfer function). In addition, the pump peak power decreases with an increase in the pump pulse repetition rate if the duty cycle

increases and the pump average power remains the same. Therefore, a higher average pump power (~ 0.84 W) is required to provide sufficient gain. To prevent wavelength drift under such a high pump power, the filter BW is set at 0.8 nm. Sample lasing spectra of the 20 GHz harmonically mode-locked FOPO are shown in Figure 5.1 (c) and the characteristics of the output pulses are shown in Figure 5.1 (d, e).

It is observed that the wavelength can be tunable from 1533.5 nm to 1551.7 nm, which is 18.2 nm in the anti-Stokes band. In total, the tuning range is 36.4 nm - smaller than that at 10 GHz. The tuning range is limited by the maximum optical power that EDFA1 can offer in this experiment. The generated pulse has a pulse width of around 11 ps and TBW product of around 0.7. The pulse width is a little shorter than that obtained in the 10 GHz operation case (~ 12.5 ps, [175]). This is because the pump pulse itself is shortened because of the nonlinear transfer function near the null point of the MZM. The RMS timing jitter is measured to be around 500 fs, which is a little bit larger than that in [175]. This might be due to the large ASE noise introduced by EDFA1. In addition, since the bias point is at the null of the MZM transfer function, the generated pulse is more vulnerable to bias variations rather than at the quadrature point. The RF spectrum shows that the SNSR is ~ 60 dB which is worse than the 10 GHz case.

Generally, the results show that this method can produce pulses with a repetition-rate of 20 GHz with similar pulse quality as in the 10 GHz case. However, a much higher average pump power is required because of the extra loss in the MZM and the increased repetition-rate of the pump pulses. As a result, it imposes a limit to the achievable tuning range with a certain power budget offered from the EDFA, and more noise is added into the cavity. In principle, we can multiply the pump repetition rate by four times (40 GHz) by cascading another MZM in the pump branch or by biasing the MZM in the transmission peak with appropriate modulation voltage [176]. However, it is not practical in our case since more power consumption is required and the residual 10 GHz and 20 GHz frequency components will degrade the mode-locking strength. It is indeed reported that using an intra-cavity fiber FP filter to suppress lower-order modulation sides is helpful for frequency multiplication and amplitude stabilization [150].

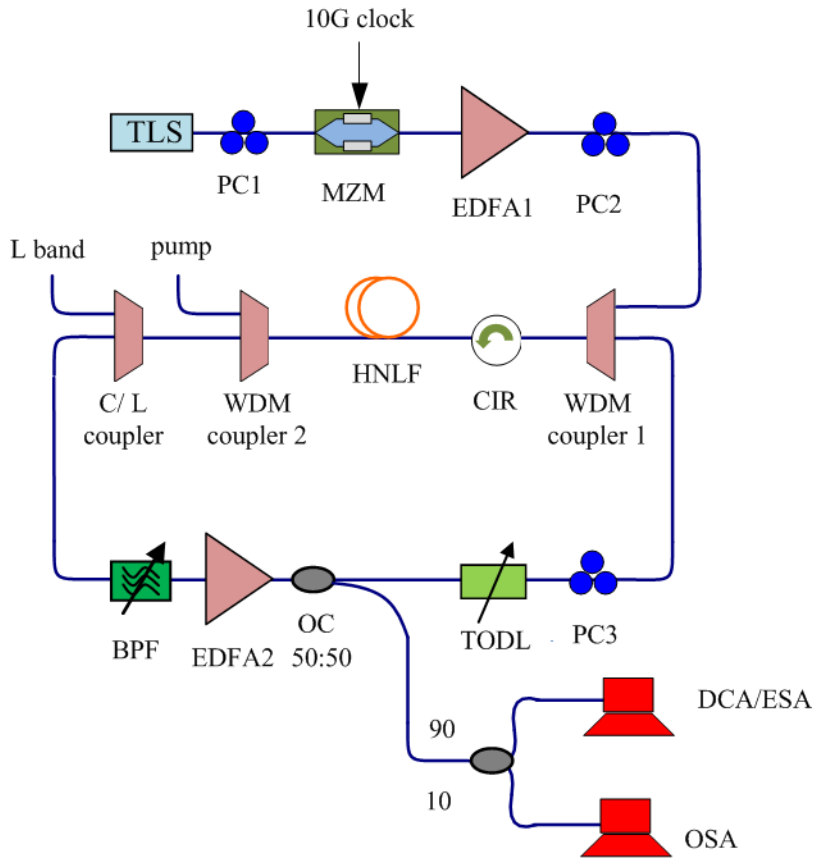

Figure 5.2 Experimental setup of a rational harmonic mode-locked FOPO working at 10 - 30 GHz.

5.3 RHML from 10 GHz to 30 GHz

5.3.1 Operating principle and experimental setup

The experimental setup of the rational harmonic mode-locked FOPO is shown in Figure 5.2. A TLS at 1556.5 nm serves as the pump signal which is modulated by a 10 GHz sinusoidal wave using a MZM. The duty cycle of the optical clock signal is 33%. Then, it is amplified by EDFA1 to an average power of 70 mW before being launched into a spool of HNLF. The HNLF has the same characteristics as the one used in the previous experiment (see Table 4.2). A circulator is used to ensure unidirectional operation. Two WDMCs are used to combine and split the pump and the oscillating signals, respectively. A C/L band coupler is also used to suppress the undesired L-band idlers and noise. A BPF with a bandwidth of 1.6 nm is used to select the desired output wavelength.

The cavity loss (without EDFA2) is measured to be 15.4 dB, which mainly comes from the BPF (~ 6 dB) and four OCs (~ 5 dB). EDFA2 can provide an open-loop small-signal gain of about 14 dB while the parametric gain overcomes the rest of the cavity loss. Since the parametric gain is low, we do not need to suppress SBS. In addition, the low gain will help to reduce amplitude variations between adjacent pulses. 50% of the oscillating light is coupled out of the cavity through a 3 dB OC while the rest is re-injected in the cavity. As we have discussed before, in RHML repetition rate multiplication is achieved by detuning the modulation frequency (i.e., RF signal applied to the MZM) of the pump from the harmonic frequency by a fraction of the cavity resonance frequency. This can be achieved by either changing the modulation frequency of the electrical source or by simply changing the cavity resonance frequency through adjusting the ODL. We choose the latter method in our characterization in order to keep the modulation frequency constant. In this case, an ODL is used to adjust the cavity length so that the cavity resonance frequency is changed correspondingly.

Since none of the optical components in the laser cavity is polarization-maintaining, polarization controllers PC2 and PC3 are used to align the SOP of the pump and the signal so that maximum parametric gain can be achieved. The output pulses are monitored and measured using the same OSA, DCA and ESA as described in section 4.2. During the measurements, only the ODL needs to be adjusted. This is because the cavity length will drift with time due to temperature changes and environmental perturbations, which can desynchronize the modulation frequency and the cavity resonance frequency. For long-term operation, the stability can be increased by adding a feedback loop, as we have discussed in section 4.1.2.

The cavity gain of our rational harmonic mode-locked FOPO is provided by both an EDFA and parametric gain. The EDFA gain is set below the cavity threshold so that CW operation will not occur. The parametric gain is provided by an optical pump (i.e., an optical clock signal) through energy conversion from the pump to the signal and the idler in silica fiber. The time-varying pump signal modulates the cavity gain above and below the cavity threshold periodically so that active mode-locking is achieved. Thus, the parametric gain functions as both a gain medium and an all-optical mode-locker.

If the modulation frequency of the pump signal is n times that of the cavity resonance frequency, there will be n pulses circulating in the cavity; each pulse passes through the mode-locker at the time when there is also an incoming pulse from the pump signal (i.e., the mode-locker provides the maximum gain) in each round trip. This kind of active harmonic mode-locking has been discussed in Chapter Chapter 4 . However, in the case of rational harmonic mode-locking, the modulation frequency of the pump signal is detuned from the harmonic frequency by a fraction of the cavity resonance frequency f_{cav}/p. If the modulation frequency is decreased by $f_{cav}/2$, then each pulse is delayed by half of the modulation period. So, it will pass through the mode-locker when there is no parametric gain in the second round trip. But the pulse will not vanish because the EDFA gain can still compensate part of the cavity loss until the pulse arrives at the mode-locker at its maximum gain point in the next round trip. Since every pulse experiences the maximum gain in every second round trip, the repetition rate is doubled. Higher-order rational harmonic mode-locking can be explained in the same manner. It can be seen that the function of the intra-cavity EDFA is used to keep the signal pulse oscillating in the cavity even when there is no gain in the mode-locker. Otherwise, the signal might die out after several round-trips with pure loss (note that a round-trip cavity loss is ~ 15.4 dB). On the other hand, adding an intra-cavity EDFA constrains the wavelength tuning range of the FOPO to the bandwidth of conventional EDFAs. However, the intra-cavity amplifier does not need to be an EDFA. We believe that any type of amplifier within the gain region of interest, for example other specially-doped amplifiers or SOAs, can be used.

Since adjacent pulses will experience different gain/loss in one round-trip, there is intrinsic amplitude fluctuation in the rational harmonic mode-locking process [164]. This fluctuation is larger for higher rational harmonic order. At the same time, the proposed FOPO will suffer from supermode noise due to the long relaxation time of the erbium ions and the small cavity resonance mode spacing. These constitute the main sources of amplitude noise in rational harmonic mode-locking.

5.3.2 Results and discussions

5.3.2.1 20 GHz pulse train generation

10 GHz optical pulse train generation has been discussed in section 4.3.6. Next, we change the cavity length so that the modulation frequency is detuned from the harmonic frequency by half of the cavity resonance frequency. In this way, second-order rational harmonic mode-locking is realized and a 20 GHz pulse train is generated as shown in Figure 5.3. The wavelength can be tunable from 1532.5 nm to 1551.7 nm, corresponding to a tuning range of 19.2 nm. Since a larger cavity loss is applied to each circulating pulse while the parametric gain remains the same, the tuning range for 20 GHz operation is smaller than that for 10 GHz. Although the parametric gain bandwidth can be increased by increasing the pump power, amplitude fluctuations will appear on the pulses because of a higher saturation power of the parametric gain. In the end, this is a trade-off between broader wavelength tuning range and smaller amplitude fluctuations. So the gain bandwidth can only be increased by optimizing the HNLF parameters. The RMS timing jitter is around 300 fs from 1540.8 nm to 1551.7 nm and is higher at the shorter wavelengths. The pulsewidth is again around 9 ps and the TBW product is around 0.7 over most of the tuning range, which is similar to the results obtained for 10 GHz mode-locking. The spectral peaks in the OSA trace now have a wavelength spacing of ~0.16 nm which indicates that the pulse train has a repetition rate of 20 GHz. There are also small 10 GHz spectral peaks observed in the spectrum which cause very small amplitude fluctuations in the waveform as shown in Figure 5.3 (a). The average output power is around 3 mW. However, the output power cannot be increased by increasing the EDFA gain and the pump power, because it can lead to greater amplitude fluctuations between adjacent pulses due to a higher saturation power of the amplifier. One possible means to increase the output power is to increase the output coupling ratio.

5.3.2.2 30 GHz pulse train generation

Finally, 30 GHz rational harmonic mode-locking is realized by changing the cavity length so that the modulation frequency is detuned by a third of the cavity resonance frequency from the harmonic frequency. The waveform and the corresponding characteristics are shown in Figure 5.4. The tuning range of the FOPO is 19.4 nm from

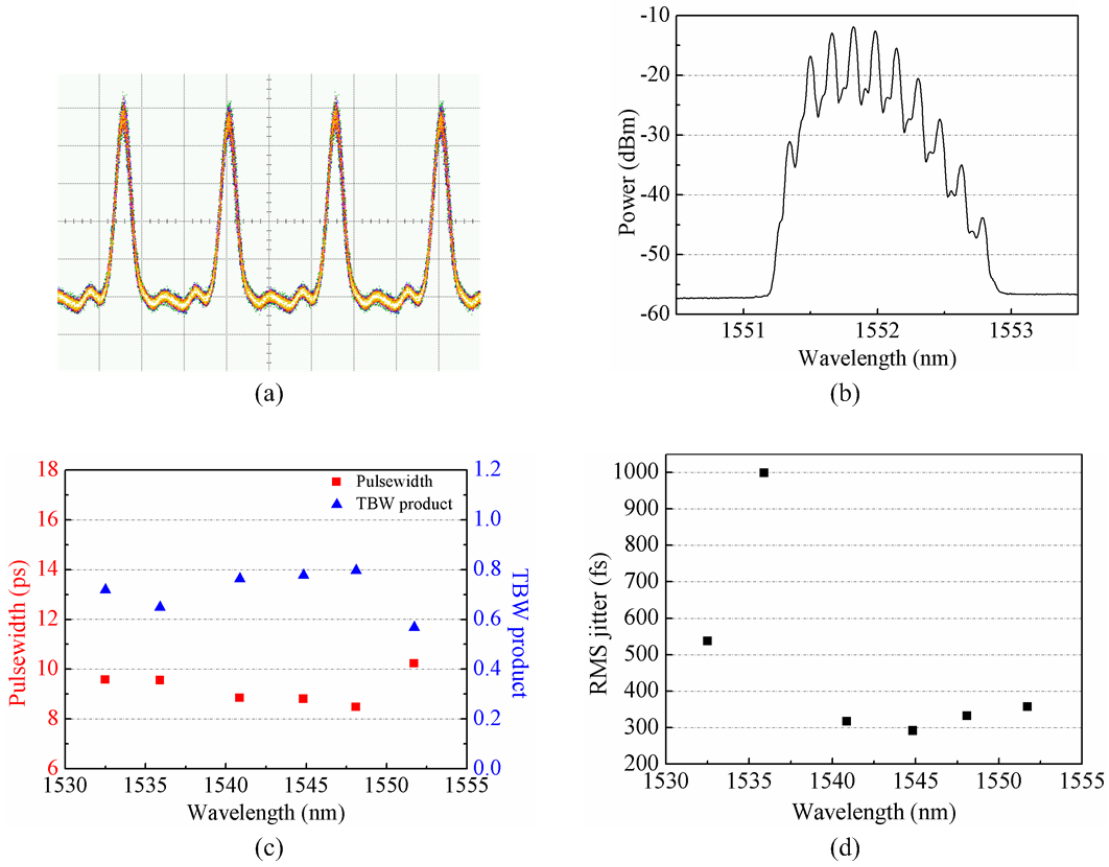

Figure 5.3 (a) Waveform of 20 GHz mode-locked pulses at 1551.7 nm. Time scale: 20 ps/div. (b) Optical spectrum of the mode-locked pulses at 20 GHz. (c) Pulsewidth and TBW product vs. wavelength. (d) RMS timing jitter vs. wavelength.

1532.4 nm to 1551.8 nm, which is almost the same as the 20 GHz mode-locking result. The RMS timing jitter increases to around 400 fs, which indicates that the FOPO becomes more unstable under a higher-order rational harmonic order. This is expected because each pulse has to travel three cavity round trips in order to be amplified at the mode-locker. So the effective cavity length is tripled compared with the conventional harmonic mode-locking and therefore operation is more vulnerable to environmental perturbations. Less timing jitter could be obtained with shorter cavity length by using HNLF with higher nonlinearity [177]. The pulsewidth decreases to about 8 ps compared with 10 GHz and 20 GHz operation. This agrees with the theoretical predictions shown in [178]. The TBW product increases to about 0.8. From the OSA trace, it can be found that the wavelength spacing between the dominant spectral peaks is ~0.24 nm while some

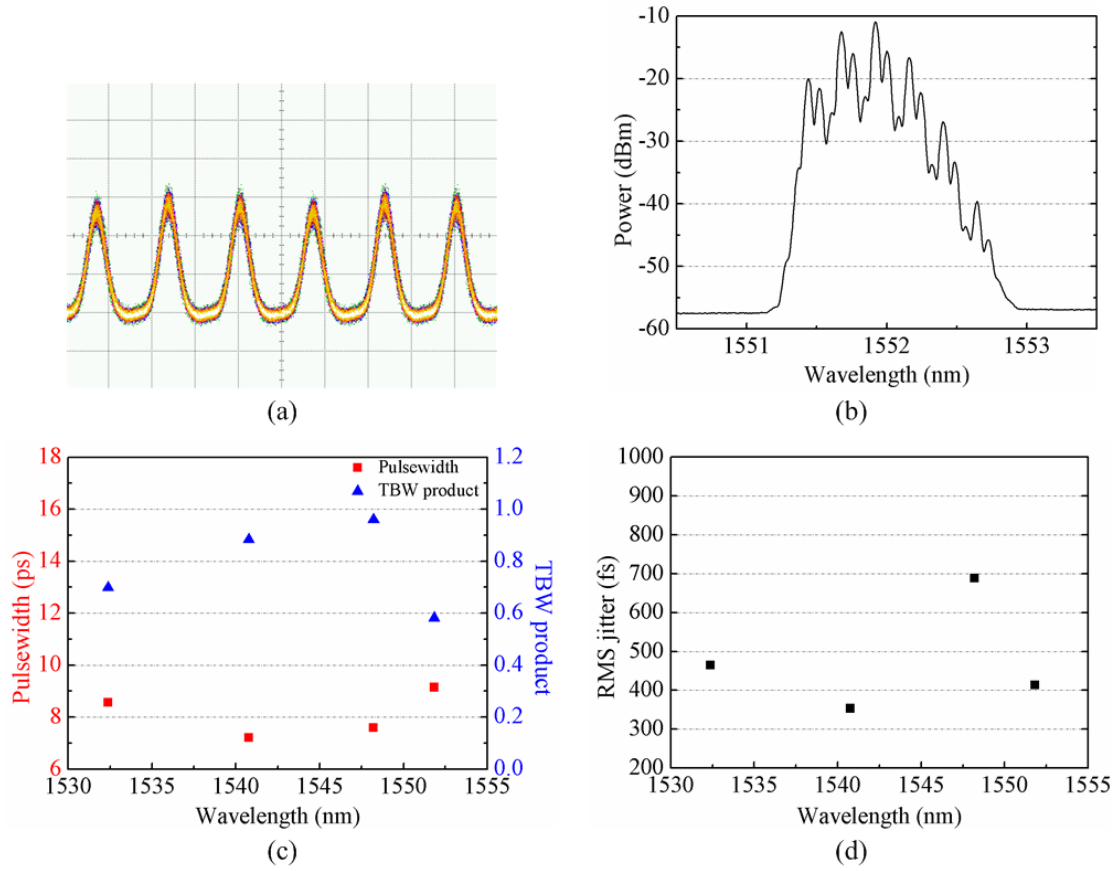

Figure 5.4 (a) Waveform of 30 GHz mode-locked pulses at 1551.8 nm. Time scale: 20 ps/div. (b) Optical spectrum of the mode-locked pulses at 30 GHz. (c) Pulsewidth and TBW product vs. wavelength. (d) RMS timing jitter vs. wavelength.

small peaks also appear which are 0.08 nm and 0.16 nm away from their adjacent peaks. These 10 GHz and 20 GHz spectral components cause the small amplitude variations between adjacent pulses as shown in Figure 5.4 (a). This is an intrinsic problem in higher-order rational harmonic mode-locking which is due to the random oscillation of the lower-order rational harmonic modes (i.e., 10 GHz and 20 GHz modes). Again, the average output power is around 3 mW, which can be increased by changing the output coupling ratio.

5.3.2.3 Discussions

It can also be seen from Figure 5.3 and Figure 5.4 that the pulses generated from the second-order and third-order RHML exhibit significant amplitude fluctuations. The

amplitude fluctuations come from two sources. The first is the supermode noise as we have discussed previously with regards to harmonic mode-locking. The second is the oscillation of lower-order rational harmonic modes. From the perspective of the time domain, this is because adjacent pulses experience different gain/loss in each round-trip. From the perspective of the frequency domain, this is due to the random oscillation of lower-order rational harmonic modes (e.g., 10 GHz and 20 GHz modes for the 30 GHz RHML case) in the cavity. The oscillation of lower-order modes can be clearly seen from the optical spectra shown in Figure 5.3 (b) and Figure 5.4 (b). Compared with the contribution from supermode noise, the oscillation of lower-order rational harmonic modes causes more amplitude fluctuations and it increases with increasing rational harmonic orders. The uneven pulse amplitude distribution is an intrinsic problem of the RHML technique and thus cannot be eliminated by changing the parameter settings in our approach, although we can minimize the amplitude fluctuations by keeping the parametric gain as low as possible since a saturated parametric amplifier can be used as a nonlinear amplitude limiter [147]. Besides, it is reported that uneven pulse amplitude distribution can be equalized by means of post-processing methods such as using a saturated SOA as an amplitude limiter [174], adding an optical feedback loop with pulse intensity matching [172], or using an additional equalizing fiber laser comprising a NALM and Faraday rotating mirror laser cavity [169].

Compared with the method of biasing the MZM at the null point, the method of RHML is much simpler in terms of the experimental setup, especially for higher-order frequency multiplication, since only the ODL needs to be adjusted rather than cascading MZMs and incorporating intra-cavity Fabry-Pérot filters with specific spectral response. In terms of wavelength tuning characteristics, both approaches have the same wavelength tuning range, which is narrower than that measured in the harmonic mode-locking case. This is due to the extra loss suffered either from the signal travelling through multiple round-trip time or from the MZMs working at the null transmission point. The pulses generated from RHML exhibit shorter pulse duration and less RMS timing jitter than those generated from biasing the MZMs, however at the expense of larger amplitude fluctuations. In summary, the method of RHML is superior to the method of biasing the

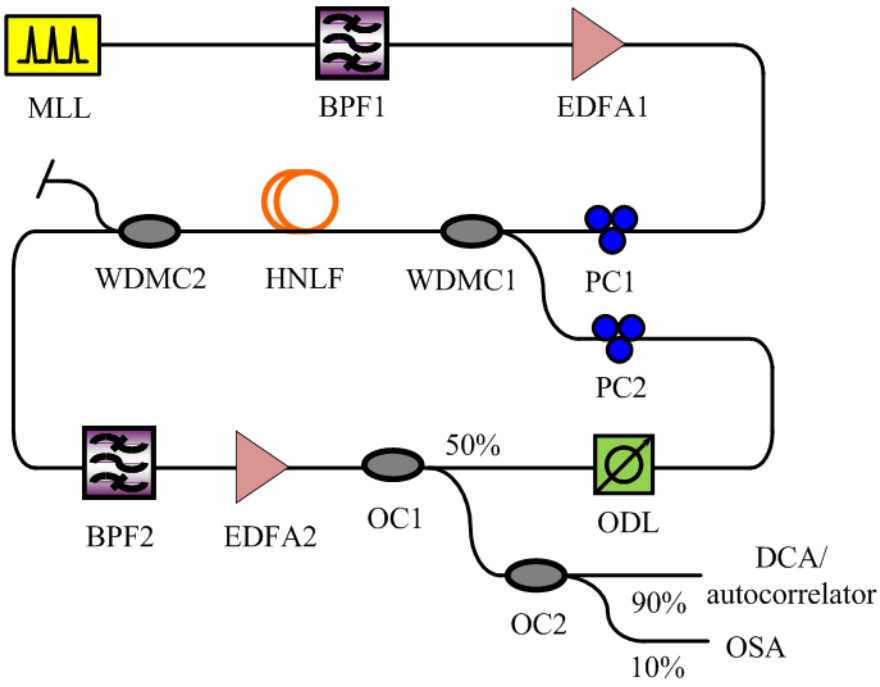

Figure 5.5 Experimental setup for a rational harmonic mode-locked FOPO working at 40 – 240 GHz.

MZMs in terms of simpler setup, easier for extension to higher-speed operation, better pulse quality, and less power consumption.

5.4 RHML from 40 GHz to 240 GHz

We have discussed the advantages and the limitations of RHML in the previous section. Actually, another constraint that prevents the above configuration from generating the fourth- or higher-order RHML pulses is because the duration of the generated pulses is too broad. We can solve this problem by reducing the pump pulse duty cycle or duration as discussed in section 4.3.1. Since the mode-locking element of the FOPO is optically controlled (i.e., through parametric amplification), the easiest way is to use a pulsed source such as a MLL as the pump. Besides, as we have mentioned before, higher rational harmonic orders generate larger amplitude fluctuations of the output pulses due to the random oscillation of lower-order modes. As a result, complex configurations are usually required to equalize the amplitudes of the mode-locked pulses as we mentioned above [169, 172, 174]. An alternative method is to use intermediate-frequency

modulation signals with lower rational harmonic orders. As an example, in [165], a 200 GHz pulse train was generated with a 40 GHz driving signal.

In general, the experimental setup for the RHML-FOPO working at 40 GHz and beyond is similar to the one shown in Figure 5.2. One major difference is that the 10 GHz pump pulse generation part is replaced by an erbium-doped fiber based MLL working at 40 GHz. The wavelength from the MLL is centered at 1558 nm and the pulse duration is 3.6 ps (measured using an autocorrelator) after the BPF1. The pump pulse is amplified by EDFA1 to around 0.09 W before being launched into the FOPO cavity. Another difference is that the C/L band coupler and the circulator are abandoned to further reduce the cavity loss, which is crucial to increase the wavelength tuning range of the output pulses as we have discussed in the previous section. In addition, BPF2 has a 3 dB bandwidth of 4 nm and EDFA2 has a fixed output power of 68 mW. RHML is achieved by tuning the ODL in the cavity.

In our experiments, we characterize the waveforms of the output pulses by means of a DCA, an autocorrelator and an optical sampling oscilloscope (OSO), depending on the availability of the equipment at the time of our measurements. The OSO has >500 GHz optical bandwidth and ~50 fs typical RMS timing jitter.

First, we characterize the impact of FBW on the output pulse quality. The results are shown in Figure 5.6. It is observed that the pulse width decreases as a function of the increasing FBW and approaches a constant value when the FBW is larger than 4 nm. The TBW product keeps almost constant of around 0.65. So does the RMS timing jitter (of around 400 fs). Note that the timing jitter measurement is not accurate in this case because of the limited bandwidth (65 GHz) of the optical sampling module in the DCA. In the end, we choose the FBW to be 4 nm in the later measurements.

After choosing a proper FBW, we characterize the wavelength tuning characteristics of the FOPO working at 40 GHz and 80 GHz using the autocorrelator and the OSA. Since the DCA has a limited impulse response (of 7.7 ps), and the autocorrelator does not reflect the waveform in real-time or sampling fashion (though it can be used to measure the pulse width), we use the OSO to measure the pulses with higher repetition rates in the later measurements. However, the timing jitter measurements on the OSO cannot be compared directly to those from the DCA since the

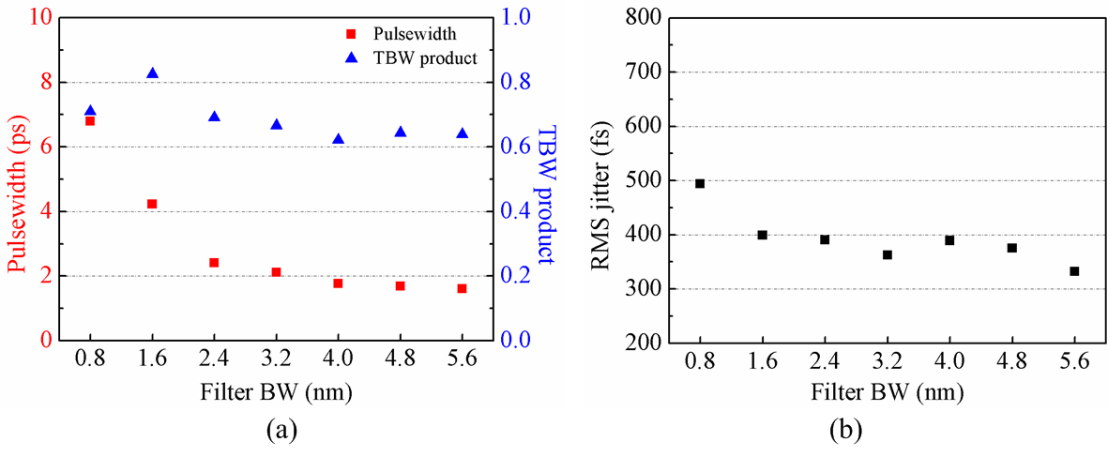

Figure 5.6 Impact of FBW on the characteristics of the output pulses at 40 GHz.

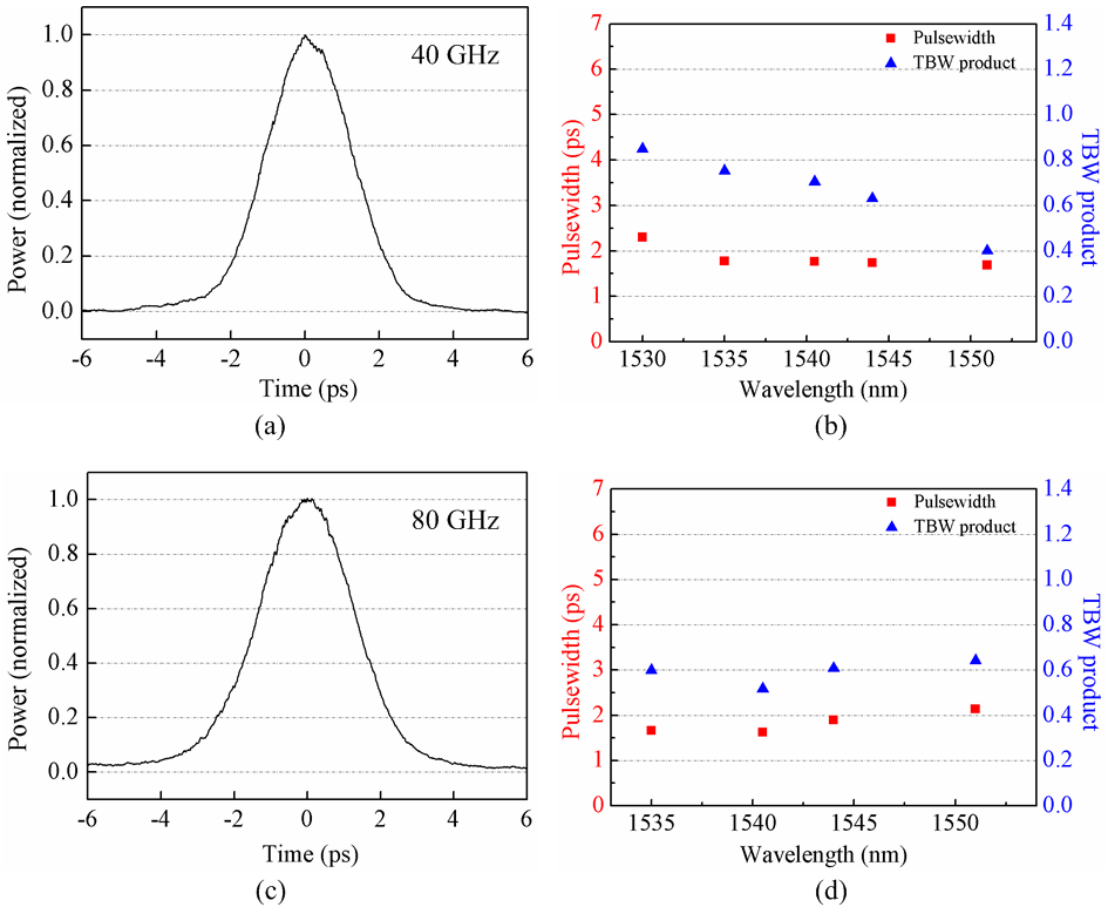

Figure 5.7 Wavelength tuning characteristics of a RHML FOPO working at 40 GHz (a, b) and 80 GHz (c, d). (a, c) show the autocorrelation traces of the 40 GHz and 80 GHz pulses.

jitter floors and the measurement techniques varied for different test instruments. From the results in Figure 5.7, we can find out that the tuning range for a 40 GHz RHML FOPO is 21 nm from 1530 nm to 1551 nm, and for an 80 GHz RHML FOPO it is 16 nm from 1535 nm to 1551 nm, both in the anti-Stokes band. So the total tuning range is 42 nm and 32 nm for 40 GHz and 80 GHz FOPO, respectively. The pulse width is measured using the autocorrelator and we confirm that the output pulse has a sech^2 profile by fitting the measured trace with the calculated autocorrelation of a sech^2 function in MATLAB. The pulse width is measured to be around 1.7 ps for 40 GHz and 1.9 ps for 80 GHz pulses. The TBW product is around 0.7 for 40 GHz and 0.6 for 80 GHz pulses. We can see that the pulse duration is reduced compared with the input in both cases which is in consistency with the results shown before. The reduced tuning range for 80 GHz pulses compared with 40 GHz case is expected because of the larger loss experienced by the higher-order rational harmonic modes.

At last, we characterize the pulse quality for even higher-order RHML pulses (up to 6^{th}-order). We did not measure the tuning range for all cases since they are expected to have almost the same amount as in the case of 80 GHz operation. The pulse properties are measured using an OSO with 500 GHz bandwidth. The waveforms are shown in Figure 5.8. Very clear waveforms can be obtained with various repetition rates from 40 GHz up to 240 GHz. It is also observed that the pulse amplitude starts to decrease with an increasing repetition rate and the amplitude variation becomes more severe as well. For the 240 GHz pulse train, we used an optical amplifier to amplify the weak signal before detection in the OSO. The pulse width, RMS timing jitter, and amplitude fluctuations of the output pulses are shown in Figure 5.9. The pulse width decreases from 2.4 ps to 2.05 ps with an increasing repetition rate from 40 GHz to 240 GHz. However, the RMS timing jitter increases from 65 fs to 152 fs accordingly. The amplitude fluctuation value is defined as the ratio between the peak to peak amplitude difference and the mean of the pulse peak amplitude. It can be seen that the amplitude fluctuations increase from 2.7% to 26.3% when repetition rate increases from 40 GHz to 240 GHz.

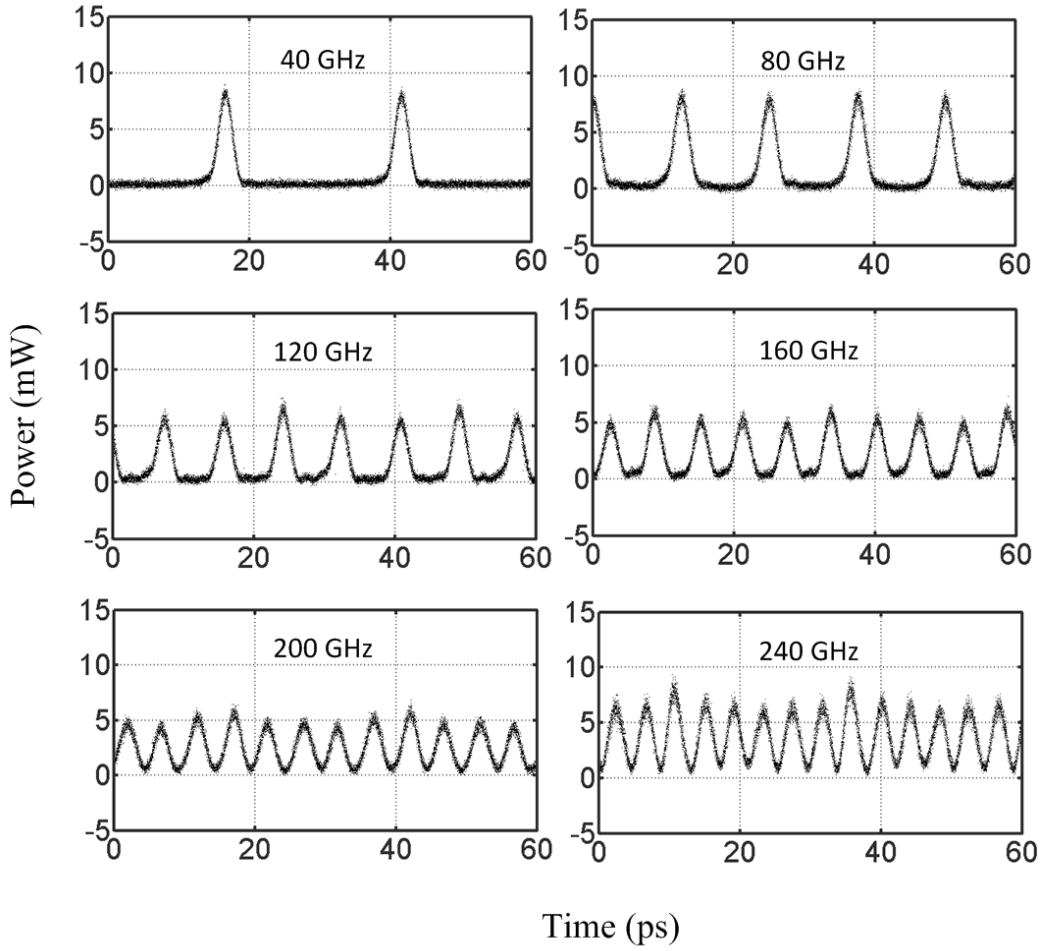

Figure 5.8 Waveforms of the pulses with various repetition rates generated from a RHML FOPO.

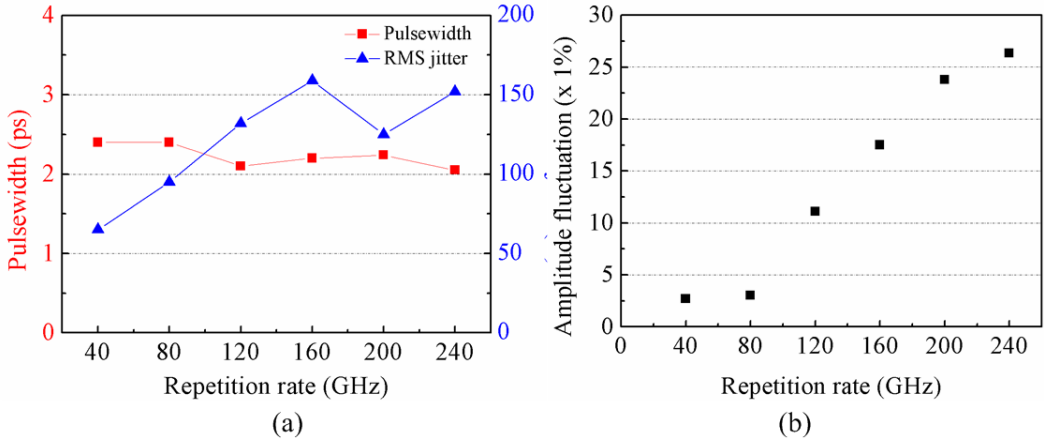

Figure 5.9 Characteristics of the pulses with various repetition rates generated from a RHML FOPO.

Table 5.1 Comparison of pulse characteristics using different schemes and with different repetition rates.

Type	Rep rate (GHz)	Pump power (W)	Pump phase modulation	Pulse width (ps)	RMS jitter (fs)	Tuning range (nm)
Harmonic mode-locking	10	0.35	Yes	9	400	44.6
Frequency doubling by biasing MZM	20	0.84	Yes	11	500	36.4
RHML from 10 GHz	10	0.07	No	9	300	47.6
	20			9	350	38.4
	30			8	450	38.8
RHML from 40 GHz	40	0.09	No	2.4	65	42
	80			2.4	95	32
	120			2.1	132	
	160			2.2	159	
	200			2.24	125	
	240			2.05	152	N/A

5.5 Conclusions

In this chapter, the repetition rate of the actively mode-locked FOPO is increased in two ways: nonlinear frequency doubling in a MZM by biasing the MZM in its minimum transmission point, and RHML. We find that the method of biasing the MZM can produce good quality pulses in general, however at the expense of larger pump power and larger timing jitter. Moreover, the configuration becomes very complex if we want to realize higher-order frequency multiplication. On the other hand, the method of RHML is much simpler to be implemented. In our experiment, frequency multiplication is achieved by simply tuning the ODL in the cavity. Since an EDFA is used in the cavity, the pump power can be kept relatively low. Therefore, there is no need for the pump phase modulation, which reduces the RMS timing jitter of the mode-locked pulses. In our experiment, we have successfully generated good quality pulses with repetition rate from 10 to 30 GHz using a 10 GHz optical pump source, and from 40 to 240 GHz using a 40 GHz optical pump source. The characteristics of the pulses generated using different

schemes and with different repetition rates are summarized in Table 5.1. It can be seen that very short optical pulses with low RMS timing jitter are generated from a RHML FOPO working at very high frequency. The drawback of this approach is the uneven amplitude distributions of the RHML pulses due to the random oscillation of lower-order rational harmonic modes. Post-processing will be needed in order to equalize the pulse amplitudes.

Chapter 6 All-optical Clock Recovery Based on a FOPO

All-optical signal processing is an enabling technology for future high-speed all-optical transport networks because it allows direct processing of optical signals which is an important feature for specific network locations and applications where optical signals are preferred to be preserved in the optical domain rather than being converted back and forward between the optical and electrical domain. In particular, all-optical signal processing techniques are capable of processing signals at a very high line-rate by utilizing the huge bandwidth offered by photonic devices and subsystems which is hard and/or expensive to be realized using electronic circuits.

Among the entire signal processing functions, clock recovery is a fundamental building block in all digital communication devices and systems, and therefore is of crucial importance especially for the OTDM systems because it can retrieve the clock information from the high-speed data traffic which is used for accurate timing in the decision circuit of the receivers, synchronization of an external optical source to the current traffic signals, and many other signal processing functions such as optical de-multiplexing of high-speed OTDM signals, packet switching, 3R (reamplifying, reshaping, and retiming) regeneration, optical logic operation, etc. A good all-optical clock recovery circuit should be robust against system impairments such as variation of signal duty cycle, extinction ratio, OSNR, etc., and be able to recover the clock signal with little timing jitter, amplitude fluctuation, and pulse chirp.

A number of all-optical clock recovery schemes have been proposed and demonstrated in the past decades, which can be roughly divided into two categories: active pulsating and passive filtering [179]. Active pulsating methods use active devices such as self-pulsating lasers, opto-electronic oscillators (OEOs), or actively mode-locked fiber ring lasers. The operating frequency of these active pulsating devices is locked to the data rate of the incoming data stream so that clock pulses can be recovered. High quality clock signals can be recovered using this type of method, but usually at the price of higher complexity and cost. Alternatively, passive filtering method simply preserves

the clock frequency components of the incoming data signal while filtering out the rest of the spectral components through periodical optical filters. Passive filtering is simpler and cost-effective compared with the active pulsating method, however usually at the cost of quality of the recovered clock signal.

In this chapter, we consider how FOPOs can be used to perform all-optical clock recovery. The rest of this chapter is organized as follows. Section 6.1 will review and compare various all-optical clock recovery approaches. Section 6.2 will give an introduction to the basic configuration and operating principle of a FOPO-based all-optical clock recovery circuit. Section 6.3 will perform a detailed analysis of the FOPO-based all-optical clock recovery in terms of the circuit robustness to various system impairments applied to the traffic channels such as the duty cycle, average input power, extinction ratio, OSNR, residual dispersion, and differential group delay (DGD). Section 6.4 will demonstrate 40 Gb/s all-optical clock recovery using the FOPO-based approach, and conclusions will be made in the last section.

6.1 Review of clock recovery approaches

6.1.1 PLLs

Electrical PLLs are widely used for clock recovery, in which the frequency and the phase information of the incoming data streams are obtained during the synchronization process between the local oscillator and the external source. A conventional PLL is consisted of three basic components: a phase detector, a voltage-controlled oscillator (VCO) and a feedback loop. The VCO is tuned such that the cross-correlation value of the local signal and the reference is maximized at the phase detector. Since the operating speed of the electrical PLL is limited by the response time of the phase detector, optical PLLs are proposed which can provide a much broader bandwidth. In optical PLLs, the frequency and phase information of the local oscillator and the incoming data stream are compared in high-speed optical gating devices such as a SOA-based NOLM [180], an electrically gated EAM [181], an optically gated EAM [182], and a LiNbO3 modulator [183].

In the optical PLLs discussed above, the VCOs could be discrete microwave sources to directly modulate the optical gating devices or to drive the optical sources such

as mode-locked lasers that could cross-correlate with the incoming data streams in the optical gates. However, instead of using the VCOs, there are other designs where the oscillating electro-optic loops (OEOLs) are used which basically realize the functions of both the VCOs and the feedback loops. For instance, in [184] the output of the MZM is converted into an electrical signal and is looped-back into the modulator RF port after amplification. In this way, the MZM is used as both the phase comparator and the intensity modulator. However, the operating speed of this configuration might be limited by the length of the feedback loop. As a solution, a narrow-band RF filter can be added into the feedback loop that is used to select the desired harmonic of the base resonator frequency. This kind of configuration has been demonstrated in [185, 186].

6.1.2 Self-pulsating laser

Self-pulsating laser is another device that has been widely used for clock recovery. By injecting an optical data signal into a self-pulsating laser operating in a free-running mode, the output of the laser can be locked to the clock frequency of the incoming data stream and therefore realize clock recovery. Self-pulsating laser based clock recovery typically has the advantages of simple configuration, ability to recover high quality clock signal, and enabling operation at high frequency.

One approach is based on two-section self-pulsating DFB diode laser. The bias current of the two laser sections have opposite signs so that one section is reversely biased functioning as a saturable absorber and the other one functioning as a gain medium. High-repetition-rate optical pulses can be generated in self-pulsating DFB diode lasers benefiting from the short cavity length [187, 188]. There are two operation regimes for a two-section DFB laser based clock recovery: coherent operation and incoherent operation [189]. In the incoherent operation approach, the signal is injected into the self-pulsating laser at ~1 nm away from the free-running wavelength. The process is not sensitive to the signal wavelength or the SOP. However, in the coherent operation approach, the signal is injected at the same wavelength as the free-running wavelength, and the laser can be injection locked to the incoming signal if the frequency is within the locking range. However, the coherent approach is dependent on the wavelength and the polarization of the input signal. SOA based wavelength conversion can be used before

launching the signal into the DFB laser to achieve wavelength and polarization independence [190]. Multi-section diode lasers with unequal section lengths have also been demonstrated for clock recovery. Three-section self-pulsating lasers have been demonstrated in which the first section provides the gain, while the middle section tunes the phase and the last section provides the optical feedback [191].

6.1.3 Spectral filtering

We have discussed clock recovery approaches based on PPLs and self-pulsating diode lasers. However, clock recovery can be achieved by using purely passive methods such as spectral filtering. Among different kinds of optical filters, FP filters are commonly used for clock recovery. The scheme was first demonstrated in [192], in which an optical tank circuit or a free-space FP resonator was used for clock recovery. The center wavelength of the FP filter needed to be aligned with the center wavelength of the incoming data signal, and the FSR had to match the clock frequency of the data signal in order to recover clock signal with good quality. Later, 40 GHz all-optical clock recovery was demonstrated by using a high-fineness FP filter and an SOA [193]. The center wavelength of the FP filter can be tuned by using an ultra-fine Peltier cooler. However, the quality of the recovered clock signal depends on the pattern of the input data stream and the resonator time constant. Large amplitude fluctuation can be observed if the incoming data stream contains long strings of the consecutive '0' bits, and the resonator time constant is very short. The amplitude fluctuation of the output clock signal can be equalized by a number of approaches such as using a nonlinear interferometer [194] or a MZI switch [195] . Ultrafast power limiter based on a HNLF followed by a BPF has been used for amplitude equalization [196]. SOAs operating near the gain-saturation regime can be used for amplitude equalization as well [193, 197]. In addition to FP filters, FBGs are often used as spectral filters for clock recovery application. It has been demonstrated that clock signal can be recovered from a 40 Gb/s NRZ data signal by using FBGs [198]. As we have discussed in section 5.1.3, temporal Talbot effect, which functions as a spectral phase filter, can be used to replicate the input optical pulses or produce pulse trains with repetition rate multiple times of the original pulse train depending on the transmission length and the dispersion of the first-order dispersion medium. Based on the

temporal Talbot effect, single and multiple wavelength clock recovery have been demonstrated in [199].

6.1.4 Actively mode-locked fiber ring laser

Similar to the idea of self-pulsating diode laser, fiber ring lasers are also widely used for the generation of mode-locked pulses and optical clock recovery. Fiber ring lasers use conventional atomic energy-state transition based amplifiers such as EDFAs and SOAs, or nonlinear parametric conversion and scattering based amplifiers such as fiber optical parametric amplifiers, Raman amplifiers, and Brillouin amplifiers. Passively mode-locked fiber ring laser based optical clock recovery has been proposed and demonstrated in [200]. A multiple-quantum well semiconductor saturable absorber (SSA) is used as the mode-locking component. The laser is mode-locked by injecting an optical signal into the cavity and cross-saturating the SSA. However, the operating speed of this method is limited by the FSR of the longitudinal modes which is only 14.13 MHz due to the long fiber cavity. Therefore, actively mode-locked fiber laser is a preferred scheme since it has the potential to recover optical signals at very high data rate which is only limited by the operating speed of the mode-locker and the response time of the cavity gain medium. As a result, many linear and nonlinear phenomena based all-optical mode-lockers have been proposed for clock recovery application. For example, SOA-based mode-locked fiber laser has been demonstrated for clock recovery in [201-203], in which the SOAs provides the cavity gain as well as the mode-locking. Incoming data streams saturate the SOA gain of the recovered clock signal through XGM which forces laser mode locking. Similarly, optical clock recovery has been demonstrated in SOA- or linear optical amplifier (LOA)-based fiber lasers [118, 204]. In these types of fiber lasers, EAMs are used as the mode-locker in which the device loss is modulated by the incoming data signals through XAM. In addition to using SOAs as the nonlinear medium, HNLFs have also been exploited for mode-locking through various nonlinear effects. For example, XPM modulation has been used in the HNLF for FM mode-locking of an EDFA-based fiber laser [205]. NOLMs are well-known as ultrafast optical gates which are also demonstrated as all-optical mode-locker in the actively mode-locked fiber

laser for high-speed clock recovery [126, 206, 207]. Moreover, NPR based optical mode-locker has been demonstrated for clock recovery in [129].

Actively mode-locked FOPOs, which are based on the ultrafast Kerr effect (~fs) in optical fiber, provide a promising solution to ultra-high-speed all-optical clock recovery. Such experiments have been reported in [93, 208, 209] for 14.14 MHz $2^7 - 1$ and 40 Gb/s $2^{11} - 1$ RZ-OOK input signals. However, the pattern lengths used are too short and would not be representative of the types of data that may be found in real situations. Moreover, the authors only consider ideal input signals, i.e., input signals that have not been degraded. In most clock recovery applications, we may expect that the characteristics of the input signals have been degraded along the transmission links before entering into the clock recovery circuit. To date, a detailed investigation on FOPO based clock recovery has not been reported. In this chapter, a thorough analysis of FOPO based all-optical clock recovery is performed. In particular, we investigate the impact of duty cycle, average power, extinction ratio, OSNR, residual dispersion, and DGD of the input signal on the RMS timing jitter, pulsewidth, and TBW product of the recovered clock. Wavelength tunability is also investigated. The permissible range for each of these characteristics is identified in terms of the RMS timing jitter of the recovered clock signal being less than 2 ps [210]. By analyzing such impacts, we are able to quantify the requirements of the input signal in order to obtain a recovered clock with good performance.

6.2 Experimental setup of a FOPO based all-optical clock recovery

The experimental setup of an all-optical clock recovery circuit using a FOPO is shown in Figure 6.1. It is composed of two parts: the upper block of the setup is for generating the 10 Gb/s RZ-OOK signal while the lower block of the setup is the clock recovery circuit. To generate the RZ-OOK PRBS, two MZMs are used: one for data modulation and the other for pulse carving (the length of the PRBS is $2^{31} - 1$). Phase modulation is not required in this case because the bandwidth of the RZ-PRBS signal is broader than the SBS gain bandwidth. The data is then amplified by EDFA1. VOA1 is

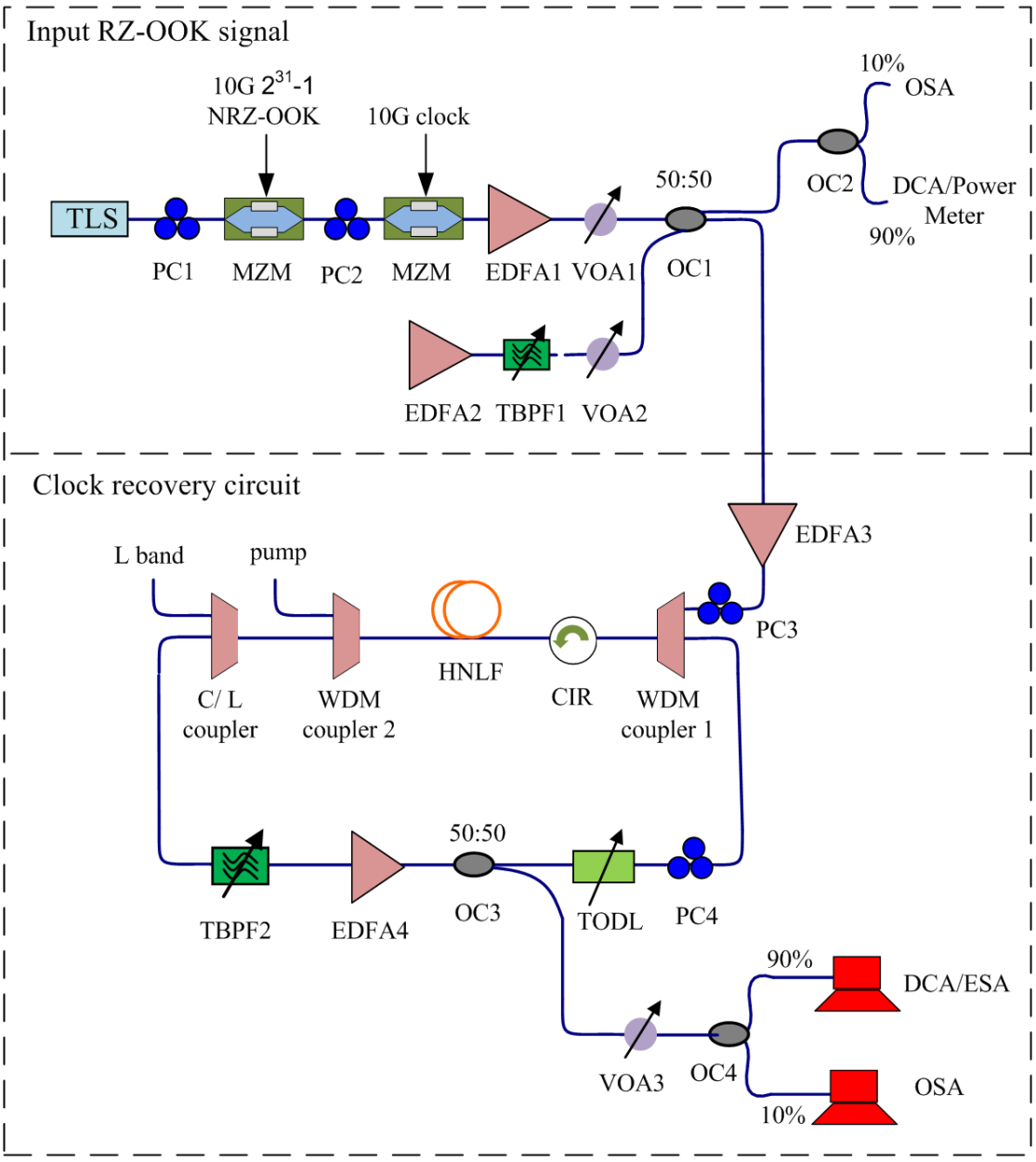

Figure 6.1 Experimental setup of a FOPO based clock recovery circuit.

used to control the input signal power to the all-optical clock recovery circuit. EDFA2 and BPF1 are used to generate the ASE noise. VOA2 is used to control the noise power added to the input signal. The characteristics of the input signal are monitored on the OSA, DCA, and power meter through the 50% port of the 3 dB OC1.

If the input signal is a periodic pulse train, the setup functions as a mode-locked laser provided the cavity length is adjusted to match the modulation frequency of the pump. On the other hand, if the input signal comprises PRBS data, the circulating '1's will attenuate gradually if the mode-locking element (i.e., FOPO) is off, i.e., for a long string of '0' data bits. The attenuation rate depends on the cavity loss. Since the parametric gain is time dependent and the response time is very fast, if there are long strings of consecutive '0's in the input signal, the circulating '1's may die out after several round trips in the cavity. This is the reason why we need to add EDFA4 into the cavity. If the EDFA gain is larger or even a bit smaller than the cavity loss, the '1' data bits can survive for a longer time in the cavity until the FOPO is on again. At this point, the attenuated '1's will be amplified by the parametric gain and continue oscillating in the cavity. So in the FOPO based all-optical clock recovery, cavity gain is provided by both the EDFA and parametric gain while the mode-locking mechanism is provided by the parametric gain modulation. Since the parametric process is on the order of femtoseconds, this method could be potentially used for ultra-high-speed all-optical clock recovery. The tunable range of the recovered clock depends on the EDFA gain and parametric gain bandwidth. By using HNLF with low dispersion and flat dispersion slope, it is able to support phase matching over a large range.

The EDFA gain should be set a little bit lower than the cavity loss. This is because if the EDFA gain is high, the increasing input signal power to the HNLF would lower the parametric gain, which in turn decrease the mode-locking strength and the FOPO would operate in CW mode. As a solution, the pump power could be increased correspondingly, but the amplitude fluctuation of the recovered clock will increase as a result of the increased saturation power of the parametric gain. So it is a compromise between the mode-locking strength and amplitude fluctuation. The best way is to set the EDFA gain a bit lower than the cavity threshold and pump power just enough or a little higher to compensate the rest of the cavity loss.

6.3 Detailed analysis of 10 Gb/s all-optical clock recovery

In the following sub-sections, we investigate the impact of duty cycle, average power, extinction ratio, OSNR, residual dispersion, and DGD of the input signal on the

Table 6.1 Characteristics of the the input signal without impairments

Parameter	Value
Wavelength	1556.5 nm
Data rate	9.95328 Gbit/s
Pattern length	2^{31} - 1
Duty cycle	40%
Extinction ratio	13 dB
Average power	0 dBm
OSNR	41 dB
Residual dispersion	0 ps/nm
DGD	0 ps

RMS timing jitter, pulsewidth, and TBW product of the recovered clock. Degradations to the signal are deliberately added to simulate the degradation associated with transmission impairments. Although no fiber transmission experiments were performed, our analysis covers most of the linear impairments encountered in practical transmission systems. The wavelength tunability of the recovered clock is also investigated. The characteristics of the input signal without impairments (i.e., in the nominal case) are shown in Table 6.1. In each of the following measurements, only one parameter (i.e., duty cycle, average power, extinction ratio, OSNR, residual dispersion, and DGD) is changed while the others remain the same, unless otherwise mentioned. The EDFA (EDFA4) output power is set at 68 mW, and the pump power is 74 mW. The cavity loss is measured to be 14.1 dB. Both powers remain unchanged during the whole experiment. Once the polarization of the cavity is optimized at the beginning of the experiment, no further changes are required during the measurements. Polarization insensitive operation could also be realized by using polarization diversity method [42]. However, the ODL needs to be adjusted slightly because of the cavity length drift due to temperature change and environment perturbations. In practical systems, this can be controlled using a feedback loop.

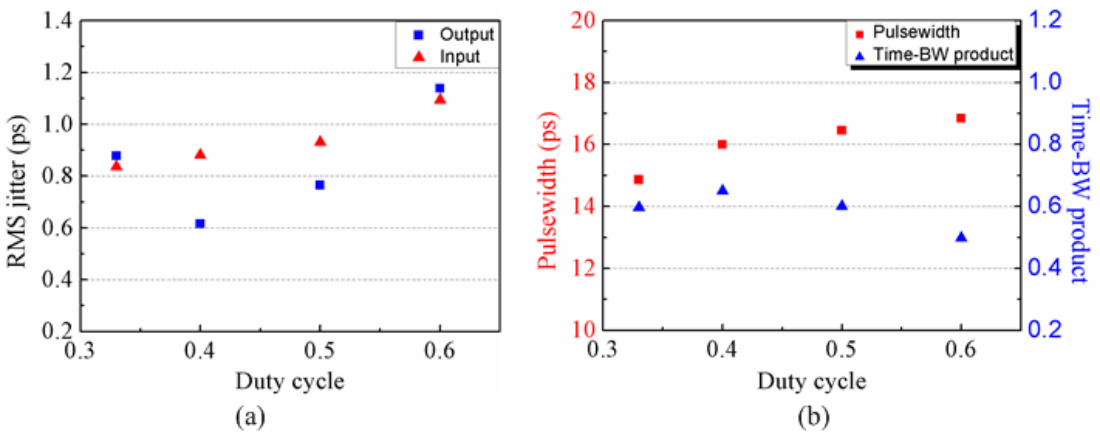

Figure 6.2 Dependence of clock recovery performance on the signal duty cycle. (a) RMS timing jitter vs. duty cycle. (b) Pulsewidth, TBW product vs. duty cycle.

6.3.1 Duty cycle

We change the duty cycle of the input signal by adjusting the bias of the MZM used for pulse carving. The peak power of the signal is kept the same for all duty cycles. The results are shown in Figure 6.2. It can be seen that the output timing jitter is less than the input when duty cycle is 40% and 50%. Besides, the output timing jitter degrades slightly for duty cycles of 33% and 60%. A possible reason for the jitter degradation is that 33% and 60% pulses are more vulnerable to cavity length drift which can cause de-synchronization between the circulating pulses and the pump pulses. Moreover, timing jitter may arise due to temperature changes and environmental perturbations. This can be avoided by using a feedback loop. The pulsewidth of the recovered clock varies from 14.9 ps to 16.8 ps while the TBW product varies from 0.50 to 0.65. It can be concluded that 40% duty cycle provides the best performance in terms of timing jitter but at the cost of a higher TBW product. Overall, the system works fine with duty cycles ranging from 33% to 60% with output timing jitter less than 1.2 ps.

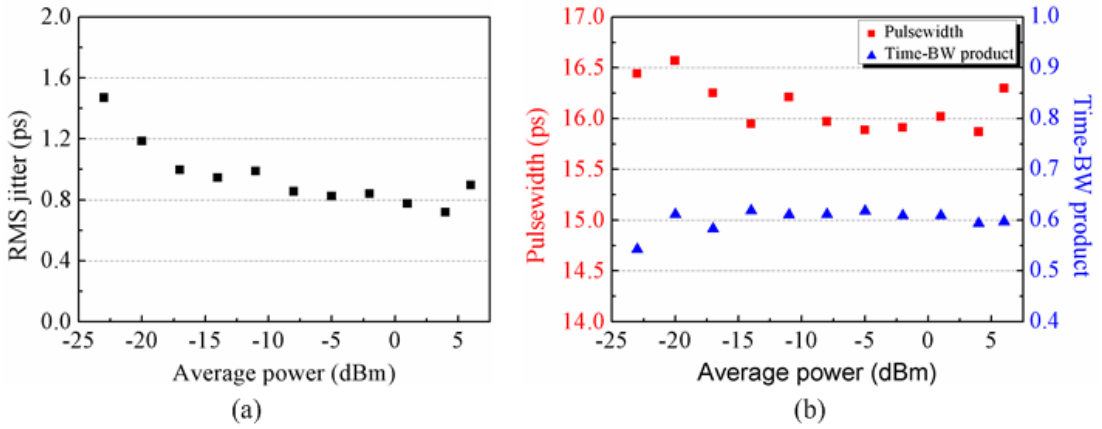

Figure 6.3 Dependence of clock recovery performance on the signal average input power. (a) RMS timing jitter vs. average input power. (b) Pulsewidth, TBW product vs. average input power.

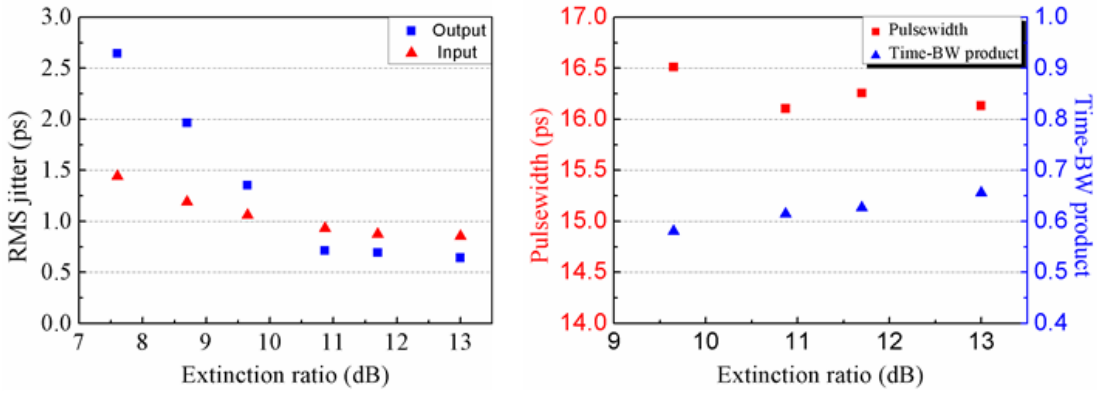

Figure 6.4 Dependence of clock recovery performance on the signal extinction ratio. (a) RMS timing jitter vs. extinction ratio. (b) Pulsewidth, TBW product vs. extinction ratio.

6.3.2 Average power

The average power of the input signal is changed by adjusting the attenuation value in VOA1. The results are shown in Figure 6.3. It is exciting to find out that the system exhibits large tolerance to the average input power. The timing jitter remains less than 1.5

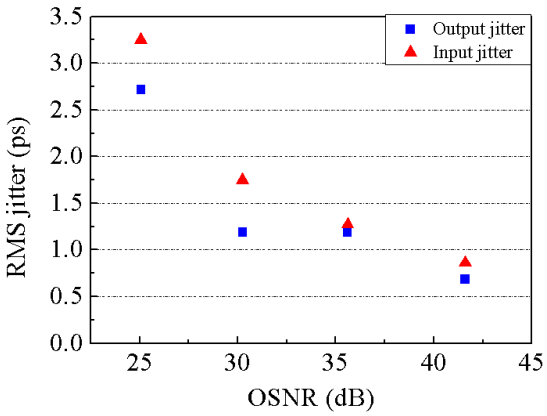

Figure 6.5 Dependence of clock recovery performance on the signal OSNR.

ps when the average input power is in the range from -23 dBm to 6 dBm. The reason is that the all-optical clock recovery circuit incorporates an EDFA which can amplify weak signals. The output pulsewidth is around 16.1 ps while the TBW product is around 0.61 for most of the input powers. Thus, we conclude that the system can retrieve stable clock signals with good quality in a large range of average input power from -23 dBm to 6 dBm.

6.3.3 Extinction ratio

The extinction ratio is changed by tuning PC1 before MZM1. The OSNR may change a bit when varying the extinction ratio. The results are shown in Figure 6.4. It can be seen that the output timing jitter is less than 2 ps for an extinction ratio larger than 8.7 dB. It is also noticeable that the output timing jitter becomes worse than the input jitter when the extinction ratio is less than 9.7 dB. The pulsewidth of the clock pulses varies from 16.1 ps to 16.5 ps while the TBW product ranges from 0.58 to 0.66 for extinction ratios larger than 9.7 dB. The measurement of pulsewidth from the DCA becomes inaccurate when the extinction ratio is below 9.7 dB. This is because the mode-locking strength becomes worse at a lower extinction ratio and CW-operation is competing with mode locking. As a result the recovered clock pulse looks quite noisy in waveform, so that the standard deviations of the measurements from the DCA become too large (~4 ps in our case) to be used. The results suggest that the extinction ratio of the input signal should be larger than about 10 dB in order to recover a clock with less timing jitter than the input.

6.3.4 OSNR

The OSNR is defined as the ratio of the signal power within the signal bandwidth to the noise power measured in 0.1 nm bandwidth. It is measured by using an OSA with 0.1 nm RBW in our experiment. The OSNR is changed by adding noise to the input signal. Specifically, noise power is controlled by adjusting the attenuation value of VOA2. But the total input power to the all-optical clock recovery circuit keeps constant in this case. The OSNR of the input signal is measured on the OSA with a RBW of 0.1 nm and a wavelength offset of 0.5 nm. The results are shown in Figure 6.5. It is observed that timing jitter of the recovered clock is less than 1.2 ps when the OSNR is larger than 30.3 dB. But it degrades to 2.7 ps when the OSNR equals 25.1 dB. So for error-free performance the input OSNR should be larger than about 27 dB. Note that the required OSNR is larger than what is typically expected (i.e., for a signal that requires regeneration); errors will arise if the OSNR is lower than this limit and this is one limitation of our approach. It is worth noting that the timing jitter for the recovered clock is less than the input when the input OSNR is larger than 25.1 dB. We did not measure the pulsewidth of the recovered clock in this case since the measurements from the DCA are not accurate in the presence of too much amplitude fluctuation when the input OSNR is below 30 dB.

6.3.5 Residual dispersion

In optical communication systems, residual dispersion usually occurs for the transmitted signal when it is not perfectly dispersion compensated. Figure 6.6shows the impact of residual dispersion of the input signal on the RMS timing jitter of the recovered clock. As can be seen, the timing jitter remains below 2 ps for residual dispersion from -600 ps/nm to 550 ps/nm (experimental result, not shown in the figure). The pulsewidth and TBW product keep around 14.5 ps and 0.7, correspondingly. The results show that FOPO based all-optical clock recovery has a large tolerance to the residual dispersion of the input signal. However, the timing jitter and amplitude fluctuation of the recovered clock signal become worse for large residual dispersion which is due to the larger pump pulse amplitude fluctuations arising from inter-symbol intereference.

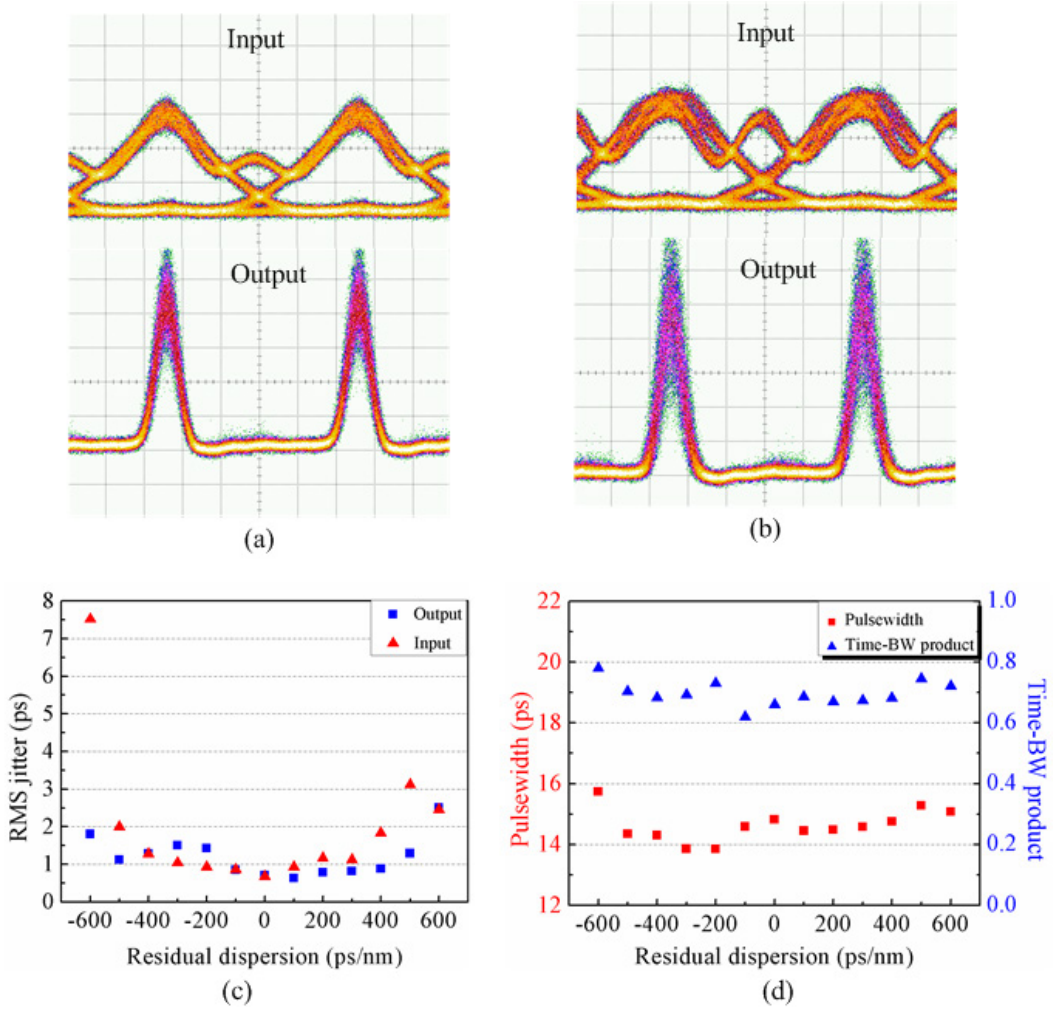

Figure 6.6 Dependence of clock recovery performance on the signal residual dispersion. (a) Waveforms of the input signal with 500 ps/nm residual dispersion and its corresponding recovered clock. (b) Waveforms of the input signal with -600 ps/nm residual dispersion and its corresponding recovered clock. (c) RMS timing jitter vs. residual dispersion. (b) Pulsewidth, TBW product vs. residual dispersion.

6.3.6 DGD

PMD is also an important factor that should be taken into account. Figure 6.7 shows the impact of DGD of the input signal on the recovered clock. It can be seen that the timing jitter remains below 2 ps for up to 48 ps of DGD. In fact, when the DGD is less than 36 ps, which is almost the FWHM of the input pulse, the clock signal can be recovered

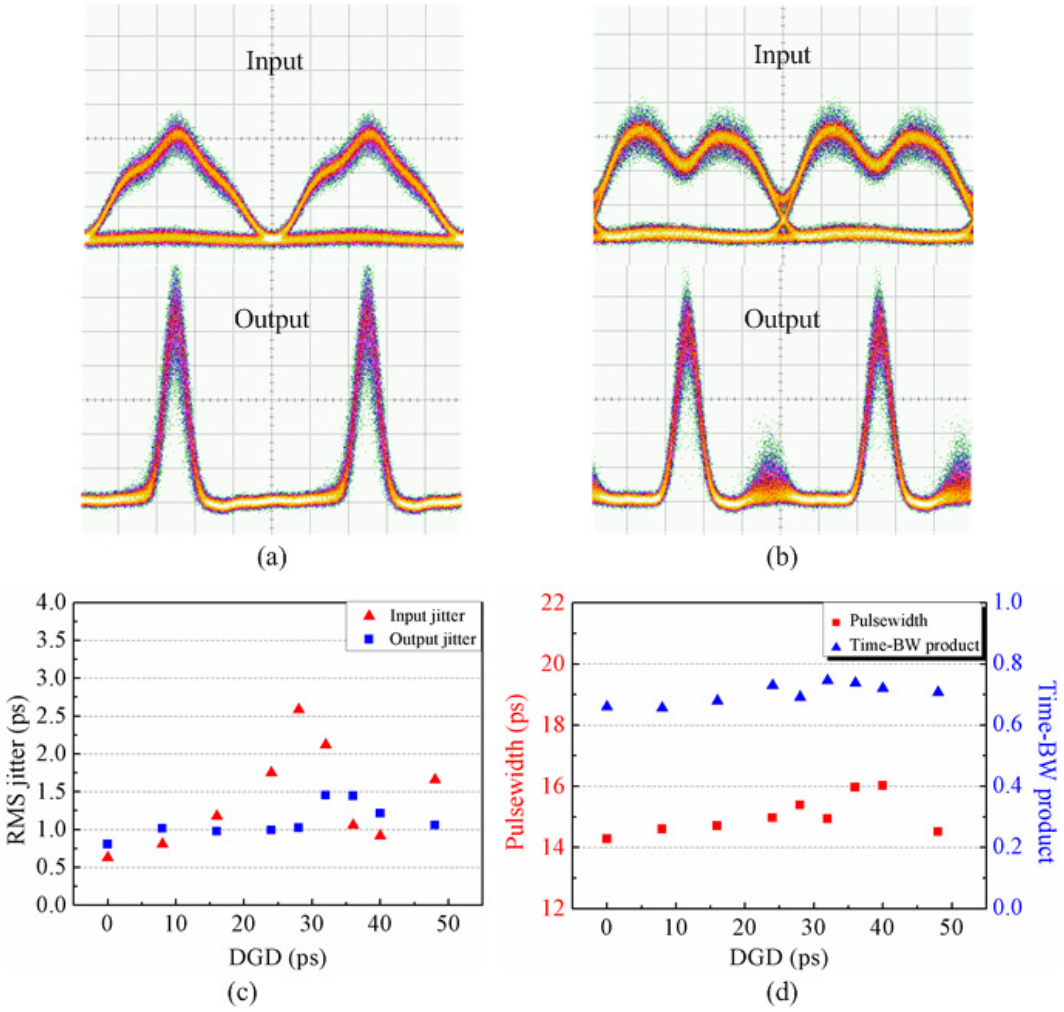

Figure 6.7 Dependence of clock recovery performance on the signal DGD. (a) Waveforms of the input signal with 36 ps DGD and its corresponding output recovered clock. 20 ps/div. (b) Waveforms of the input signal with 48 ps DGD and its corresponding output clock. 20 ps/div. (c) RMS timing jitter vs. DGD. (b) Pulsewidth, TBW product vs. DGD.

without adjusting the system parameters. But when the DGD is larger than 36 ps, the pulses in orthogonal SOPs are spaced apart in the time domain, as shown in Figure 6.7 (b). In this case, the clock signal cannot be recovered unless the SOP of the pump is adjusted to align with one of the SOPs of the pulses. So the clock signal is actually recovered from the input pulses in one SOP. The ghost pulses in the middle of the two clock pulses were generated due to the imperfect suppression of mode-locking in the orthogonal polarization state. It is observed that by changing the SOP of the pump or the

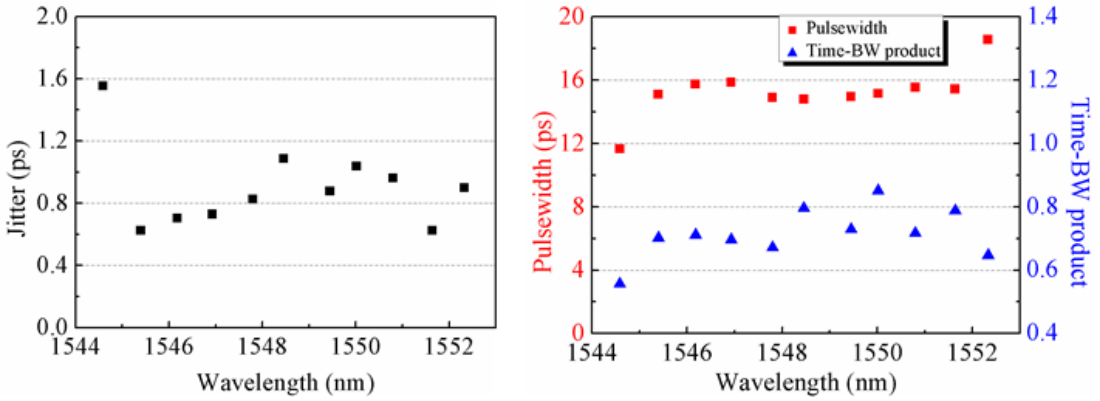

Figure 6.8 Dependence of clock recovery performance on the clock wavelength. (a) RMS timing jitter vs. clock wavelength. (b) Pulsewidth, TBW product vs. clock wavelength.

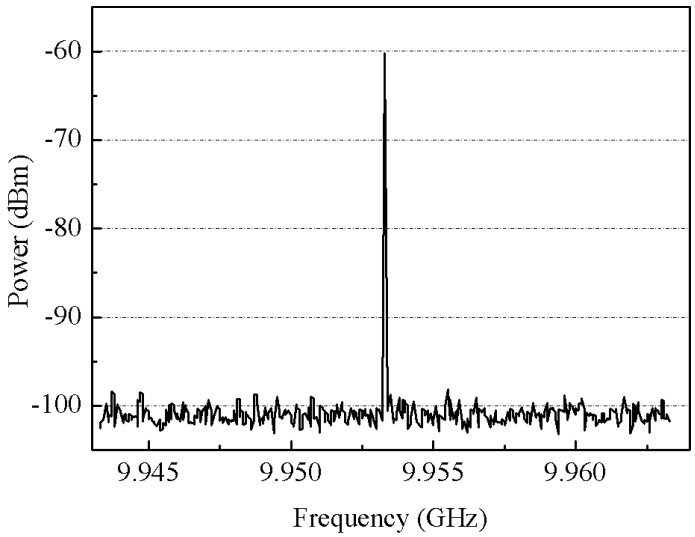

Figure 6.9 Electrical spectrum of the recovered clock from input signal without impairments. ESA RBW: 1 kHz.

signal the ghost pulses were increased in amplitude due to stronger mode-locking while the original clock signals were suppressed.

6.3.7 Tunability

An all-optical clock recovery circuit with a tunable output wavelength is important for all-optical "3R" regenerations in which the recovered clock signal can be all-optically

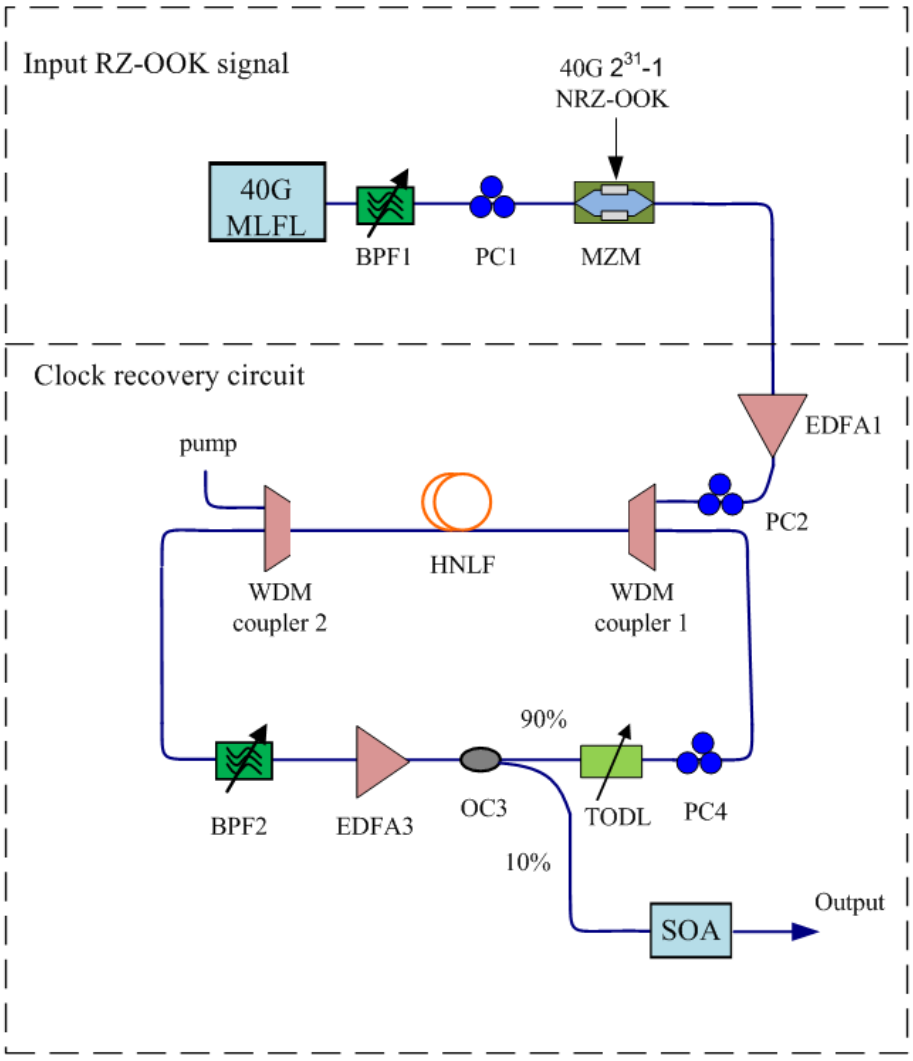

Figure 6.10 Experimental setup of FOPO based all-optical clock recovery operating at 40 Gb/s.

modulated by the NOLM or SOA interferometer. The inherent wavelength conversion feature of this approach can reduce the cost and complexity of WDM networks. We tested the tunability of the recovered clock signal by tuning the BPF in the cavity. The results are shown in Figure 6.8. It can be seen that the tuning range is from 1544.59 nm to 1552.33 nm, which is almost 8 nm. We expect that the same tuning range could also be obtained in the Stokes band, but we could not perform any measurements due to the lack of a tunable L-band filter. The tunability in the longer wavelength band is limited by the available bandwidth of the WDMC1 and WDMC2, which have a cutoff wavelength at 1551.4 nm. The tuning range is also limited by the parametric gain bandwidth which is

governed by the phase-matching condition. Since the pump power is relatively low in the clock recovery, the gain bandwidth is not large either. Larger gain bandwidth can be achieved by using shorter length of microstructure fibers or by engineering the fiber dispersion such that large range of phase-matching can be achieved. Besides, less than 1.6 ps timing jitter can be achieved over the whole tuning range. The pulsewidth is around 15.5 ps throughout the tuning range, while the TBW product scales from 0.56 to 0.85. The higher timing jitter and larger TBW product in the wavelength range from 1548.5 nm to 1551.6 nm are due to the larger parametric gain experienced in this region.

6.3.8 Electrical spectrum

Figure 6.9 shows the electrical spectrum of the recovered clock when the input is $2^{31} - 1$ RZ-OOK signal without impairments. The side-mode suppression ratio is about 40 dB, which shows the recovered clock does not have much timing jitter or amplitude fluctuation.

6.4 Demonstration of 40 Gb/s all-optical clock recovery

In the previous sections, the operating principle of all-optical clock recovery using an actively mode-locked FOPO has been introduced. The experimental results shown in section 6.3 have demonstrated that the approach is very robust to the input signal quality degradations. In order to demonstrate its ability to accommodate input signals of a higher data rate, a separate experiment is conducted using a similar setup in which the input is a 40 Gb/s RZ-OOK signal.

The experimental setup is shown in Figure 6.10. The 40 Gb/s RZ-OOK signal is generated using a 40 GHz mode-locked fiber laser modulated by a MZM driven by a $2^{31} - 1$ PRBS. The MLFL pulses are centered at 1557 nm and are broadened to 3.6 ps using a BPF1 with 0.85 nm bandwidth. The data signal pulse was broadened since FOPO based clock recovery has a better performance when the signal duty cycle is a bit larger (e.g., ~40%) according to the results obtained in the previous analysis. The signal is amplified by an EDFA1 to an average power of 13.9 dBm before being launched into the FOPO laser cavity. The cavity loss is about 11.2 dB, which is compensated mostly by EDFA2; the remainder of the loss is compensated using parametric gain in the HNLF. The

parametric gain is modulated by the input signal in an ultrafast nature so that mode-locking can be achieved. However, the parametric gain is kept low since it will help to reduce amplitude fluctuations of the recovered clock signal. The HNLF has the same characteristics as the one used in the previous chapters. Two WDMCs are used to combine/split the input signal and the recovered clock signal. BPF2 with a 3 dB bandwidth of 3.2 nm is used to select the output wavelength of the clock signal. An ODL is used to adjust the cavity length so that the signal modulation frequency is matched with the cavity resonance frequency. Ten percent of the power is coupled out of the cavity through an OC while ninety percent remains circulating inside the cavity. The recovered clock signal is amplified by an SOA (Covega, Nonlinear SOA) at the output of the cavity to reduce power fluctuations [174]. The output power before the SOA is -1.7 dBm.

First, we characterize the dependence of the RMS timing jitter and power fluctuations of the recovered clock signal on the SOA current. The RMS timing jitter is measured using a DCA triggered with a precision time base and operating in sample mode with a persistence time of 400 ms (the jitter noise floor is 200 fs). The power fluctuations are defined as the ratio between the standard deviation of the peak power and the mean value of the peak power. From Figure 6.11 it is clear that the RMS timing jitter and the power fluctuations are reduced with an increase in SOA current. In particular, the RMS timing jitter is reduced from 1.15 ps to 490 fs and the power fluctuations are reduced from 0.224 to 0.09 for the case when no SOA is used and when the SOA current is 250 mA, respectively. Sample eye diagrams are shown in Figure 6.12.

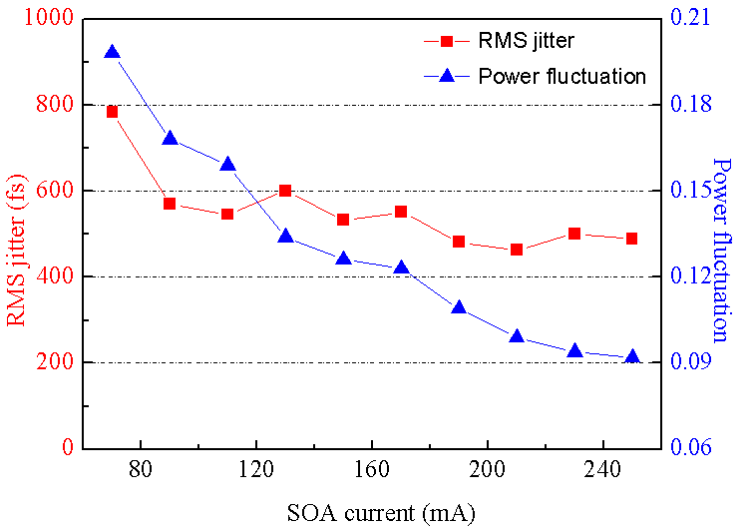

Figure 6.11 Characteristics of the recovered clock as a function as SOA current.

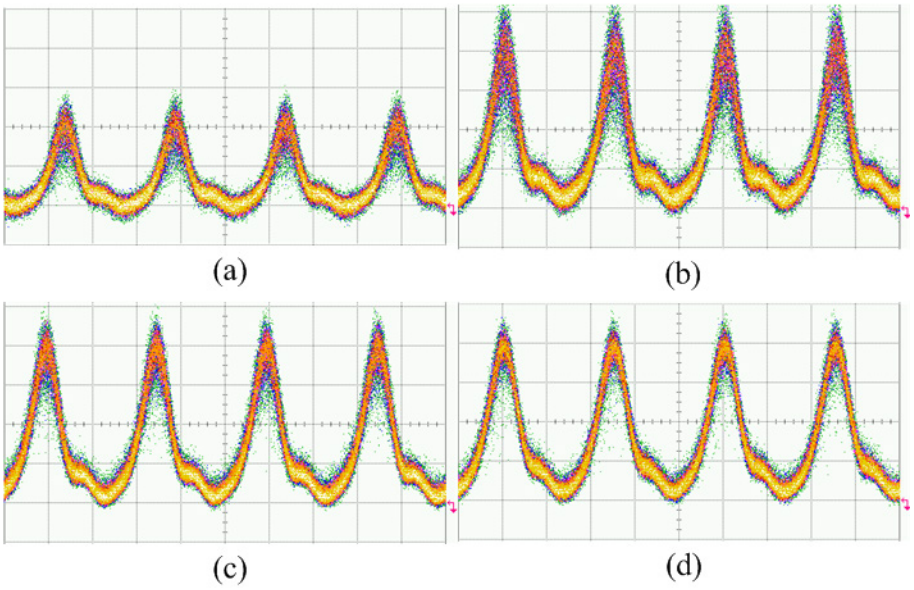

Figure 6.12 Waveforms of the recovered clock signal as a function of SOA current. (a) Waveform of the clock signal without SOA amplification. (b, c, d) Waveforms of the clock signals when the SOA operates at 70 mA, 150 mA, and 250 mA, correspondingly.

Next, we characterize the tuning range of the recovered clock signal and the corresponding variations of the RMS timing jitter and power fluctuations. The SOA

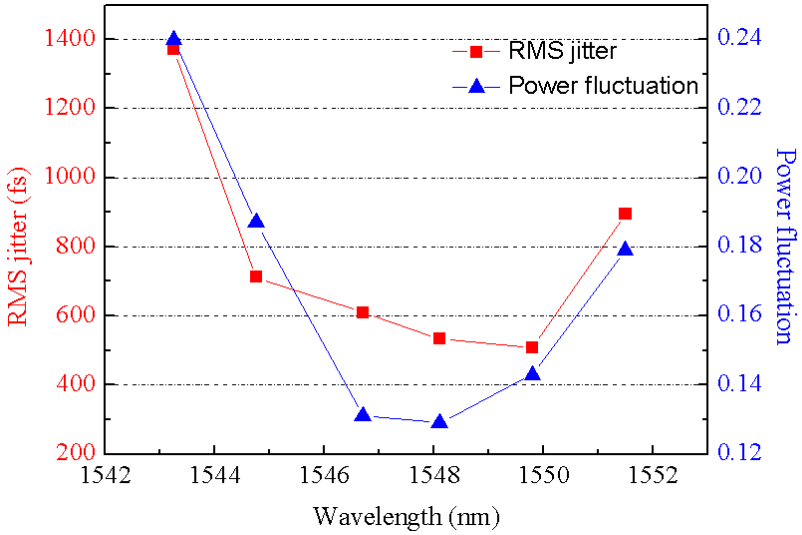

Figure 6.13 Characteristics of the recovered clock signal as a function of clock wavelength.

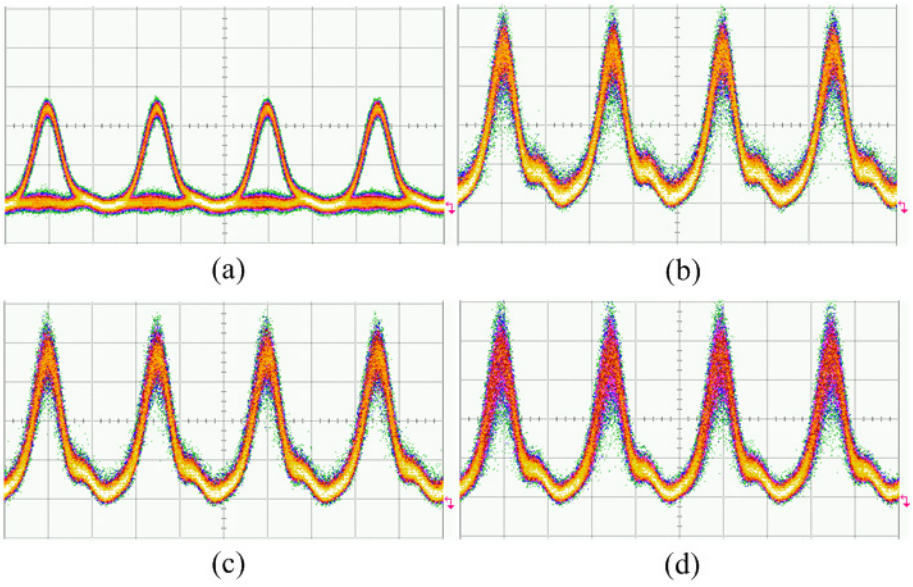

Figure 6.14 Waveforms of the recovered clock signal as a function of clock wavelength. (a) Waveform of the input signal. 10 ps/div. (b, c, d) Waveforms of the output clock at 1546.7 nm, 1549.8 nm, and 1551.5 nm, correspondingly. 10ps/div.

current is fixed at 150 mA during these measurements. It can be seen from Figure 6.13 that the clock signal is tunable over 8 nm (from 1543.3 nm to 1551.5 nm); the smallest RMS timing jitter and power fluctuations are obtained at a wavelength of ~1548 nm. Sample eye diagrams are shown in Figure 6.14. It is worth noting that all-optical clock

recovery with a tunable wavelength provides increased flexibility when performing processing functions such as all-optical 3R regeneration. In this experiment, the tuning range is limited by the bandwidth of the WDMCs and the specifications of the HNLF available.

6.5 Conclusions

In this chapter, a detailed analysis of all-optical clock recovery using FOPOs is performed. First, clock recovery using various approaches are reviewed which include using PPLs, self-pulsating lasers, spectral filtering, and actively mode-locked fiber ring lasers. Later, the experimental setup and the operating principle of FOPO based all-optical clock recovery operating at 10 Gb/s are introduced. Particularly, the way to optimize cavity parameters is explained. Later, we investigate the impact of changing the duty cycle, average power, extinction ratio, OSNR, residual dispersion and DGD of the input signal on the recovered clock characteristics in terms of the RMS timing jitter, pulsewidth and TBW product. To retrieve a clock signal with a timing jitter less than 2 ps, the input signal should have a duty cycle from 33% to 60%, an average power from -23 dBm to 6 dBm, an extinction ration larger than 8.7 dB, an OSNR better than 27 dB, a residual dispersion between -600 ps/nm and 550 ps/nm, and a DGD below 48 ps. The tunable range of the clock is also investigated which is about 8 nm in the anti-Stokes band. Although the wavelength of the input signal is fixed at 1556.5 nm in our experiment, it is not necessary unless it is located near the zero-dispersion wavelength of the HNLF in the anomalous dispersion regime. The tolerance on the input signal wavelength depends on the dispersion profile of the HNLF used and needs to be considered in the design of the all-optical clock recovery subsystem. In the end, 40 Gb/s all-optical clock recovery is demonstrated using a similar experimental setup. The performance of the all-optical clock recovery circuit is characterized in terms of the RMS timing jitter and the power fluctuation of the recovered clock pulses. In particular, it is observed that the timing jitter and power fluctuation performance can be improved significantly if a saturated SOA is placed at the output of the clock recovery circuit.

In summary, the results show that FOPO based all-optical clock recovery is promising in terms of low timing jitter with large tolerance to the input signal

impairments. The quantified requirements of input signal are useful for the future system design.

Chapter 7 Conclusions and Future work

7.1 Summary of contributions

Optical transport network is evolving at an unprecedented speed to meet the ever increasing demand for bandwidth. Various technologies such as OTDM, WDM, and coherent communication have helped us exploit the full capacity that can be provided by optical fiber. No matter what advanced technology is going to be prevailing in the future optical transport network, some of its constituent components such as amplifiers, lasers and signal processing units always play an important role. Simple design, cost-effective, versatile functionalities, and easy to be upgraded are the key requirements for the future agile optical networks. In this dissertation, a versatile platform, named FOPO, is proposed to meet such requirements. Based on parametric amplification, a third-order nonlinear effect in optical fiber, FOPOs are demonstrated to produce single wavelength or multiple wavelength CW signals, pulsed signals at various repetition rates, and can recover clock signals from incoming data stream with various data rates. Almost all designs are based on a common simple system configuration as described in section 2.3.4, while they may vary a bit according to their specific applications and requirements. Detailed analysis is performed in these applications, from which useful design guidelines are generated. The main contributions can be summarized as below.

(1) A stable multi-wavelength FOPO is demonstrated which can lase 129 wavelengths with 25-GHz spacing simultaneously. The power non-uniformity is only 4.5 dB over the entire emission spectrum. The results are limited to the available bandwidth of the programmable filter and WDMCs used in the experiment. Moreover, the proposed multi-wavelengths FOPO is tunable over the whole lasing spectrum (~25.6 nm) and reconfigurable to arbitrary lasing bands without sacrificing the performance. This demonstrates the largest wavelength number and the flattest lasing spectrum that have ever been reported to date, and the first time demonstration of a tunable and reconfigurable emission spectrum from a multi-wavelength CW FOPO.

(2) The performance of a 10 GHz actively mode-locked FOPO is investigated in detail such as the impact of pump pulse duty cycle, pump power, dispersion management

in the cavity, filter BW, and lasing wavelength on the output pulse quality. The results show that by properly configuring the experimental setups and parameters (e.g., pump pulse with smaller duty cycle, higher pump power, with intra-cavity dispersion management, without pump phase modulation, and with a proper FBW), mode-locked pulses with shorter duration, less RMS timing jitter, less TBW product and high SNSR can be generated. This represents the first detailed analysis on the actively mode-locked FOPO, and the results obtained show a significant improvement over the previous reported results using a similar configuration in terms of the pulsewidth, RMS timing jitter and wavelength tuning range.

(3) Two ways of laser repetition rate multiplication are investigated: nonlinear frequency doubling in a MZM by biasing the MZM in the null transmission point, and RHML. The results show that RHML is superior to the other one in terms of simple configuration, and easy to generate higher-order frequency multiplied optical pulses. Based on this method, optical pulses have been generated with repetition rates from 10 to 30 GHz using a 10 GHz optical pump source, and from 40 GHz to 240 GHz using a 40 GHz optical pump source. This represents the highest repetition rate that a FOPO can achieve.

(4) A detailed analysis of all-optical clock recovery at 10 Gb/s using FOPOs is presented. The proposed all-optical clock recovery method is very robust to input signal quality degradations due to the transmission line impairments. The results suggest that error-free operating can be achieved when the input signal has duty cycle from 33% to 60%, average power from -23 dBm to 6 dBm, extinction ration larger than 8.7 dB, OSNR better than 27 dB, residual dispersion from -600 ps/nm to 550 ps/nm, and DGD below 48 ps. This demonstrates for the first time a detailed and thorough investigation on the FOPO based all-optical clock recovery. 40 Gb/s all-optical clock recovery is also demonstrated successfully which proves its feasibility of being implemented in applications that require a higher operating speed.

7.2 Future work

7.2.1 > 40 Gb/s all-optical clock recovery

FOPO based all-optical clock recovery approach has the potential to be operated at a higher speed (i.e., > 40 Gb/s) since the parametric process in optical fiber has an inherent ultrafast response (~ fs). However, it is difficult to be implemented in practice due to the following reasons: first, the incoming high-data-rate OTDM signals are generated by combining several low-data-rate signals with appropriate time difference between them, as we discussed in section 1.1. The SOP of the comprised low-data-rate signals may not be the same at the input of the transmission fiber link and therefore different when they arrive at the clock recovery circuit. As we know that parametric amplification is highly sensitive to the SOP of the interacting waves (i.e., the incoming data signal and the recovered clock signal in this case). The parametric gain could fluctuate significantly if the SOP of the data signal and the clock signal are not properly aligned, which could cause failure in the laser mode-locking process. Second, as the signal data rate increases the pulse duration becomes smaller, and as a result is more vulnerable to the cavity length drift caused by temperature change and/or environment perturbation. In addition, a higher EDFA gain is required to bring up the total input power into the HNLF since the peak power needs to be maintained to be the same when the repetition rate is increased. Higher EDFA gain would introduce more ASE noise that could degrade the OSNR of the input signal. As we know from section 6.3.4 that clock recovery performance is quite sensitive to the OSNR of the input signal. Therefore, extra precautions need to be taken into account when designing the FOPO based all-optical clock recovery circuit. HNLF with a shorter length is preferred to reduce the impact of the cavity length drift, and small dispersion slope at 1550 nm is still required in order to achieve a broadband parametric gain and to reduce the walk-off between the data signal and the recovered clock signal. Polarization maintaining optical multiplexer (OMUX) is necessary to make sure the input low-data-rate signals keeps the same SOP. Low-noise high-power EDFA need to be used as a pre-amplifier at the input of the clock recovery circuit, and a following BPF would be helpful to reduce the ASE noise in the pump source.

7.2.2 Multi-wavelength mode-locking and all-optical clock recovery

Single wavelength actively mode-locked FOPO has been discussed in chapter Chapter 4 , in which a BPF is used to select the required wavelength, and an ODL to adjust the cavity length so that mode-locking condition can be satisfied. However, if we want to design a multi-wavelength actively mode-locked FOPO, different wavelength should meet the harmonic mode-locking condition simultaneously. But it is always not straight forward to design a multi-wavelength non-dispersive optical filter in practice. If the filter is dispersive, then the cavity length of each wavelength needs to be adjusted precisely and independently, which increases the cost and complexity of the system. Also a number of feedback loops are required to stabilize the cavity length of such lasers. To overcome the problems mentioned above, a cavity with high dispersion can be used in the multi-wavelength actively mode-locked fiber ring lasers. In such lasers, the wavelength can be tunable by changing the modulation frequency of the driving source or the cavity length, which is referred to as dispersion tuning.

The principle of dispersion tuning is well explained in [132]: if the cavity consists of a spool of dispersion-compensation fiber (DCF) as the dispersive medium, the *m*th harmonic frequency of the laser cavity is expressed as:

$$f = \frac{mc}{n(\lambda)L + n_d(\lambda)L_d} \tag{7.1}$$

where λ is the light wavelength, c is the light velocity in vacuum, and L is the cavity length excluding the length of the DCF, L_d is the length of DCF, and n and n_d are the group indices of SMF and DCF, respectively.

The derivative of f with respect to λ can be expressed as:

$$\frac{df}{d\lambda} = -\frac{f^2}{m}[D(\lambda)L + D_d(\lambda)L_d] \tag{7.2}$$

where $D(\lambda)$ and $D_d(\lambda)$ are the dispersion parameters of the SMF and DCF, respectively. From Eq (7.1 - 7.2), it can be found that the fundamental and harmonic frequencies are all wavelength dependent. So the emission wavelength of the laser can be tuned continuously by changing the modulation frequency so as to keep the fundamental or one of the harmonic frequencies.

Since the wavelength tuning range is much smaller than the light wavelength as well as it is far away from the ZDW of the SMF and DCF, D and D_d can be assumed to be constant in the tuning range. Then the frequency difference between the mth harmonic of the wavelength λ_l and the (m+N)th harmonic of wavelength λ_s (λ_l and λ_s are the longest and shortest wavelengths of the gain bandwidth of the gain medium) is given by:

$$\Delta f = \frac{mc}{n(\lambda_l)L + n_d(\lambda_l)L_d} - \frac{(m+N)c}{n(\lambda_l)L + n_d(\lambda_l)L_d + c(DL + D_d L_d)(\lambda_s - \lambda_l)} \tag{7.3}$$

If N=1 and f<0, the laser can only work with one wavelength in the entire tuning range when the laser is modulated at the mth or lower harmonic orders. If $\Delta f \geq 0$, (N+1) wavelengths may be mode-locked simultaneously when the laser is modulated at the mth or higher harmonic orders. It can be found from Eq. (7.3) that if we want to get single-wavelength operation at higher repetition rate we can reduce the cavity dispersion; conversely, multi-wavelength operation can be obtained at lower modulation frequencies by increasing the cavity dispersion.

Dispersion-tuned actively mode-locked FOPO has been demonstrated in [49], single wavelength 10-GHz tunable pulses can be generated by using a spool of DCF with low dispersion. Instead of DCF, linear-chirped FBG can also be used as the dispersive medium, which is more compact compared with DCF and thus is easier for integration. Moreover, the short length of LCFBGs can increase the stability of the laser to environmental perturbations. So for the future work, a single wavelength dispersion-tuned harmonic mode-locked FOPO based on LCFBGs could be investigated first. Then multi-wavelength operation could be tried with larger cavity dispersion or by decreasing the modulation frequency of the laser.

As another method, we can use a super-imposed linearly-chirped FBG as the dispersive medium in the cavity. Since each reflection band of the FBG has almost the same dispersion characteristics, different wavelength can be self-tuned and be mode-locked in the same harmonic order. The dispersion of each band enables the dispersion tuning of the emission wavelength when changing the modulation frequency or the cavity length. This method has been demonstrated in the SOA based mode-locked fiber ring lasers [133], in which 2 to 4 wavelengths mode-locked pulses can be generated. As a future work, the feasibility and performance of this approach can be investigated,

which will be very important to demonstrate that FOPO is a promising approach as a multi-wavelength pulse source and has the potential to be used for multi-wavelength all-optical clock recovery applications.

7.2.3 Silicon based optical parametric amplifier and oscillator

A considerable amount of work has been done in FOPAs and FOPOs in which the nonlinear medium is silica fiber. However, since the nonlinear refractive index n_2 is quite low in silica fiber, hundreds of meters interaction length is usually required to achieve certain nonlinear effects with moderate amount of optical power. Alternatively, silicon exhibits $\chi^{(3)}$ nonlinearity too, with n_2 two orders of magnitude larger than that in silica. Combining with even tighter confinement of light in silicon chips than in silica fiber, silicon waveguide with proper design can exhibit nonlinear coefficient γ more than three orders of magnitude larger than state-of-the-art highly-nonlinear fibers [211]. So silicon waveguide is a promising platform for all-optical signal processors with the capabilities of dense integration and massive production with low costs. Indeed, various types of nonlinear effects have been demonstrated in silicon waveguides in recent years [212], including parametric amplifiers and oscillators [213, 214]. It would definitely be interesting to continue exploiting the possibility of realizing functionalities such as multi-wavelength lasing, mode-locking, and all-optical clock recovery on the silicon platform.

REFERENCES

[1] TeleGeography. (2013). *International Bandwidth Demand is Decentralizing*. Available: http://www.telegeography.com/press/press-releases/2013/04/17/international-bandwidth-demand-is-decentralizing/index.html

[2] Cisco. (2013). *Cisco Visual Networking Index: Forecast and Methodology*. Available: http://www.cisco.com/en/US/solutions/collateral/ns341/ns525/ns537/ns705/ns827/white_paper_c11-481360.pdf

[3] IEEE. (2013). *IEEE Launches Study Group To Explore 400 Gb/s Ethernet*. Available: http://standards.ieee.org/news/2013/400gbs_ethernet.html

[4] G. P. Agrawal, *Fiber-optic Communication Systems*, 4th ed. New Jersey: John Wiley & Sons, Inc., 2010.

[5] K. Kao and G. A. Hockham, "Dielectric-fibre surface waveguides for optical frequencies," *Proc. IEE,* vol. 113, no. 7, pp. 1151-1158, 1966.

[6] T. Miya, Y. Terunuma, T. Hosaka, and T. Miyashita, "Ultimate low-loss single-mode fibre at 1.55 μm," *Electron. Lett.,* vol. 15, no. 4, pp. 106-108, 1979.

[7] T. Morioka, Y. Awaji, R. Ryf, P. Winzer, D. Richardson, and F. Poletti, "Enhancing optical communications with brand new fibers," *IEEE Comm. Mag.,* vol. 50, no. 2, pp. s31-s42, Feb. 2012.

[8] H.-G. Weber, R. Ludwig, S. Ferber, C. Schmidt-Langhorst, M. Kroh, V. Marembert, *et al.*, "Ultrahigh-speed OTDM-transmission technology," *J. Lightw. Technol.,* vol. 24, no. 12, pp. 4616-4627, Dec. 2006.

[9] M. Nakazawa, T. Yamamoto, and K. Tamura, "1.28 Tbit/s-70 km OTDM transmission using third-and fourth-order simultaneous dispersion compensation with a phase modulator," *Electron. Lett.,* vol. 36, no. 24, pp. 2027-2029, Nov. 2000.

[10] H. Weber, S. Ferber, M. Kroh, C. Schmidt-Langhorst, R. Ludwig, V. Marembert, *et al.*, "Single channel 1.28 Tbit/s and 2.56 Tbit/s DQPSK transmission," in *31st European Conference on Optical Communication*, 2005, pp. 3-4.

[11] C. Schmidt-Langhorst, R. Ludwig, D.-D. Groß, L. Molle, M. Seimetz, R. Freund, *et al.*, "Generation and coherent time-division demultiplexing of up to 5.1 Tb/s single-channel 8-PSK and 16-QAM signals," in *Conference on Optical Fiber Communication-incudes post deadline papers*, 2009, pp. 1-3.

[12] H. Hu, M. Galili, L. Oxenlowe, J. Xu, H. C. H. Mulvad, C. Peucheret, *et al.*, "Error-free transmission of serial 1.28 Tbaud RZ-DPSK signal," in *36th European Conference and Exhibition on Optical Communication (ECOC)*, 2010, pp. 1-3.

[13] H. H. Mulvad, M. Galili, L. K. Oxenløwe, H. Hu, A. T. Clausen, J. B. Jensen, *et al.*, "Demonstration of 5.1 Tbit/s data capacity on a single-wavelength channel," *Opt. Exp.,* vol. 18, no. 2, pp. 1438-1443, Jan. 2010.

[14] E. Palushani, C. Schmidt-Langhorst, T. Richter, M. Nolle, R. Ludwig, and C. Schubert, "Transmission of a serial 5.1-Tb/s data signal using 16-QAM and coherent detection," in *37th European Conference and Exhibition on Optical Communication (ECOC)*, 2011, pp. 1-3.

[15] T. Richter, E. Palushani, C. Schmidt-Langhorst, M. Nölle, R. Ludwig, and C. Schubert, "Single wavelength channel 10.2 Tb/s TDM-data capacity using 16-QAM and coherent detection," in *Optical Fiber Communication Conference*, 2011.

[16] T. Richter, E. Palushani, C. Schmidt-Langhorst, R. Ludwig, L. Molle, M. Nolle, *et al.*, "Transmission of single-channel 16-QAM data signals at terabaud symbol rates," *J. Lightw. Technol.,* vol. 30, no. 4, pp. 504-511, Feb. 2012.

[17] M. Vasilyev, I. Tomkos, M. Mehendale, J.-K. Rhee, A. Kobyakov, M. Ajgaonkar, *et al.*, "Transparent Ultra-Long-Haul DWDM Networks With "broadcast-and-select" OADM/OXC architecture," *J. Lightw. Technol.,* vol. 21, no. 11, p. 2661, 2003.

[18] A. Tzanakaki, I. Zacharopoulos, and I. Tomkos, "Optical add/drop multiplexers and optical cross-connects for wavelength routed networks," in *Proceedings of 2003 5th International Conference on Transparent Optical Networks*, 2003, pp. 41-46.

[19] K. Fukuchi, T. Kasamatsu, M. Morie, R. Ohhira, T. Ito, K. Sekiya, *et al.*, "10.92-Tb/s (273 x 40-Gb/s) triple-band/ultra-dense WDM optical-repeatered transmission experiment," in *Optical Fiber Communication Conference*, 2001.

[20] G. C. Gupta, R. E. Tench, O. Mizuhara, L. L. Wang, N. N. Dang, N. Chand, *et al.*, "3.2 Tbit/s (40× 80 Gb/s) transmission over 1000 km with 100 km span (25 dB loss) and 0.8 bit/s/Hz of spectral efficiency," in *Optical Fiber Communication Conference and Exhibit*, 2002, pp. 6-8.

[21] C. Rasmussen, T. Fjelde, J. Bennike, F. Liu, S. Dey, B. Mikkelsen, *et al.*, "DWDM 40G transmission over trans-pacific distance (10000 km) using CSRZ-DPSK, enhanced FEC, and all-Raman-amplified 100-km UltraWave fiber spans," *J. Lightw. Technol.,* vol. 22, no. 1, p. 203, Jan. 2004.

[22] R. C. Alferness, P. A. Bonenfant, C. J. Newton, K. A. Sparks, and E. L. Varma, "A practical vision for optical transport networking," *Bell Labs Technical Journal,* vol. 4, no. 1, pp. 3-18, 1999.

[23] P. J. Winzer and R.-J. Essiambre, "Advanced optical modulation formats," *Proc. IEEE,* vol. 94, no. 5, pp. 952-985, May 2006.

[24] P. J. Winzer, "High-spectral-efficiency optical modulation formats," *J. Lightw. Technol.,* vol. 30, no. 24, pp. 3824-3835, Dec. 2012.

[25] A. Sano, T. Kobayashi, S. Yamanaka, A. Matsuura, H. Kawakami, Y. Miyamoto, *et al.*, "102.3-Tb/s (224 x 548-Gb/s) C-and extended L-band all-Raman transmission over 240 km using PDM-64QAM single carrier FDM with digital pilot tone," in *Optical Fiber Communication Conference*, 2012.

[26] S. J. Savory, "Digital coherent optical receivers: algorithms and subsystems," *IEEE J. Sel. Topics Quantum Electron.,* vol. 16, no. 5, pp. 1164-1179, Sep/Oct. 2010.

[27] R.-J. Essiambre, G. Kramer, P. J. Winzer, G. J. Foschini, and B. Goebel, "Capacity limits of optical fiber networks," *J. Lightw. Technol.,* vol. 28, no. 4, pp. 662-701, Feb. 2010.

[28] L. Oxenløwe, M. Galili, H. H. Mulvad, H. Hu, H. Ji, J. Xu, *et al.*, "Ultra-high-speed optical signal processing of Tbaud data signals," in *36th European Conference and Exhibition on Optical Communication (ECOC)*, 2010, pp. 1-6.

[29] R. Driad, R. Makon, V. Hurm, K. Schneider, F. Benkhelifa, R. Losch, *et al.*, "InP DHBT-based ICs for 100 Gbit/s data transmission," in *Indium Phosphide and Related Materials, 2008. IPRM 2008. 20th International Conference on*, 2008, pp. 1-4.

[30] G. P. Agrawal, *Nonlinear Fiber Optics*, 3rd ed. San Diego, CA: Academic, 2001.

[31] M. Nikles, L. Thevenaz, and P. A. Robert, "Brillouin gain spectrum characterization in single-mode optical fibers," *J. Lightw. Technol.,* vol. 15, no. 10, pp. 1842-1851, 1997.

[32] D. Dougherty, F. Kärtner, H. Haus, and E. Ippen, "Measurement of the Raman gain spectrum of optical fibers," *Opt. Lett.,* vol. 20, no. 1, pp. 31-33, 1995.

[33] J. Hansryd, P. A. Andrekson, M. Westlund, J. Li, and P. O. Hedekvist, "Fiber-based optical parametric amplifiers and their applications," *IEEE J. Sel. Topics Quantum Electron.,* vol. 8, no. 3, pp. 506-520, May/Jun. 2002.

[34] S. Radic, C. McKinstrie, R. Jopson, J. Centanni, Q. Lin, and G. Agrawal, "Record performance of parametric amplifier constructed with highly nonlinear fibre," *Electron. Lett.,* vol. 39, no. 11, pp. 838-839, 2003.

[35] T. Torounidis, P. A. Andrekson, and B.-E. Olsson, "Fiber-optical parametric amplifier with 70-dB gain," *IEEE Photon. Technol. Lett.,* vol. 18, no. 10, pp. 1194-1196, May 2006.

[36] K. K. Wong, K. Shimizu, K. Uesaka, G. Kalogerakis, M. E. Marhic, and L. G. Kazovsky, "Continuous-wave fiber optical parametric amplifier with 60-dB gain using a novel two-segment design," *IEEE Photon. Technol. Lett.,* vol. 15, no. 12, pp. 1707-1709, Dec. 2003.
[37] T. Torounidis and P. Andrekson, "Broadband single-pumped fiber-optic parametric amplifiers," *IEEE Photon. Technol. Lett.,* vol. 19, no. 9, pp. 650-652, May 2007.
[38] M. E. Marhic, K.-Y. Wong, and L. G. Kazovsky, "Wide-band tuning of the gain spectra of one-pump fiber optical parametric amplifiers," *IEEE J. Sel. Topics Quantum Electron.,* vol. 10, no. 5, pp. 1133-1141, Sep/Oct. 2004.
[39] J. D. Marconi, J. M. Chavez Boggio, H. L. Fragnito, and S. R. Bickham, "Nearly 100 nm bandwidth of flat gain with a double-pumped fiber optic parametric amplifier," in *Optical Fiber Communication Conference*, 2007.
[40] J. L. Blows and S. E. French, "Low-noise-figure optical parametric amplifier with a continuous-wave frequency-modulated pump," *Opt. Lett.,* vol. 27, no. 7, pp. 491-493, 2002 2002.
[41] P. L. Voss, R. Tang, and P. Kumar, "Measurement of the photon statistics and the noise figure of a fiber-optic parametric amplifier," *Opt. Lett.,* vol. 28, no. 7, pp. 549-551, 2003 2003.
[42] K. K. Y. Wong, M. E. Marhic, K. Uesaka, and L. G. Kazovsky, "Polarization-independent one-pump fiber-optical parametric amplifier," *IEEE Photon. Technol. Lett.,* vol. 14, no. 11, pp. 1506-1508, Nov. 2002.
[43] K. K. Y. Wong, M. E. Marhic, K. Uesaka, and L. G. Kazovsky, "Polarization-independent two-pump fiber optical parametric amplifier," *IEEE Photon. Technol. Lett.,* vol. 14, no. 7, pp. 911-913, Jul. 2002.
[44] M. E. Marhic, K. K. Y. Wong, L. G. Kazovsky, and T. E. Tsai, "Continuous-wave fiber optical parametric oscillator," *Opt. Lett.,* vol. 27, no. 16, pp. 1439-1441, Aug. 2002.
[45] C. J. S. De Matos, J. R. Taylor, and K. P. Hansen, "Continuous-wave, totally fiber integrated optical parametric oscillator using holey fiber," *Opt. Lett.,* vol. 29, no. 9, pp. 983-985, May 2004.
[46] S. Yang, X. Xu, Y. Zhou, K. K. Y. Cheung, and K. K. Y. Wong, "Continuous-wave single-longitudinal-mode fiber-optical parametric oscillator with reduced pump threshold," *IEEE Photon. Technol. Lett.,* vol. 21, no. 24, pp. 1870-1872, Dec. 2009.
[47] S. Yang, K. K. Y. Cheung, Y. Zhou, and K. K. Y. Wong, "Tunable single-longitudinal-mode fiber optical parametric oscillator," *Opt. Lett.,* vol. 35, no. 4, pp. 481-483, Feb. 2010.
[48] S. Yang, Y. Zhou, J. Li, and K. K. Y. Wong, "Actively mode-locked fiber optical parametric oscillator," *IEEE J. Sel. Topics Quantum Electron.,* vol. 15, no. 2, pp. 393-398, Mar/Apr. 2009.
[49] S. Yang, K. K. Cheung, Y. Zhou, and K. K. Wong, "Dispersion-tuned harmonically mode-locked fiber-optical parametric oscillator," *IEEE Photon. Technol. Lett.,* vol. 22, no. 8, pp. 580-582, Apr. 2010.
[50] D. K. Serkland, G. D. Bartolini, A. Agarwal, P. Kumar, and W. L. Kath, "Pulsed degenerate optical parametric oscillator based on a nonlinear-fiber Sagnac interferometer," *Opt. Lett.,* vol. 23, no. 10, pp. 795-797, May 1998.
[51] D. K. Serkland and P. Kumar, "Tunable fiber-optic parametric oscillator," *Opt. Lett.,* vol. 24, no. 2, pp. 92-94, Jan. 1999.
[52] J. E. Sharping, M. Fiorentino, A. Coker, P. Kumar, and R. S. Windeler, "Four-wave mixing in microstructure fiber," *Opt. Lett.,* vol. 26, no. 14, pp. 1048-1050, Jul. 2001.
[53] J. E. Sharping, M. Fiorentino, P. Kumar, and R. S. Windeler, "Optical parametric oscillator based on four-wave mixing in microstructure fiber," *Opt. Lett.,* vol. 27, no. 19, pp. 1675-1677, Oct. 2002.

[54] J. E. Sharping, M. A. Foster, A. L. Gaeta, J. Lasri, O. Lyngnes, and K. Vogel, "Octave-spanning, high-power microstructure-fiber-based optical parametric oscillators," *Opt. Exp.,* vol. 15, no. 4, pp. 1474-1479, Feb. 2007.

[55] J. Lasri, P. Devgan, R. Tang, J. E. Sharping, and P. Kumar, "A microstructure-fiber-based 10-GHz synchronized tunable optical parametric oscillator in the 1550-nm regime," *IEEE Photon. Technol. Lett.,* vol. 15, no. 8, pp. 1058-1060, Aug. 2003.

[56] J. E. Sharping, "Microstructure fiber based optical parametric oscillators," *J. Lightw. Technol.,* vol. 26, no. 14, pp. 2184-2191, Jul. 2008.

[57] J. D. Harvey, R. Leonhardt, S. Coen, G. K. Wong, J. Knight, W. J. Wadsworth, *et al.*, "Scalar modulation instability in the normal dispersion regime by use of a photonic crystal fiber," *Opt. Lett.,* vol. 28, no. 22, pp. 2225-2227, 2003.

[58] A. Y. H. Chen, G. K. L. Wong, S. G. Murdoch, R. Leonhardt, J. D. Harvey, J. C. Knight, *et al.*, "Widely tunable optical parametric generation in a photonic crystal fiber," *Opt. Lett.,* vol. 30, no. 7, pp. 762-764, Apr. 2005.

[59] Y. Q. Xu, S. G. Murdoch, R. Leonhardt, and J. D. Harvey, "Widely tunable photonic crystal fiber Fabry-Perot optical parametric oscillator," *Opt. Lett.,* vol. 33, no. 12, pp. 1351-1353, Jun. 2008.

[60] G. K. L. Wong, S. G. Murdoch, R. Leonhardt, J. D. Harvey, and V. Marie, "High-conversion-efficiency widely-tunable all-fiber optical parametric oscillator," *Opt. Exp.,* vol. 15, no. 6, pp. 2947-2952, Mar. 2007.

[61] Y. Q. Xu, S. G. Murdoch, R. Leonhardt, and J. D. Harvey, "Raman-assisted continuous-wave tunable all-fiber optical parametric oscillator," *J. Opt. Soc. Am. B.,* vol. 26, no. 7, pp. 1351-1356, Jul. 2009.

[62] Y. Zhou, B. P. Kuo, K. K. Y. Cheung, S. Yang, P. C. Chui, and K. K. Y. Wong, "Wide-band generation of picosecond pulse using fiber optical parametric amplifier and oscillator," *IEEE J. Quantum Electron.,* vol. 45, no. 11, pp. 1350-1356, Nov. 2009.

[63] Y. Zhou, K. K. Cheung, S. Yang, P. Chui, and K. K. Wong, "Ultra-widely tunable, narrow linewidth picosecond fiber-optical parametric oscillator," *IEEE Photon. Technol. Lett.,* vol. 22, no. 23, pp. 1756-1758, Dec. 2010.

[64] A. Gershikov, E. Shumakher, A. Willinger, and G. Eisenstein, "Fiber parametric oscillator for the 2 μm wavelength range based on narrowband optical parametric amplification," *Opt. Lett.,* vol. 35, no. 19, pp. 3198-3200, Oct. 2010.

[65] B. P.-P. Kuo, N. Alic, P. F. Wysocki, and S. Radic, "Simultaneous wavelength-swept generation in NIR and SWIR bands over combined 329-nm band using swept-pump fiber optical parametric oscillator," *J. Lightw. Technol.,* vol. 29, no. 4, pp. 410-416, Feb. 2011.

[66] A. Bellemare, M. Rochette, S. LaRochelle, and M. Tetu, "Room temperature multifrequency erbium-doped fiber lasers anchored on the ITU frequency grid," *J. Lightw. Technol.,* vol. 18, no. 6, pp. 825-831, Jun. 2000.

[67] L. Talaverano, S. Abad, S. Jarabo, and M. Lopez-Amo, "Multiwavelength fiber laser sources with Bragg-grating sensor multiplexing capability," *J. Lightw. Technol.,* vol. 19, no. 4, p. 553, Apr. 2001.

[68] Z. G. Lu, F. G. Sun, G. Z. Xiao, and C. P. Grover, "A tunable multiwavelength fiber ring laser for measuring polarization-mode dispersion in optical fibers," *IEEE Photon. Technol. Lett.,* vol. 16, no. 5, pp. 1280-1282, May 2004.

[69] L. R. Chen and V. Page, "Tunable photonic microwave filter using semiconductor fibre laser," *Electron. Lett.,* vol. 41, no. 21, pp. 1183-1184, Oct. 2005.

[70] K. R. Poguntke, J. B. D. Soole, A. Scherer, H. P. LeBlanc, C. Caneau, R. Bhat, *et al.*, "Simultaneous multiple wavelength operation of a multistripe array grating integrated cavity laser," *Appl. Phys. Lett.,* vol. 62, no. 17, pp. 2024-2026, Apr. 1993.

[71] M. Zirngibl, C. H. Joyner, C. R. Doerr, L. W. Stulz, and H. M. Presby, "An 18-channel multifrequency laser," *IEEE Photon. Technol. Lett.,* vol. 8, no. 7, pp. 870-872, Jul. 1996.

[72] N. Park and P. F. Wysocki, "24-line multiwavelength operation of erbium-doped fiber-ring laser," *IEEE Photon. Technol. Lett.,* vol. 8, no. 11, pp. 1459-1461, Nov. 1996.

[73] K. Zhou, D. Zhou, F. Dong, and N. Q. Ngo, "Room-temperature multiwavelength erbium-doped fiber ring laser employing sinusoidal phase-modulation feedback," *Opt. Lett.,* vol. 28, no. 11, pp. 893-895, Jun. 2003.

[74] J. Yao, J. Yao, Z. Deng, and J. Liu, "Investigation of room-temperature multiwavelength fiber-ring laser that incorporates an SOA-based phase modulator in the laser cavity," *J. Lightw. Technol.,* vol. 23, no. 8, pp. 2484-2490, Aug. 2005.

[75] S. Pan, C. Lou, and Y. Gao, "Multiwavelength erbium-doped fiber laser based on inhomogeneous loss mechanism by use of a highly nonlinear fiber and a Fabry-Perot filter," *Opt. Exp.,* vol. 14, no. 3, pp. 1113-1118, Jan. 2006.

[76] Z. Zhang, L. Zhan, K. Xu, J. Wu, Y. Xia, and J. Lin, "Multiwavelength fiber laser with fine adjustment, based on nonlinear polarization rotation and birefringence fiber filter," *Opt. Lett.,* vol. 33, no. 4, pp. 324-326, Feb. 2008.

[77] X. Liu and C. Lu, "Self-stabilizing effect of four-wave mixing and its applications on multiwavelength erbium-doped fiber lasers," *IEEE Photon. Technol. Lett.,* vol. 17, no. 12, pp. 2541-2543, Dec. 2005.

[78] X. Liu, X. Zhou, X. Tang, J. Ng, J. Hao, T. Y. Chai, *et al.*, "Switchable and tunable multiwavelength erbium-doped fiber laser with fiber Bragg gratings and photonic crystal fiber," *IEEE Photon. Technol. Lett.,* vol. 17, no. 8, pp. 1626-1628, Aug. 2005.

[79] A. Zhang, H. Liu, M. S. Demokan, and H. Y. Tam, "Stable and broad bandwidth multiwavelength fiber ring laser incorporating a highly nonlinear photonic crystal fiber," *IEEE Photon. Technol. Lett.,* vol. 17, no. 12, pp. 2535-2537, Dec. 2005.

[80] X. Feng, H.-Y. Tam, and P. K. A. Wai, "Switchable multiwavelength erbium-doped fiber laser with a multimode fiber Bragg grating and photonic crystal fiber," *IEEE Photon. Technol. Lett.,* vol. 18, no. 9, pp. 1088-1090, May 2006.

[81] X. Feng, P.-K. A. Wai, H.-Y. Tam, J. Li, B.-O. Guan, and C. Lu, "Investigation of a multiwavelength erbium-doped fiber laser employing a nonlinear high-birefringence fiber loop mirror," *Opt. Eng.,* vol. 49, no. 7, pp. 074202-074202-6, 2010.

[82] L. Xia, P. Shum, Y. Wang, and T. H. Cheng, "Stable triple-wavelength fiber ring laser with ultranarrow wavelength spacing using a triple-transmission-band fiber Bragg grating filter," *IEEE Photon. Technol. Lett.,* vol. 18, no. 20, pp. 2162-2164, 2006.

[83] N. Pleros, C. Bintjas, M. Kalyvas, G. Theophilopoulos, K. Yiannopoulos, S. Sygletos, *et al.*, "Multiwavelength and power equalized SOA laser sources," *IEEE Photon. Technol. Lett.,* vol. 14, no. 5, pp. 693-695, 2002.

[84] V. Baby, L. R. Chen, S. Doucet, and S. LaRochelle, "Continuous-wave operation of semiconductor optical amplifier-based multiwavelength tunable fiber lasers with 25-GHz spacing," *IEEE J. Sel. Topics Quantum Electron.,* vol. 13, no. 3, pp. 764-769, May/Jun. 2007.

[85] Z. Zhang, J. Wu, K. Xu, X. Hong, and J. Lin, "Tunable multiwavelength SOA fiber laser with ultra-narrow wavelength spacing based on nonlinear polarization rotation," *Opt. Exp.,* vol. 17, no. 19, pp. 17200-17205, Sep. 2009.

[86] Y. W. Lee, J. Jung, and B. Lee, "Multiwavelength-switchable SOA-fiber ring laser based on polarization-maintaining fiber loop mirror and polarization beam splitter," *IEEE Photon. Technol. Lett.,* vol. 16, no. 1, pp. 54-56, Jan. 2004.

[87] B.-A. Yu, J. Kwon, S. Chung, S.-W. Seo, and B. Lee, "Multiwavelength-switchable SOA-fibre ring laser using sampled Hi-Bi fibre grating," *Electron. Lett.,* vol. 39, no. 8, pp. 649-650, 2003.

[88] D. S. Moon, B. H. Kim, A. Lin, G. Sun, W.-T. Han, Y.-G. Han, *et al.*, "Tunable multi-wavelength SOA fiber laser based on a Sagnac loop mirror using an elliptical core side-hole fiber," *Opt. Exp.,* vol. 15, no. 13, pp. 8371-8376, 2007.

[89] Z. Luo, W.-D. Zhong, Z. Cai, C. Ye, H. Xu, X. Dong, *et al.*, "Multiwavelength fiber optical parametric oscillator," *IEEE Photon. Technol. Lett.,* vol. 21, no. 21, pp. 1609-1611, Nov. 2009.

[90] D. Chen and B. Sun, "Multi-wavelength fiber optical parametric oscillator with ultra-narrow wavelength spacing," *Opt. Exp.,* vol. 18, no. 17, pp. 18425-18430, Aug. 2010.

[91] B. Sun, K. Hu, D. Chen, Y. Wei, S. Gao, and S. He, "Wavelength-spacing-tunable double-pumped multiwavelength optical parametric oscillator based on a Mach–Zehnder interferometer," *J. Lightw. Technol.,* vol. 30, no. 12, pp. 1937-1942, Jun. 2012.

[92] R. Slavík, S. Doucet, and S. LaRochelle, "High-performance all-fiber Fabry-Perot filters with superimposed chirped Bragg gratings," *J. Lightw. Technol.,* vol. 21, no. 4, p. 1059, Apr. 2003.

[93] X. Xu, Y. Yao, and D. Chen, "Numerical analysis of multiwavelength erbium-doped fiber ring laser exploiting four-wave mixing," *Opt. Exp.,* vol. 16, no. 16, pp. 12397-12402, 2008.

[94] A. Shen, S. Bouchoule, P. Crozat, D. Mathoorasing, J.-M. Lourtioz, and C. Kazmierski, "Low timing jitter of gain-and Q-switched laser diodes for high bit rate OTDM applications," *Electron. Lett.,* vol. 33, no. 22, pp. 1875-1877, 1997.

[95] A. Aschwanden, D. Lorenser, H. Unold, R. Paschotta, E. Gini, and U. Keller, "2.1-W picosecond passively mode-locked external-cavity semiconductor laser," *Opt. Lett.,* vol. 30, no. 3, pp. 272-274, 2005.

[96] Y. Akage, K. Kawano, S. Oku, R. Iga, H. Okamoto, Y. Miyamoto, *et al.*, "Wide bandwidth of over 50 GHz travelling-wave electrode electroabsorption modulator integrated DFB lasers," *Electron. Lett.,* vol. 37, no. 5, pp. 299-300, 2001.

[97] M. Shirane, Y. Hashimoto, H. Yamada, and H. Yokoyama, "A compact optical sampling measurement system using mode-locked laser-diode modules," *IEEE Photon. Technol. Lett.,* vol. 12, no. 11, pp. 1537-1539, Nov. 2000.

[98] P. J. Delfyett, S. Gee, M.-T. Choi, H. Izadpanah, W. Lee, S. Ozharar, *et al.*, "Optical frequency combs from semiconductor lasers and applications in ultrawideband signal processing and communications," *J. Lightw. Technol.,* vol. 24, no. 7, p. 2701, Jul. 2006.

[99] S. B. Yoo, "Optical packet and burst switching technologies for the future photonic internet," *J. Lightw. Technol.,* vol. 24, no. 12, pp. 4468-4492, Dec. 2006.

[100] A. E. Siegman, *Lasers*. Mill Valley, CA: University Science Books, 1986.

[101] H. Haus, "A theory of forced mode locking," *IEEE J. Quantum Electron.,* vol. 11, no. 7, pp. 323-330, Jul. 1975.

[102] C. Yeh, *Applied Photonics*. San Diego, CA: Academic Press, 1994.

[103] H. Takara, S. Kawanishi, M. Saruwatari, and K. Noguchi, "Generation of highly stable 20 GHz transform-limited optical pulses from actively mode-locked Er-doped fibre lasers with an all-polarisation maintaining ring cavity," *Electron. Lett.,* vol. 28, no. 22, pp. 2095-2096, Oct. 1992.

[104] T. Pfeiffer and G. Veith, "40 GHz pulse generation using a widely tunable all-polarisation preserving erbium fibre ring laser," *Electron. Lett.,* vol. 29, no. 21, pp. 1849-1850, Oct. 1993.

[105] H. Takara, S. Kawanishi, and M. Saruwatari, "Stabilisation of a modelocked Er-doped fibre laser by suppressing the relaxation oscillation frequency component," *Electron. Lett.,* vol. 31, no. 4, pp. 292-293, Feb. 1995.

[106] X. Shan, T. Widdowson, A. Ellis, and A. Siddiqui, "Very simple method to stabilise mode-locked erbium fibre lasers," *Electron. Lett.,* vol. 32, no. 11, pp. 1015-1016, May 1996.

[107] E. Yoshida and M. Nakazawa, "Wavelength tunable 1.0 ps pulse generation in 1.530-1.555 μm region from PLL, regeneratively modelocked fibre laser," *Electron. Lett.,* vol. 34, no. 18, pp. 1753-1754, Sep. 1998.

[108] A. Ellis, R. Manning, I. Phillips, and D. Nesset, "1.6 ps pulse generation at 40 GHz in phaselocked ring laser incorporating highly nonlinear fibre for application to 160 Gbit/s OTDM networks," *Electron. Lett.,* vol. 35, no. 8, pp. 645-646, Apr. 1999.
[109] M. Horowitz, C. R. Menyuk, T. F. Carruthers, and I. N. DulingIII, "Theoretical and experimental study of harmonically modelocked fiber lasers for optical communication systems," *J. Lightw. Technol.,* vol. 18, no. 11, p. 1565, 2000.
[110] L. Duan, C. J. Richardson, Z. Hu, M. Dagenais, and J. Goldhar, "A stable smoothly wavelength-tunable picosecond pulse generator," *IEEE Photon. Technol. Lett.,* vol. 14, no. 6, pp. 840-842, Jun. 2002.
[111] X. Shan, D. Cleland, and A. Ellis, "Stabilising Er fibre soliton laser with pulse phase locking," *Electron. Lett.,* vol. 28, no. 2, pp. 182-184, Jan. 1992.
[112] M. Nakazawa, E. Yoshida, and Y. Kimura, "Ultrastable harmonically and regeneratively modelocked polarisation-maintaining erbium fibre ring laser," *Electron. Lett.,* vol. 30, no. 19, pp. 1603-1605, Sep. 1994.
[113] C. Doerr, H. Haus, E. Ippen, M. Shirasaki, and K. Tamura, "Additive-pulse limiting," *Opt. Lett.,* vol. 19, no. 1, pp. 31-33, Jan. 1994.
[114] M. Nakazawa, K. Tamura, and E. Yoshida, "Supermode noise suppression in a harmonically modelocked fibre laser by selfphase modulation and spectral filtering," *Electron. Lett.,* vol. 32, no. 5, pp. 461-463, February 1996.
[115] G. T. Harvey and L. F. Mollenauer, "Harmonically mode-locked fiber ring laser with an internal Fabry-Perot stabilizer for soliton transmission," *Opt. Lett.,* vol. 18, no. 2, pp. 107-109, Jan. 1993.
[116] L. Duan, M. Dagenais, and J. Goldhar, "Smoothly wavelength-tunable picosecond pulse generation using a harmonically mode-locked fiber ring laser," *J. Lightw. Technol.,* vol. 21, no. 4, p. 930, Apr. 2003.
[117] M. Guy, J. Taylor, D. Moodie, and A. Kelly, "10 GHz 3 ps actively mode-locked ring laser incorporating a semiconductor laser amplifier and an electroabsorption modulator," *Electron. Lett.,* vol. 32, no. 24, pp. 2240-2241, Nov. 1996.
[118] L. R. Chen and J. C. Cartledge, "Mode-locking in a semiconductor fiber laser using cross-absorption modulation in an electroabsorption modulator and application to all-optical clock recovery," *J. Lightw. Technol.,* vol. 26, no. 7, pp. 799-806, Apr. 2008.
[119] W. Tang, M. Fok, and C. Shu, "10 GHz pulses generated across a~ 100 nm tuning range using a gain-shifted mode-locked SOA ring laser," *Opt. Exp.,* vol. 14, no. 6, pp. 2158-2163, March 2006.
[120] D. Patrick, "Modelocked ring laser using nonlinearity in a semiconductor laser amplifier," *Electron. Lett.,* vol. 30, no. 1, pp. 43-44, Jan. 1994.
[121] K. Vlachos, K. Zoiros, T. Houbavlis, and H. Avramopoulos, "10 x 30 GHz pulse train generation from semiconductor amplifier fiber ring laser," *IEEE Photon. Technol. Lett.,* vol. 12, no. 1, pp. 25-27, Jan. 2000.
[122] J. He and K. Chan, "Generation and wavelength switching of picosecond pulses by optically modulating a semiconductor optical amplifier in a fiber laser with optical delay line," *IEEE Photon. Technol. Lett.,* vol. 15, no. 6, pp. 798-800, June 2003.
[123] K. Vlachos, C. Bintjas, N. Pleros, and H. Avramopoulos, "Ultrafast semiconductor-based fiber laser sources," *IEEE J. Sel. Topics Quantum Electron.,* vol. 10, no. 1, pp. 147-154, Jan/Feb. 2004.
[124] L. Schares, L. Occhi, and G. Guekos, "80-160-GHz mode-locked fiber ring laser synchronized to external optical pulse stream," *IEEE Photon. Technol. Lett.,* vol. 15, no. 10, pp. 1348-1350, Oct. 2003.
[125] L. Schares, R. Paschotta, L. Occhi, and G. Guekos, "40-GHz mode-locked fiber-ring laser using a Mach-Zehnder interferometer with integrated SOAs," *J. Lightw. Technol.,* vol. 22, no. 3, p. 859, Mar. 2004.

[126] S. Bigo and E. Desurvire, "20 GHz all-optical clock recovery based on fibre laser mode-locking with fibre nonlinear loop mirror as variable intensity/phase modulator," *Electron. Lett.,* vol. 31, no. 21, pp. 1855-1857, Oct. 1995.
[127] W. Tang, C. Shu, and K. Lee, "Rational harmonic mode locking of an optically triggered fiber laser incorporating a nonlinear optical loop modulator," *IEEE Photon. Technol. Lett.,* vol. 13, no. 1, pp. 16-18, Jan. 2001.
[128] T. Cai and L. R. Chen, "40-80-160 GHz tunable mode-locked semiconductor fiber laser incorporating a nonlinear optical loop mirror," *Opt. Exp.,* vol. 18, no. 17, pp. 18113-18118, Aug. 2010.
[129] T. Huang, J. Sun, J. Li, and L. R. Chen, "40-Gb/s All-Optical Clock Recovery Based on an Mode-Locked Semiconductor Fiber Laser Using Nonlinear Polarization Rotation," *IEEE Photon. Technol. Lett.,* vol. 24, no. 8, pp. 682-684, Apr. 2012.
[130] R. Stolen, C. Lin, and R. Jain, "A time-dispersion-tuned fiber Raman oscillator," *Appl. Phys. Lett.,* vol. 30, no. 7, pp. 340-342, Apr. 1977.
[131] K. Tamura and M. Nakazawa, "Dispersion-tuned harmonically mode-locked fiber ring laser for self-synchronization to an external clock," *Opt. Lett.,* vol. 21, no. 24, pp. 1984-1986, Dec. 1996.
[132] S. Li and K. Chan, "Electrical wavelength tunable and multiwavelength actively mode-locked fiber ring laser," *Appl. Phys. Lett.,* vol. 72, no. 16, pp. 1954-1956, Apr. 1998.
[133] H. Cao and L. R. Chen, "Wavelength tuning in optically mode-locked semiconductor fiber ring lasers with linearly chirped fiber Bragg gratings," *Appl. Opt.,* vol. 44, no. 17, pp. 3545-3551, Jun. 2005.
[134] M. E. Marhic, *Fiber optical parametric amplifiers, oscillators and related devices*. Cambridge, U.K.: Cambridge University Press, 2007.
[135] J. E. Sharping, C. Pailo, C. Gu, L. Kiani, and J. R. Sanborn, "Microstructure fiber optical parametric oscillator with femtosecond output in the 1200 to 1350 nm wavelength range," *Opt. Exp.,* vol. 18, no. 4, pp. 3911-3916, Feb. 2010.
[136] Y. Zhou, K. K. Cheung, S. Yang, P. Chui, and K. K. Wong, "A time-dispersion-tuned picosecond fiber-optical parametric oscillator," *IEEE Photon. Technol. Lett.,* vol. 21, no. 17, pp. 1223-1225, Sep. 2009.
[137] Y. Zhou, K. K. Y. Cheung, S. Yang, P. C. Chui, and K. K. Y. Wong, "Widely tunable picosecond optical parametric oscillator using highly nonlinear fiber," *Opt. Lett.,* vol. 34, no. 7, pp. 989-991, Apr. 2009.
[138] B. P. P. Kuo, N. Alic, P. F. Wysocki, and S. Radic, "Simultaneous wavelength-swept generation in NIR and SWIR bands over combined 329-nm band using swept-pump fiber optical parametric oscillator," *J. Lightw. Technol.,* vol. 29, no. 4, pp. 410-416, Feb. 2011.
[139] Y. Deng, Q. Lin, F. Lu, G. P. Agrawal, and W. H. Knox, "Broadly tunable femtosecond parametric oscillator using a photonic crystal fiber," *Opt. Lett.,* vol. 30, no. 10, pp. 1234-1236, May 2005.
[140] C. Gu, H. Wei, S. Chen, W. Tong, and J. E. Sharping, "Fiber optical parametric oscillator for sub-50 fs pulse generation: optimization of fiber length," *Opt. Lett.,* vol. 35, no. 20, pp. 3516-3518, Oct. 2010.
[141] J. Lasri, P. Devgan, R. Tang, V. Grigoryan, W. Kath, and P. Kumar, "Regeneratively modelocked dual-wavelength soliton-pulse fibre-optical parametric oscillator in C-and L-bands," *Electron. Lett.,* vol. 40, no. 10, pp. 622-623, May 2004.
[142] P. S. Devgan, J. Lasri, R. Tang, V. S. Grigoryan, W. L. Kath, and P. Kumar, "10-GHz dispersion-managed soliton fiber-optical parametric oscillator using regenerative mode locking," *Opt. Lett.,* vol. 30, no. 5, pp. 528-530, Mar. 2005.
[143] D. Von der Linde, "Characterization of the noise in continuously operating mode-locked lasers," *Appl. Phys.,* vol. 39, no. 4, pp. 201-217, 1986.

[144] T. Torounidis, M. Karlsson, and P. A. Andrekson, "Fiber optical parametric amplifier pulse source: Theory and experiments," *J. Lightw. Technol.,* vol. 23, no. 12, pp. 4067-4073, Dec. 2005.
[145] C. Gu, C. Goulart, and J. E. Sharping, "Cross-phase-modulation-induced spectral effects in high-efficiency picosecond fiber optical parametric oscillators," *Opt. Lett.,* vol. 36, no. 8, pp. 1488-1490, 2011.
[146] R. Paschotta, "Timing jitter and phase noise of mode-locked fiber lasers," *Opt. Exp.,* vol. 18, no. 5, pp. 5041-5054, Mar. 2010.
[147] Y. Su, L. Wang, A. Agarwal, and P. Kumar, "All-optical limiter using gain flattened fibre parametric amplifier," *Electron. Lett.,* vol. 36, no. 13, pp. 1103-1105, Jun. 2000.
[148] A. Mussot, A. Durecu-Legrand, E. Lantz, C. Simonneau, D. Bayart, H. Maillotte, *et al.*, "Impact of pump phase modulation on the gain of fiber optical parametric amplifier," *IEEE Photon. Technol. Lett.,* vol. 16, no. 5, pp. 1289-1291, 2004.
[149] K. Tai, A. Tomita, J. Jewell, and A. Hasegawa, "Generation of subpicosecond solitonlike optical pulses at 0.3 THz repetition rate by induced modulational instability," *Appl. Phys. Lett.,* vol. 49, no. 5, pp. 236-238, Jun. 1986.
[150] K. K. Gupta, N. Onodera, K. S. Abedin, and M. Hyodo, "Pulse repetition frequency multiplication via intracavity optical filtering in AM mode-locked fiber ring lasers," *IEEE Photon. Technol. Lett.,* vol. 14, no. 3, pp. 284-286, Mar. 2002.
[151] K. Sarwar Abedin, N. Onodera, and M. Hyodo, "Repetition-rate multiplication in actively mode-locked fiber lasers by higher-order FM mode locking using a high-finesse Fabry–Perot filter," *Appl. Phys. Lett.,* vol. 73, no. 10, pp. 1311-1313, Sep. 1998.
[152] K. Yiannopoulos, K. Vyrsokinos, E. Kehayas, N. Pleros, K. Vlachos, H. Avramopoulos, *et al.*, "Rate multiplication by double-passing Fabry-Perot filtering," *IEEE Photon. Technol. Lett.,* vol. 15, no. 9, pp. 1294-1296, Sep. 2003.
[153] N. K. Berger, B. Levit, S. Atkins, and B. Fischer, "Repetition-rate multiplication of optical pulses using uniform fiber Bragg gratings," *Opt. Comm.,* vol. 221, no. 4, pp. 331-335, 2003.
[154] P. Petropoulos, M. Ibsen, M. N. Zervas, and D. J. Richardson, "Generation of a 40-GHz pulse stream by pulse multiplication with a sampled fiber Bragg grating," *Opt. Lett.,* vol. 25, no. 8, pp. 521-523, Apr. 2000.
[155] J. Azaña, R. Slavìk, P. Kockaert, L. R. Chen, and S. LaRochelle, "Generation of customized ultrahigh repetition rate pulse sequences using superimposed fiber Bragg gratings," *J. Lightw. Technol.,* vol. 21, no. 6, pp. 1490-1498, Jun. 2003.
[156] J. Azaña, P. Kockaert, R. Slavìk, L. R. Chen, and S. LaRochelle, "Generation of a 100-GHz optical pulse train by pulse repetition-rate multiplication using superimposed fiber Bragg gratings," *IEEE Photon. Technol. Lett.,* vol. 15, no. 3, pp. 413-415, Mar. 2003.
[157] A. M. Weiner and D. Leaird, "Generation of terahertz-rate trains of femtosecond pulses by phase-only filtering," *Opt. Lett.,* vol. 15, no. 1, pp. 51-53, Jan. 1990.
[158] J. Caraquitena, Z. Jiang, D. E. Leaird, and A. M. Weiner, "Tunable pulse repetition-rate multiplication using phase-only line-by-line pulse shaping," *Opt. Lett.,* vol. 32, no. 6, pp. 716-718, Mar. 2007.
[159] J. Azaña and M. A. Muriel, "Temporal self-imaging effects: theory and application for multiplying pulse repetition rates," *IEEE J. Sel. Topics Quantum Electron.,* vol. 7, no. 4, pp. 728-744, Jul/Aug. 2001.
[160] S. Arahira, S. Kutsuzawa, Y. Matsui, D. Kunimatsu, and Y. Ogawa, "Repetition-frequency multiplication of mode-locked pulses using fiber dispersion," *J. Lightw. Technol.,* vol. 16, no. 3, pp. 405-410, Mar. 1998.
[161] J. Azaña and M. A. Muriel, "Technique for multiplying the repetition rates of periodic trains of pulses by means of a temporal self-imaging effect in chirped fiber gratings," *Opt. Lett.,* vol. 24, no. 23, pp. 1672-1674, Dec. 1999.

[162] J. H. Lee, Y. Chang, Y.-G. Han, S. Kim, and S. Lee, "2~ 5 times tunable repetition-rate multiplication of a 10 GHz pulse source using a linearly tunable, chirped fiber Bragg grating," *Opt. Exp.,* vol. 12, no. 17, pp. 3900-3905, Aug. 2004.

[163] N. Onodera, A. Lowery, L. Zhai, Z. Ahmed, and R. Tucker, "Frequency multiplication in actively mode-locked semiconductor lasers," *Appl. Phys. Lett.,* vol. 62, no. 12, pp. 1329-1331, 1993.

[164] Z. Ahmed and N. Onodera, "High repetition rate optical pulse generation by frequency multiplication in actively modelocked fibre ring lasers," *Electron. Lett.,* vol. 32, no. 5, pp. 455-457, Feb. 1996.

[165] E. Yoshida and M. Nakazawa, "80~ 200 GHz erbium doped fibre laser using a rational harmonic mode-locking technique," *Electron. Lett.,* vol. 32, no. 15, pp. 1370-1372, Jul. 1996.

[166] C. Wu and N. K. Dutta, "High-repetition-rate optical pulse generation using a rational harmonic mode-locked fiber laser," *IEEE J. Quantum Electron.,* vol. 36, no. 2, pp. 145-150, Feb. 2000.

[167] G.-R. Lin, Y.-C. Chang, and J.-R. Wu, "Rational harmonic mode-locking of erbium-doped fiber laser at 40 GHz using a loss-modulated Fabry-Perot laser diode," *IEEE Photon. Technol. Lett.,* vol. 16, no. 8, pp. 1810-1812, Aug. 2004.

[168] M.-Y. Jeon, H. K. Lee, J. T. Ahn, K. H. Kim, D. S. Lim, and E.-H. Lee, "Pulse-amplitude-equalized output from a rational harmonic mode-locked fiber laser," *Opt. Lett.,* vol. 23, no. 11, pp. 855-857, Jun. 1998.

[169] M.-Y. Jeon, H. K. Lee, J. T. Ahn, D. S. Lim, H. Y. Kim, K. H. Kim*, et al.*, "External fibre laser based pulse amplitude equalisation scheme for rational harmonic modelocking in a ring-type fibre laser," *Electron. Lett.,* vol. 34, no. 2, pp. 182-184, Jan. 1998.

[170] H. J. Lee, K. Kim, and H. G. Kim, "Pulse-amplitude equalization of rational harmonic mode-locked fiber laser using a semiconductor optical amplifier loop mirror," *Opt. Comm.,* vol. 160, no. 1, pp. 51-56, Feb. 1999.

[171] Z. Li, C. Lou, K. T. Chan, Y. Li, and Y. Gao, "Theoretical and experimental study of pulse-amplitude-equalization in a rational harmonic mode-locked fiber ring laser," *IEEE J. Quantum Electron.,* vol. 37, no. 1, pp. 33-37, Jan. 2001.

[172] C. G. Lee, Y. J. Kim, H. K. Choi, and C.-S. Park, "Pulse-amplitude equalization in a rational harmonic mode-locked semiconductor ring laser using optical feedback," *Opt. Comm.,* vol. 209, no. 4, pp. 417-425, 2002.

[173] Y. Kim, C. Lee, Y. Chun, and C.-S. Park, "Pulse-amplitude equalization in a rational harmonic mode-locked semiconductor fiber ring laser using a dual-drive Mach-Zehnder modulator," *Opt. Exp.,* vol. 12, no. 5, pp. 907-915, Mar. 2004.

[174] G. Contestabile, M. Presi, R. Proietti, N. Calabretta, and E. Ciaramella, "A simple and low-power optical limiter for multi-GHz pulse trains," *Opt. Exp.,* vol. 15, no. 15, pp. 9849-9858, Jul. 2007.

[175] J. Li, T. Huang, and L. R. Chen, "Detailed analysis of all-optical clock recovery at 10 Gb/s based on a fiber optical parametric oscillator," *IEEE J. Sel. Topics Quantum Electron.,* vol. 18, no. 2, pp. 701-708, Mar/Apr. 2012.

[176] K. Gupta and D. Novak, "Millimetre-wave repetition-rate optical pulse train generation in harmonically modelocked fibre ring laser," *Electron. Lett.,* vol. 33, no. 15, pp. 1330-1331, Jul. 1997.

[177] Y. Fukuchi and J. Maeda, "Characteristics of Wavelength-Tunable Harmonically Mode-Locked Short-Cavity Fiber Ring Laser Using a Bismuth-Oxide-Based Erbium-Doped Fiber and a Bismuth-Oxide-Based Highly Nonlinear Fiber," *IEEE J. Quantum Electron.,* vol. 48, no. 7, pp. 897-902, Jul. 2012.

[178] G. Zhu, H. Chen, and N. Dutta, "Time domain analysis of a rational harmonic mode locked ring fiber laser," *J. App. Phys.,* vol. 90, no. 5, pp. 2143-2147, Sep. 2001.

[179] T. Von Lerber, S. Honkanen, A. Tervonen, H. Ludvigsen, and F. Küppers, "Optical clock recovery methods: Review," *Opt. Fiber Technol.,* vol. 15, no. 4, pp. 363-372, 2009.
[180] I. Phillips, A. Gloag, P. Kean, N. Doran, I. Bennion, and A. Ellis, "Simultaneous demultiplexing, data regeneration, and clock recovery with a single semiconductor optical amplifier-based nonlinear-optical loop mirror," *Opt. Lett.,* vol. 22, no. 17, pp. 1326-1328, 1997.
[181] J. Turkiewicz, E. Tangdiongga, G. Khoe, and H. de Waardt, "Clock recovery and demultiplexing performance of 160-Gb/s OTDM field experiments," *IEEE Photon. Technol. Lett.,* vol. 16, no. 6, pp. 1555-1557, Jun. 2004.
[182] E. S. Awad, P. S. Cho, and J. Goldhar, "Simultaneous four-wave mixing and cross-absorption modulation inside a single EAM for high-speed optical demultiplexing and clock recovery," *IEEE Photon. Technol. Lett.,* vol. 17, no. 7, pp. 1534-1536, Jul. 2005.
[183] G. Zhu, Q. Wang, H. Dong, H. Sun, and N. Dutta, "80Gb/s clock recovery with phase locked loop based on LiNbO3 modulators," *Opt. Exp.,* vol. 12, no. 15, pp. 3488-3492, Jul. 2004.
[184] M. W. Chbat, P. Perrier, and P. Prucnal, "Optical clock recovery demonstration using periodic oscillations of a hybrid electrooptic bistable system," *IEEE Photon. Technol. Lett.,* vol. 3, no. 1, pp. 65-67, Jan. 1991.
[185] H. Tsuchida, "160-Gb/s optical clock recovery using a regeneratively mode-locked laser diode," *IEEE Photon. Technol. Lett.,* vol. 18, no. 16, pp. 1687-1689, Aug. 2006.
[186] J. Lasri, P. Devgan, R. Tang, and P. Kumar, "Ultralow timing jitter 40-Gb/s clock recovery using a self-starting optoelectronic oscillator," *IEEE Photon. Technol. Lett.,* vol. 16, no. 1, pp. 263-265, Jan. 2004.
[187] S. Arahira, S. Sasaki, K. Tachibana, and Y. Ogawa, "All-optical 160-Gb/s clock extraction with a mode-locked laser diode module," *IEEE Photon. Technol. Lett.,* vol. 16, no. 6, pp. 1558-1560, Jun. 2004.
[188] S. Arahira, H. Takahashi, K. Nakamura, S. Miyamura, H. Yaegashi, and Y. Ogawa, "Polarization-insensitive clock recovery operation in a monolithic passively mode-locked distributed-Bragg-reflector laser integrated with a tensile-strained multiple-quantum-well saturable absorber," *IEEE Photon. Technol. Lett.,* vol. 19, no. 16, pp. 1263-1265, Aug. 2007.
[189] I. Kim, C. Kim, P. L. LiKamWa, and G. Li, "Dynamics of all-optical clock recovery using two-section index-and gain-coupled DFB lasers," *J. Lightw. Technol.,* vol. 23, no. 4, pp. 1704-1712, Apr. 2005.
[190] W. Mao, Y. Li, M. Al-Mumin, and G. Li, "All-optical clock recovery from RZ-format data by using a two-section gain-coupled DFB laser," *J. Lightw. Technol.,* vol. 20, no. 9, p. 1705, Sep. 2002.
[191] Y. A. Leem, D.-S. Yee, E. Sim, S.-B. Kim, D. C. Kim, and K. H. Park, "Self-pulsation in multisection laser diodes with a DFB reflector," *IEEE Photon. Technol. Lett.,* vol. 18, no. 4, pp. 622-624, Feb. 2006.
[192] M. Jinno, T. Matsumoto, and M. Koga, "All-optical timing extraction using an optical tank circuit," *IEEE Photon. Technol. Lett.,* vol. 2, no. 3, pp. 203-204, Mar. 1990.
[193] G. Contestabile, A. D'Errico, M. Presi, and E. Ciaramella, "40-GHz all-optical clock extraction using a semiconductor-assisted fabry-Pe´ rot filter," *IEEE Photon. Technol. Lett.,* vol. 16, no. 11, pp. 2523-2525, Nov. 2004.
[194] E. Kehayas, L. Stampoulidis, H. Avramopoulos, Y. Liu, E. Tangdiongga, and H. Dorren, "40 Gb/s all-optical packet clock recovery with ultrafast lock-in time and low inter-packet guardbands," *Opt. Exp.,* vol. 13, no. 2, pp. 475-480, Jan. 2005.
[195] P. Bakopoulos, D. Tsiokos, O. Zouraraki, H. Avramopoulos, G. Maxwell, and A. Poustie, "Compact all-optical packet clock and data recovery circuit using generic integrated MZI switches," *Opt. Exp.,* vol. 13, no. 17, pp. 6401-6406, Aug. 2005.

[196] C. Kouloumentas, A. Tzanakaki, and I. Tomkos, "Clock recovery at 160 Gb/s and beyond, using a fiber-based optical power limiter," *IEEE Photon. Technol. Lett.,* vol. 18, no. 22, pp. 2365-2367, Nov. 2006.
[197] G. Contestabile, M. Presi, N. Calabretta, and E. Ciaramella, "All-optical clock recovery for NRZ-DPSK signals," *IEEE Photon. Technol. Lett.,* vol. 18, no. 23, pp. 2544-2546, Dec. 2006.
[198] J. Lee, H. Cho, and J. S. Ko, "Enhancement of clock component in a nonreturn-to-zero signal through beating process," *Opt. Fiber Technol.,* vol. 12, no. 1, pp. 59-70, 2006.
[199] D. Pudo, M. Depa, and L. R. Chen, "Single and multiwavelength all-optical clock recovery in single-mode fiber using the temporal Talbot effect," *J. Lightw. Technol.,* vol. 25, no. 10, pp. 2898-2903, Oct. 2007.
[200] L. Wang, Y. Su, A. Agarwal, and P. Kumar, "Polarization insensitive widely tunable all-optical clock recovery based on AM mode-locking of a fiber ring laser," *IEEE Photon. Technol. Lett.,* vol. 12, no. 2, pp. 211-213, Feb. 2000.
[201] K. G. Vlachos, "Optical clock recovery and clock division at 20 Gb/s using a tunable semiconductor fiber ring laser," *Opt. Comm.,* vol. 222, no. 1, pp. 249-255, 2003.
[202] K. Vlachos, G. Theophilopoulos, A. Hatziefremidis, and H. Avramopoulos, "30 Gb/s all-optical clock recovery circuit," *IEEE Photon. Technol. Lett.,* vol. 12, no. 6, pp. 705-707, Jun. 2000.
[203] J. He and K. Chan, "Wavelength-switchable all optical clock recovery at 10Gbit/s based on semiconductor fiber ring laser," *Opt. Exp.,* vol. 13, no. 1, pp. 327-335, Jan. 2005.
[204] L. Lui, L. Xu, C. Lee, P. Wai, H. Tam, and C. Lu, "All-optical clock recovery using erbium-doped fiber laser incorporating an electroabsorption modulator and a linear optical amplifier," *IEEE Photon. Technol. Lett.,* vol. 19, no. 10, pp. 720-722, May 2007.
[205] A. Ellis, K. Smith, and D. Patrick, "All optical clock recovery at bit rates up to 40 Gbit/s," *Electron. Lett.,* vol. 29, no. 15, pp. 1323-1324, Jul. 1993.
[206] T. Huang, S. Fu, J. Sun, J. Li, and L. R. Chen, "Comparison of nonlinear fiber-based approaches for all-optical clock recovery at 40 Gb/s," *Opt. Comm.,* vol. 298-299, pp. 213-221, Jul. 2013.
[207] L. Adams, E. Kintzer, and J. Fujimoto, "All-optical timing extraction at 40 GHz using a mode-locked figure-eight laser with an SLA," *Electron. Lett.,* vol. 31, no. 20, pp. 1759-1761, Sep. 1995.
[208] Y. Su, L. Wang, A. Agarwal, and P. Kumar, "Wavelength-tunable all-optical clock recovery using a fiber-optic parametric oscillator," *Opt. Comm.,* vol. 184, no. 1, pp. 151-156, 2000.
[209] L. Lui, A. Zhang, P. Wai, H. Tam, and M. Demokan, "40 Gb/s All-optical clock recovery based on an optical parametric oscillator with photonic crystal fiber," in *Proceedings to Lasers and Electro-Optics, 2008 and 2008 Conference on Quantum Electronics and Laser Science*, 2008, pp. 1-2.
[210] I. Monfils and J. C. Cartledge, "Detailed theoretical and experimental characterization of 10 Gb/s clock recovery using a Q-switched self-pulsating laser," *J. Lightw. Technol.,* vol. 27, no. 5, pp. 619-626, Mar. 2009.
[211] C. Koos, L. Jacome, C. Poulton, J. Leuthold, and W. Freude, "Nonlinear silicon-on-insulator waveguides for all-optical signal processing," *Opt. Exp.,* vol. 15, no. 10, pp. 5976-5990, 2007.
[212] J. Leuthold, C. Koos, and W. Freude, "Nonlinear silicon photonics," *Nature Photonics,* vol. 4, no. 8, 2010.
[213] J. S. Levy, A. Gondarenko, M. A. Foster, A. C. Turner-Foster, A. L. Gaeta, and M. Lipson, "CMOS-compatible multiple-wavelength oscillator for on-chip optical interconnects," *Nature Photonics,* vol. 4, no. 1, pp. 37-40, 2010.

[214] M. A. Foster, A. C. Turner, J. E. Sharping, B. S. Schmidt, M. Lipson, and A. L. Gaeta, "Broad-band optical parametric gain on a silicon photonic chip," *Nature,* vol. 441, no. 7096, pp. 960-963, 2006.